Theses

12-2019

Improvements to a Thermally Actuated MEMS Viscosity Sensor

Shreyas Choudhary

sc3355@rit.edu

IMPROVEMENTS TO A THERMALLY ACTUATED MEMS VISCOSITY SENSOR

by

SHREYAS CHOUDHARY

Thesis submitted in partial fulfillment of the requirements for the degree of

MASTER OF SCIENCE IN MICROELECTRONIC ENGINEERING

Approved by:

Professor _____
Thesis Advisor – Dr. Ivan Puchades

Professor _____
Committee Member – Dr. Robert E. Pearson

Professor _____
Committee Member – Dr. Karl D. Hirschman

Professor _____
Committee Member – Dr. Patricia Iglesias Victoria

Professor _____
Program Director – Dr. Sean L. Rommel

Professor _____
Department Head- Dr. Sohail A. Dianat

DEPARTMENT OF ELECTRICAL AND MICROELECTRONIC ENGINEERING
KATE GLEASON COLLEGE OF ENGINEERING
ROCHESTER INSTITUTE OF TECHNOLOGY
ROCHESTER, NEW YORK
December, 2019

ACKNOWLEDGEMENTS

ABSTRACT

Being able to measure and monitor the viscosity of a fluid **accurately** and in **real-time** can provide insights and prevent field failures of lubricated mechanical elements. A micro electro mechanical system (MEMS) viscosity sensor that measures the properties of liquids through thermal vibrations of a silicon membrane has been previously developed. The device measures viscosity through three different characteristics: the frequency, amplitude and the quality factor of the vibrating membrane. The membrane is actuated via a short pulse of heat delivered by the heater resistor provided by an external voltage. The pulse width is controlled by a waveform generator and a power MOSFET. The movement of the membrane is measured with an in-situ piezoresistor Wheatstone bridge, which is powered by an external voltage source, and amplified with and instrumentational amplifier before the resulting vibrating signal is analyzed in LabView. The end goal of this work is to characterize the **sensitivity** and **real-time response** of a thermally actuated MEMS viscosity sensor. In addition, a process modification to include a deep reactive ion etch instead of a KOH etch, has been developed. As viscosity is dependent on temperature, when the membrane is actuated by heat, the effects of locally changing the fluid temperature will affect the **sensitivity** of the sensor. Optimized test bias condition results were, Wheatstone bridge bias voltage when increased over 7 V, the natural frequency of vibration of the sensor is modified. Pulse width and heater bias value can be adjusted for optimum sensor response. With these established bias conditions, the **real-time response** of the system was investigated. Epoxy was used to cover the sensor perimeter, protect the 25 - micron aluminum wire bond connections to a copper PCB and to glue the sensor onto the PCB. Test result show a spike in frequency and amplitude when different oils were added. As shown with additional tests, the spike is mainly caused by slight temperature variations that are introduced with new oil and how they affect the sensor packaging. Spikes were reduced by lowering the bridge bias voltage from 7 V to 3 V, which minimized the sensor heating. Furthermore, addition of oil in very small quantities, in the ~ µL range, reduced the changes in temperature. Figure 1 shows frequency and amplitude response with varying viscosities without agitation. During testing, when oil is added, the amplitude shows an immediate overdamped response which takes about 1-2 minutes to stabilize, whereas frequency is characterized by an underdamped response with response time 5-7 minutes. Frequency response time was slower as it is very dependent on intrinsic stresses of both sensor and packaging, whereas amplitude of oscillations seems to be more independent to these properties changing and shows faster response.
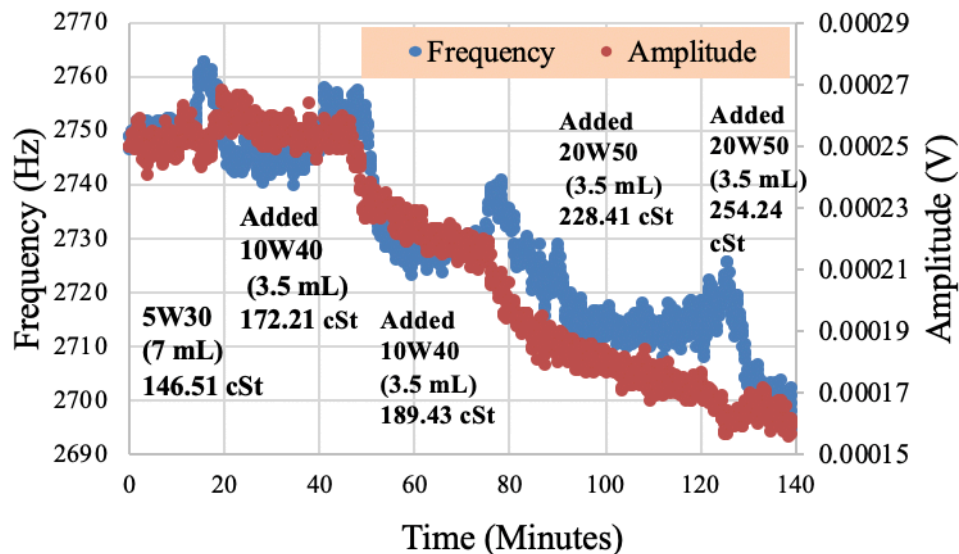
Figure 1: Frequency and amplitude response of thermally actuated MEMS sensor to changes in viscosity of commercial motor oils.

TABLE OF CONTENTS

LIST OF TABLES

LIST OF FIGURES

CHAPTER 1

INTRODUCTION

While the flow rate of fluids is a well understood concept, there is a general lack of understanding of what viscosity is and how it plays into fluid mechanics. As a baseline, viscosity is a measure to define a liquid's resistance to flow, where a fluid with high viscosity is much more resistant to change than a fluid with low viscosity. In addition to a basic understanding of pure viscosity sensors, there is an increasing need for real-time sensors, which can detect the change in viscosity over time. Some applications of this real-time response are to monitor oil life in auto applications, characterize real time polymerization reactions, and monitor blood viscosity to detect any cardiovascular events. In all of these cases, there are numerous important factors which play into the full characterization. In particular, to measure the progress of a chemical reaction, the initial viscosity needs to be measured and the end product viscosity should also be known to allow for conclusive testing. Thus, by measuring the viscosity at any point during the system operation, the proportion of reaction completed can be calculated, giving information on both what is happening as well as what issues there might be.

This work serves to introduce the basics of viscosity, its importance, and its applications in both general markets and microelectronics. Most MEMS viscosity sensors measure flow properties of liquids through vibrations of a beam or diaphragm. For example, a thermally actuated MEMS viscosity sensor integrates actuation and Piezo-resistive sensing in a silicon membrane, which results in a simple and reliable device structure. Furthermore, numerous methods have been identified to design and construct any particular MEMS sensor, making it important to understand

the benefits and drawbacks of each. For example, in some cases it might be better to use an in-line sensor which might give more accurate viscosity measurements but at the cost of system interference. The sensor could also be designed in a CMOS compatible by making it small and easily manufactured at the cost of some ultimate precision.

The device in this work measures viscosity through three different characteristics, the frequency, the amplitude, and the quality factor of the vibrating diaphragm. The main challenge with this approach is that the vibrational characteristics are also affected by thermal stresses due to changes in temperature. The signals produced by these thermal stresses could be larger than the produced by changes in viscosity. Various improvements made to the original thermally actuated MEMS viscosity sensor include process flow changes to incorporate anisotropic etch process, to eliminate bubble formation, and to optimize bias conditions.

As viscosity is dependent on temperature, when the membrane is actuated by heat the effects of locally changing the fluid temperature will affect the sensitivity of the sensor. As such, it is necessary to determine appropriate test bias conditions that do not affect the measurement. Finally, the sensitivity and real-time response of a thermally actuated MEMS viscosity sensor is characterized.

CHAPTER 2

LITERATURE REVIEW

2.1   Viscosity Fundamentals

Viscosity arises from the shear stress during the movement of a particular fluid. The coefficient of viscosity is a guide to the relationship between this stress and the rate of deformation, which is really just another word for the strain rate. Viscosity is broken up into a dynamic component and the kinematic component. Dynamic viscosity is focused primarily on the measurement of the resistance when an external force is applied, which is often measured in Poise [P], which is defined as 0.1 Pascal Second [1]. From a practicality standpoint, this is important for understanding how molecules interact due to mechanical stress, such as pumping systems or similar [2]. On the other hand, kinematic viscosity is a ratio of the dynamic viscosity to the fluid density, which provides much different metrics. This is really a diffusivity rate which is calculated in units of Stokes [St], which is equivalent to one cm^2 per second. Being that this provides a value in terms of movement, it is more popular when the fluid motion is the main concern, which comes into play for flow rates [3]. Figure 2 shows an example of a low viscous liquid compared to a high viscous liquid.
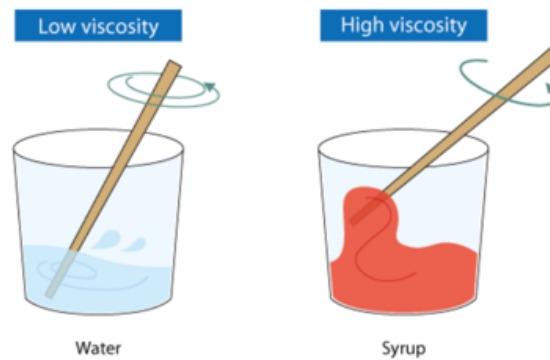
Figure 2: Drawing depicting the resistance one could encounter while stirring a fluid with low viscosity (left) and high viscosity (right) [3]. © 2017 Careerdune Free PCS Study Materials (open access)

Simply understanding what is viscosity is not particularly useful, so it is important to highlight the industries where this is important, as well as why it is important. One of the industries where viscosity plays an important role is the lubricating oil industry, which require a strong understanding of viscosity in almost all aspects. In particular, this is important due to all of the different oil forms, so depending on where in the manufacturing process the oil is, the viscosity might be vastly different. Starting with the raw crude, this is generally a very tar-like material, and will thus have an extremely high coefficient of viscosity. It is important for engineers to understand so that they can ensure that the pumps are strong enough to force it out of the ground as well as to ensure that it can be appropriately pumped into a cleaning facility. Following the initial cleaning, the oil is broken into different forms depending on the eventual destination. So, in this case the vast number of byproducts need to be properly characterized in order to move appropriate volumes as quickly as possible [4]. Due to strong government regulations, all oil-based pumps have strict guidelines on flow rates, which are strongly impacted by the viscosity of the specific liquid [4].

Additionally, other major industries such as the medical industry relies heavily on knowledge of fluid viscosity [5]. One common application is in devices for implants and various biomedical coatings. Often, fluid viscosity comes into play for coating technology as by adjusting specific material properties, coatings can be specifically designed to reach any necessary thickness. In the development of medicines there is often a strong need for extremely uniform coatings, whether that be for ensuring proper lifetime or other. Viscosity can often be used to measure the concentration of coating molecules, which in turn provides a method to verify the uniformity of a coating process [5]. Furthermore, outside of medicine itself, a lot of the medical testing relies on the knowledge of expected viscosities to diagnose illnesses. One such example is through the measurement of blood viscosity, which can be used to diagnose cardiovascular events [6].

Furthermore, the entire field of hemorheology is dedicated to understanding blood flow, where it has been noted that the viscosity of blood can also be used to provide information on the red blood cell count, plasma properties, and the amount of oxygen being carried in blood flow. This field of study is a particularly interesting application of viscosity knowledge because blood acts as a non-Newtonian fluid, which means that the viscosity varies based on the shear-rate. In this application, the viscosity increases when the shear rate goes down, which is characterized by regions of small blood vessel diameter.

Moving on from the importance of viscosity, it is important to know how viscosity can be reliably measured. The methods to measure viscosity can be broken into two main methods, viscometers and rheometers [7]. Capillary viscometers are perhaps the most used methods of measuring the kinematic viscosity due to the practicality and ease of design. This is done by passing fluid through a U-shaped tube as shown in Figure 3 and measuring the movement time, which does require prior knowledge of the fluid density and volume of the sample.
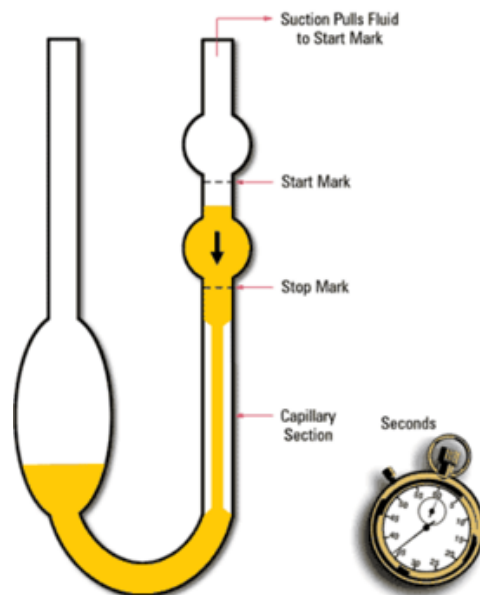
Figure 3: Working principle of a capillary viscometer by timing the fluid flow from start mark to stop mark [7]
© 2002 Noria Corporation.

Vibrational viscometers can also be used to great effect, particularly for fluids with an extremely high viscosity coefficient [8]. This method relies on vibrations at known frequencies, which are followed by monitoring the damping effects of the fluid. On the other hand, a rheometer can also be used to provide better dynamic measurements. Rotational, microfluidic, and non-contact rheology all are a part of this category, which are defined by the use of applying force to encourage deformation in some manner.

One final important discussion in terms of viscosity fundamentals is to understand the effects of temperature on various liquids. In general, it is seen that at higher temperatures, the viscosity of liquid decreases. However, this is seen to be the opposite for gases, where a higher temperature leads to a higher viscosity due to the energy involved. Figure 4 shows the viscosity of some fluids plotted against the temperature.
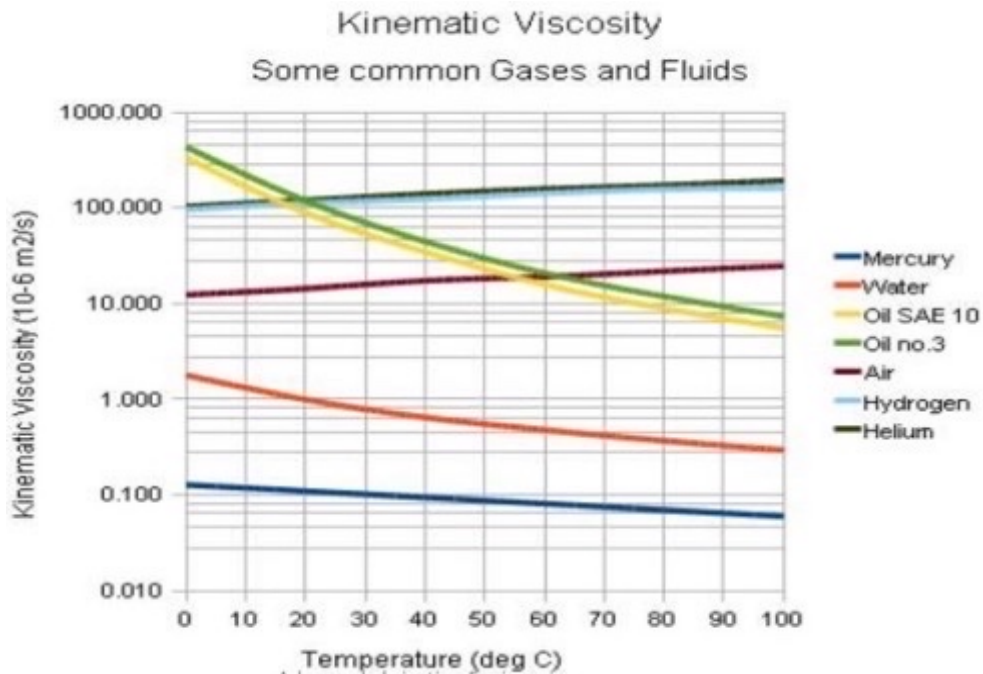
Figure 4: Kinematic viscosity vs temperature relationship using Reynolds equation [9]
© 2003 Engineering ToolBox (open access).

These plots are given using the Reynolds equation 2.1, which suggest that the shear viscosity $\mu(T)$ is related to the temperature in Kelvin (T) in an exponential fashion, where a constant in the exponent (b) provides the characterization for different liquids and gasses [10].

$$\mu(T) = \mu_0{}^{-bT} \tag{2.1}$$

Ultimately, fluid movement is much more complicated than a single constant. The specific usage circumstances need to be understood, as well as the environment that the movement is taking place. In particular, environments where the temperature changes make consistent calculation difficult, leading to the need for more developed models or a more controlled ambient environment. In some cases, such as the medical field this is possible, however in more exposed environments robust fluid control systems are needed to regulate flow [6].

2.2 MEMS Viscosity Sensors

Based on the working principle and viscosity sensing, MEMS viscosity sensors can be classified into different types such as vibrational cantilever structures, ultrasonic transducer, capillary based and piezoelectric resonators. Perhaps the most important sensor to discuss is that of the vibrational cantilever, as shown by their wide use and popularity [10]. Their basic operation is similar to an accelerometer, where a weighted beam is suspended by one end and allowed to vibrate. However, unlike an accelerometer, whose goal is to deflect for a measurement, these designs are focused on vibrating at a specific resonant frequency. In air this will be some value, but where there are fluids with different viscosities, the resonating frequency will be different [10]. Additionally, by looking at the shear stress as well, it becomes possible to characterize both the viscosity and density of any fluid at the same time, which is an important advantage. The basic design of a vibrational cantilever is shown in Figure 5.
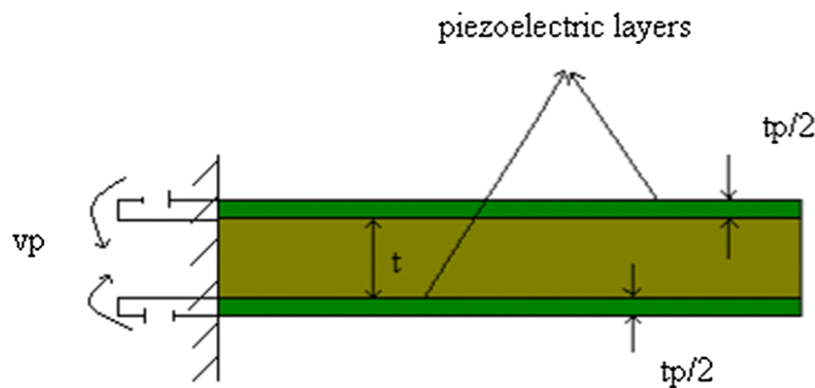
Figure 5: Vibrational Cantilever using piezoelectric layers [10].
© License Number: 4721400431746 Springer Nature.

The sensor allows the measurement of the two different signals, one due to the shear force, which is measured from the sensing element, and another one due to the longitudinal force from the piezoelectric layers. Focusing on the shear force, this impacts the resonant frequency, which can be measured using an optical tool such as a vibrometer. This will then give a ratio of the

viscosity of the fluid compared to the known base. The longitudinal force created by the fluid density then provides a phase shift and can be easily calculated. The top and bottom layers of the beam are made of a piezoelectric material, which often will lead to contamination issues [10].
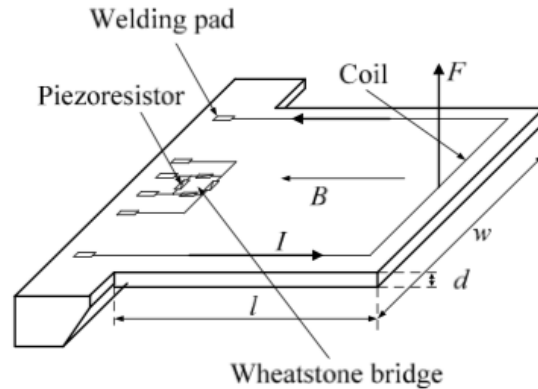
Figure 6: Schematic of a Wheatstone bridge-based cantilever beam [11].
© 2016 license MDPI (open access).

Second method of design is shown in Figure 6. This design uses a Wheatstone bride on the attached end of the cantilever beam to measure the generated deflection stress [11]. A magnetic current is then used to vibrate the cantilever and a resonant curve can be constructed using the voltage differential output. This kind of design requires more secondary processing, but is often much simpler in design, which gives it a distinct advantage.

These designs are not without flaws though. In particular, through the use of thin cantilever beams, there are obvious reliability issues, which are compounded by the fact that the beam material properties may change over long periods of operation. As designs attempt to be more and more accurate, they move to longer beams, which in turn reduce the reliability even more. Additionally, depending on the movement method such as magnetic actuation, this can cause potential interference to the fluid itself, leading to incorrect measurement [11].

Ultrasonic transducers and cantilever beam-based systems are very similar, ultrasonic transducers operate to measure the shear relaxation, which in turn allows for the calculation of shear viscosity of the fluid [12]. In general, these devices operate by sending an acoustic wave of some kind through the fluid to a measurement device which then measures the received strength of the signal, which will provide viscosity information. At higher viscosity coefficients, the wave will be significantly dampened providing valuable system information. One such example of this design is a sensor designed to use capacitive micro-machined ultrasonic transducer (CMUT) [12]. These designs provide significant advantages over others due to things such as the large bandwidth and better axial resolution. Even further, these devices can be fabricated extremely small and do not rely on long etch times, making them ideal for system integration. Figure 7 shows the basic design of one such sensor.
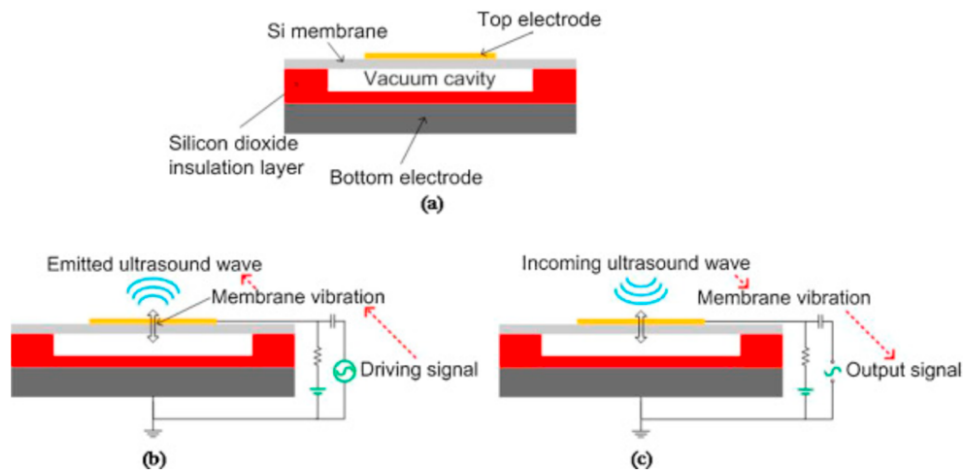
Figure 7: Schematic of basic CMUT in various operational modes [12]
© License Number: 4721481372519 Elsevier.

Under transmission mode, an AC signal with a DC bias is applied between the electrodes, leading to system vibration into whatever fluid it is in contact with. These vibrational waves generally are between 1-10 MHz, and a longer travel distance is ideal to obtain more precise measurement. By allowing the propagating waves to dampen further gives a better average result,

particularly in solutions where the viscosity might be different at the edge of the fluidic channel. In receiving mode, only the DC offset is applied and the effective AC input is read as the incoming wave. Additional designs make use of piezoresistive sensors to more accurately detect the incoming waveforms [13]. In full designs, a total of two CMUT units are used, one to act as the transmitter while the other acts as the received. The received signal is then processed using a Fourier transform to find the frequency differences. The center frequency is the most important, however the change in bandwidth is also important. This style of design is particularly useful because it is extremely small and can often be done in line without impacting the fluidic flow. The one downside to this design is usually only the viscosity is measured and not the density, unlike the cantilever beam design.

Capillary-based viscometers arise due to the need for in situ and in vivo measurements, leading to a desire for laser-based techniques. Unlike the cantilever beam-based designs, these rely on a completely different operating method than building a structure to flow the solution through, allowing for non-invasive measurement. The structure in [14] relies on a microfluidic channel to carry the sample, where an external laser is used to induce capillary waves. These waves can then be captured by measuring the damping oscillation, which is done by an intersection of heated beam intersection to produce an optical fringe pattern. Thus, by measuring the temporal behavior, it becomes possible to measure the viscosity of the liquid. A basic design of this is shown in Figure 8 [14].
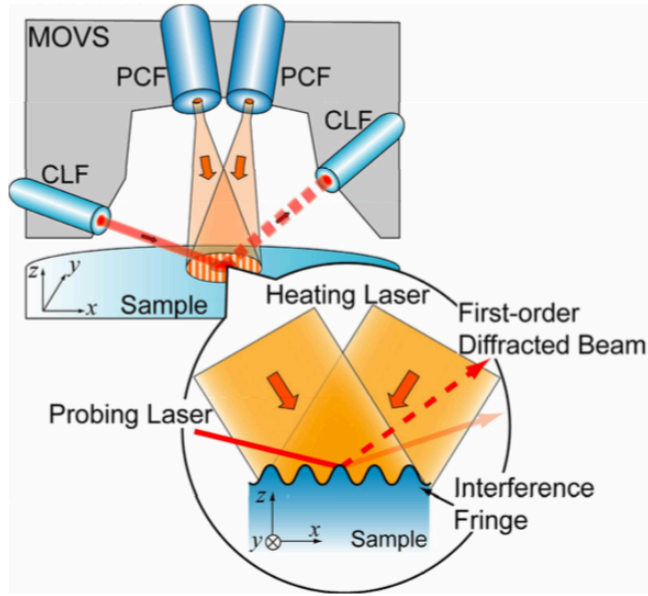
Figure 8: Basic system design of a capillary viscometer [14].
© 2008 Society of Photo-Optical Instrumentation Engineers (SPIE).

A second design which uses a probing head, has also been shown to work effectively to measure the viscosity of fluids over time [15]. Using a hollow capillary tube attached to a single mode fiber, the absorbed fluid can be measured using a two-wave interferometer to find the change in displacement after the probe is removed from the sampling fluid. Figure 9 gives a diagram of the basic design of this system. The device has a hollow silica capillary tube, and a splicing machine so this can be made for an extremely low cost. This does come at a tradeoff of being invasive to the system, unlike other traditional capillary-based designs. [15]
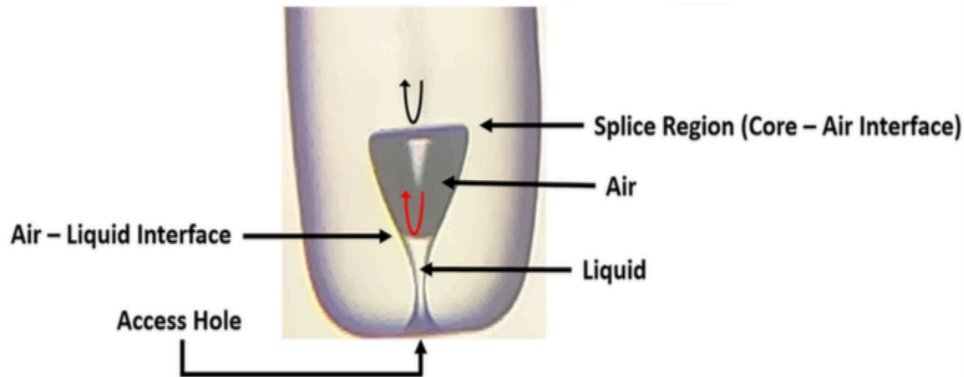
Figure 9: Inlet for hollow capillary-based design [15] © 2019 IEEE.

12

Primarily, these devices have the ability to be extremely high speed, with resolution rates of less than a microsecond, as well as extremely small sample size need of often less than 50 microliters. There are a number of downsides though which include the need for significant external equipment, which makes it not useful for a variety of applications.

Resonator based sensors are another popular type of viscosity sensor, which makes use of a piezoelectric material such as PZT or quartz to resonate at a particular frequency. From this dampening, the viscosity as well as density can be measured on a secondary electrode, similar to the ultrasonic transducer designs [12]. Depending on the fluid confinement, it is possible to separate the density and viscosity by making the resonances a function of the device separation. By constructing resonators using piezoelectric material, an external voltage can be applied leading to acoustic resonance. This driving electrode then impacts the liquid, which then dampens on the way to the sensing resonator, which operates by using the reverse effect, where a resonant change leads to a measured voltage change. Figure 10 shows top-down designs of resonators, showing the fluidic channel between the two resonators [16]. There are some proposed structures which use a single port design as well, but these have been seen to have significant parasitic capacitance, making it better to use a two-port design [16].
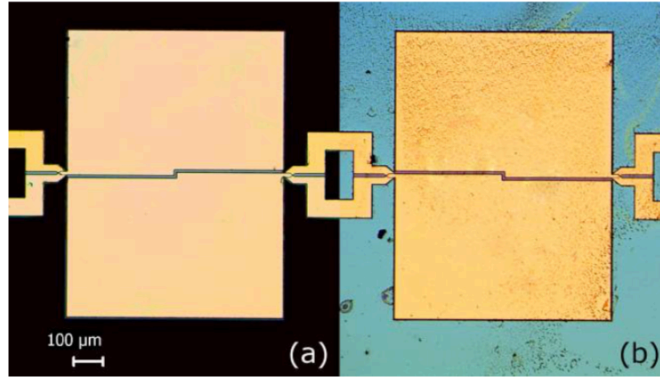
Figure 10: Example two-port designs of piezoelectric resonators [16] © 2014 IEEE.

Resonator viscometers are different than vibrational viscometers. Vibrational sensors work through actuations produced using electromagnetic forces from cantilever beams, while resonator sensors measure viscosity by the use of a piezoelectric resonator, which vibrates due to an ultrasonic frequency from a secondary source. Other designs show that these sensors are particularly well done for low-viscosity fluids, where other sensors tend to fail [17]. Furthermore, absorption modules can be used to limit the parasitic capacitances between the ports, which is important to minimize the required external signal conditioning. In particular, a lot of extra sensing circuitry is often needed, as shown in Figure 11. Due to the extremely small voltage measurements, a lot of amplification is needed to collect a valuable signal, which means that these devices are often unsuited for noisy environments.
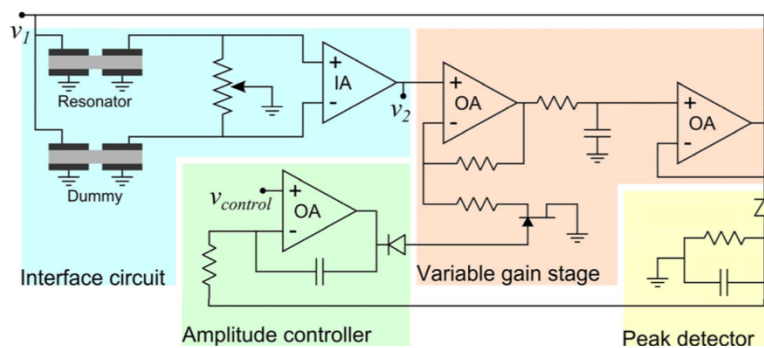
Figure 11: Circuit diagram of a resonator circuit [16] © 2014 IEEE.

14

While these sensors can independently find the density and viscosity of liquids, they are not without significant downsides. These designs were shown to have reasonably accuracy compared to their counterparts, so they might be worth constructing in an environment which needs low-cost MEMS devices. They do require a fair amount of calibration as well and tend to have lower lifetimes but are easily integrated into small-scale circuit designs, but struggle to shrink past a certain size, where the piezoelectric properties are altered [17].

2.3   Measurement Response in Several Viscosity Sensors

MEMS viscosity sensors promise to be more reliable, to consume less power, and to withstand extreme weather conditions. However, another important property that should be examined is the response time of the sensor to change in viscosity. Examples of such sensors include devices used to monitor oil life in auto applications [18], devices used to monitor real time polymerization [19], [20], [22] and devices used for monitoring the lifetime of oils in machinery [21]. These examples are discussed in this section to understand response times of different viscosity sensors.

M K Ghatkesar et al [18] discuss a micro cantilever sensor fabricated and tested for viscosity detection. A cantilever beam on a piezo sensing element is excited from a sinusoidal signal using a function generator which makes the sensor resonate at its natural frequency. A laser beam is setup as a detection mechanism to scan any changes to the amplitude and phase-spectra of vibration of the cantilever. The data is then collected in a custom developed software and processed to obtain the values for Eigen frequency (natural frequency), peak frequency and quality factor. The cantilever's real time response is examined by placing the sensor in a closed tank submerged with the fluid in test and the fluid properties like viscosity and density are changed while

monitoring the frequency and quality factor. Figure 12 shows the response of different liquids that were injected in the following order: water, 5% glycerol, 12 % ethylene glycol, 5% glycerol, 5% ethylene glycol and water where the goal during the first half was to keep density constant (section I – III) and for second half was to keep viscosity constant (section IV to VI).
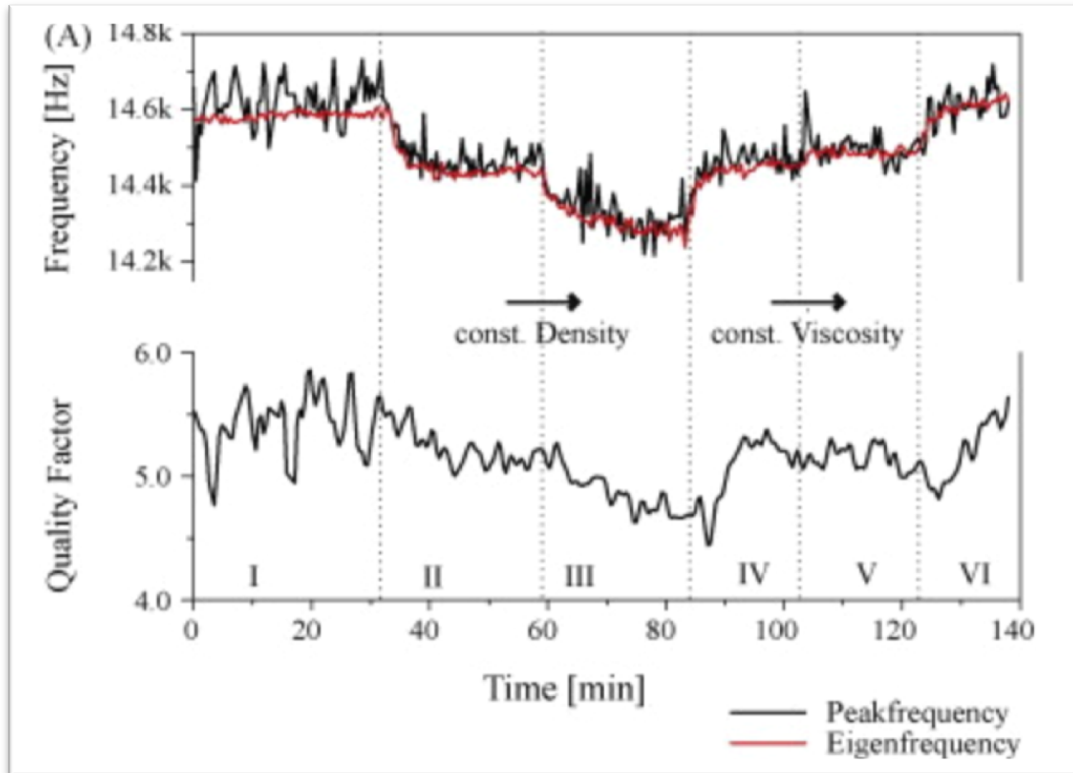
Figure 12: Frequency and quality factor response for different viscosity and density fluids [18]
© License Number: 4721501402136 Elsevier.

In Figure 12, the 5% Glycerol injected in section II and 12% ethylene glycol section III have the same density but varying viscosity whereas 5% glycerol section IV and 5% ethylene glycol section V have the same viscosity but varying density. Based on the density and viscosity values of the fluids, theoretical frequency values were calculated and compared to the shifts observed during experimental testing. It is seen that injecting 5% glycerol after pump out of water shows a downward shift as expected in all three parameters (eigen frequency, peak frequency and

16

quality factor). Additionally, there is an exponential response seen after the injections, with the majority of the signal spiking occurring directly after changing modes. These plots are taken over a large time period, with 30 minutes in between sample changes but it requires significant time (5-10 minutes) to stabilize. The 5% glycerol has higher viscosity than water so the damping force of the fluid reduces the frequency and the quality factor, while a similar decrease in all parameters is seen when 12% ethylene glycol is injected in section III due to the higher viscosity value. Again 5% glycerol is injected in section IV and the eigen frequency, peak frequency and quality factor values are a match to section II values, but in section V when 5% ethylene glycol is injected no change in the quality factor is seen with only a small change in frequency. This is due to the fact that viscosity is the same for 5% glycerol and 5% ethylene glycol where the density is the only difference. The response seen is overdamped, the frequency does not oscillate and takes time to reach a steady state. As we know, viscosity is the change in resistance of the fluid flow this directly affects the number of vibrations (quality factor) and peak frequency whereas the density of fluid only affects the frequency and has no impact on quality factor which is what we observe in section V. The response time of the sensor is within 3-4 minutes but it takes the sensor about 10 minutes for the reading to stabilize to the new fluid. This sensor has a wide variety of uses such as monitoring chemical reactions in oil industry to know the quality of fluid at any instance, or in medical applications such as measuring blood viscosity, which could help in the diagnosis of cardiovascular events [18].

In [19] a group from the Center for Cellular Imaging and Nano Analytics at University of Basel, show response of a vibrating MEMS viscosity sensor to polymerization reactions. A micro cantilever is embedded in fluid cell in order to observe real time response characterization of chemical reactions and/or sudden changes in biopolymers. In Figure 13 the immersed micro

17

cantilever is photothermally excited by a known signal and the intensity of deflection is monitored by a laser pointed at the free end of the beam, converted to a readable data by a position-sensitive detector and collected using LABVIEW. The phase and amplitude are recorded and using damped harmonic oscillator model the values are converted to eigen frequency and quality factor, further using the Hydro-Dynamic model the viscosity and density vs time graphs are plotted.
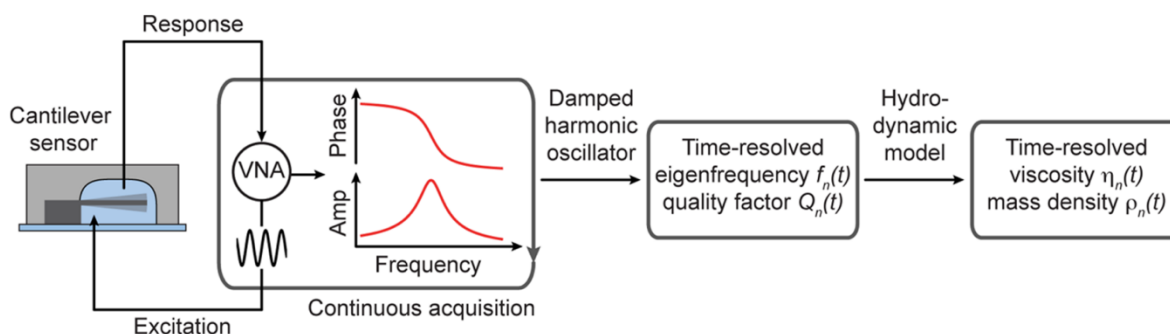
Figure 13: Experimental setup where micro-cantilever is photothermally excited and the intensity of deflection is monitored [19] © 2013 ACS Author Choice.

The sample being tested is injected sequentially into the fluid cell, through PEEK tubes, using a carrier fluid (either water or hydrocarbon oil) at a flow rate in the range of 0.1-50 µL/min. Figure 14 shows the response of radical polymerization to time where in order to monitor the polymerization process, the sample is aspirated into the fluid cell continuously. For measurements, the fuel cell made of polydimethylsiloxane has a cantilever chip inserted, where the cantilever arrays have different lengths. And all the cantilevers are cleaned with piranha solution, washed with water and isopropanol, dried in air, and passivated [19].
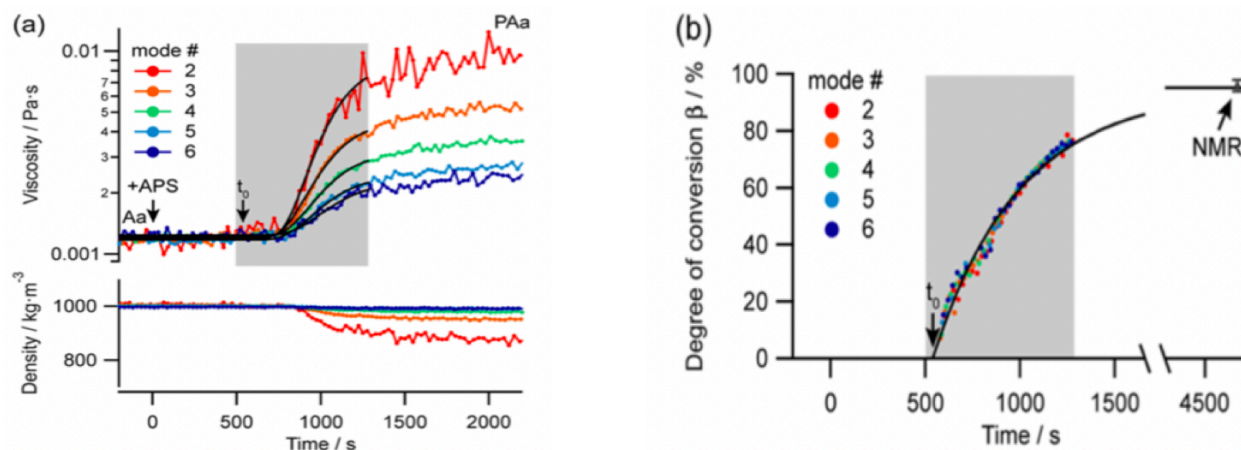
Figure 14: Response of free radical polymerization vs time to monitor the polymerization process [19]
© 2013 ACS Author Choice.

This paper demonstrated that it is possible to use resonating cantilevers to measure changes in fluid viscosity over time. In Figure 14 the shape of response is overdamped and response time reported was 40 seconds, however it is clear that several minutes are needed for the response to begin stabilizing [19]. Some spikes are seen in Response of free radical polymerization in Figure 14 which could be due to the any sudden movements during the addition of new fluid. It is important to note that significant spiking was seen several minutes after the polymerization, which is likely due to the detection of much longer strands, which would throw off the measurements compared to other fluids. Non-Newtonian shear-thinning behavior was observed, which raised questions as to how strictly the theoretical framework could be used. In the future, this design could be used in numerous other applications such as bio-catalysts, micro reactors, and other small-scale reactions. It was mentioned that future work needs to use more complex models which can extrapolate behaviors to extremely small fluid amounts [19].

There is a high need for accurate viscosity sensors in the biomedical industry, particularly in measuring properties of blood plasma. O. Cakmak et. al. developed a MEMS viscometer with a resolution better than 0.01 cP in the range of 0.8-13.1 cP while requiring a sample of less than 50 μl [20]. This range is sufficient to measure blood plasma, which sits at the lower end of the range

19

at 1.1-1.3 cP. The sensor is based on a cantilever design, with a device size of a length of 200 μm, a width of 20 μm, and a thickness of 2.5 μm, where the chips are placed inside of a microfluidic channel to allow flow through the sensor and the frequency response is monitored through phase difference between the coil drive and the photodetector. The devices were tested in varying glycerol solutions to show the resolution as well as the time needed to change. Figure 15 shows the measurements taken from a number of different solutions. For large phase differences, the values seem to converge extremely quickly, however for small differences there is a non-trivial adjustment period, which is surprising.
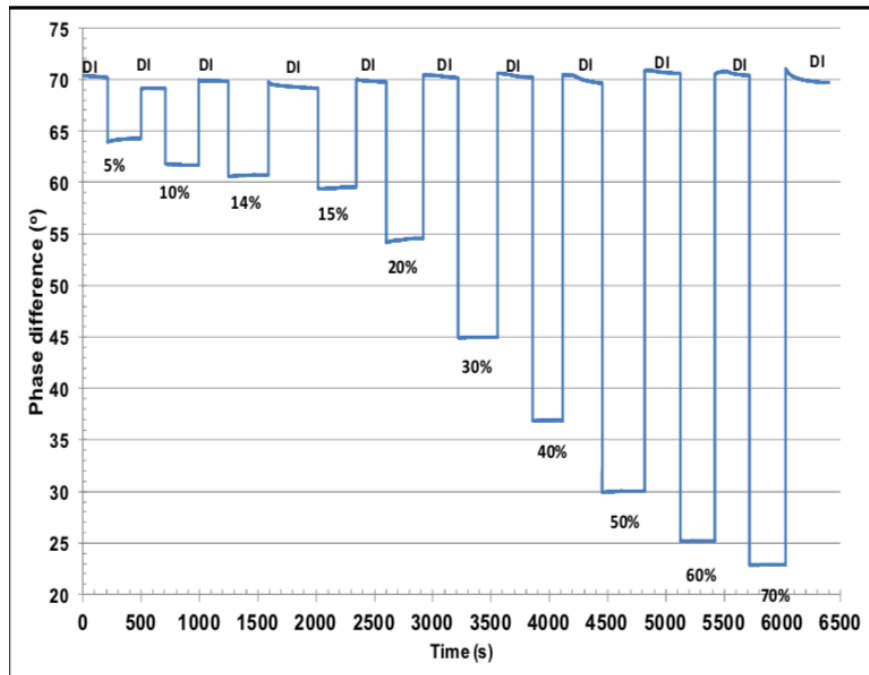
Figure 15: Response monitoring for phase difference with DI water and varying glycerol solutions [20]
© 2013 IEEE.

Following the device verification, testing was done on blood plasma to verify measurement readings. Figure 16 shows the phase change as respect to the viscosity, as well as a polynomial fit over the range that blood plasma would sit. Using these two sets of data, it was seen that the system can distinguish between extremely small viscosity differences consistently and has a response time

20

of 1 minute although sometimes significant time (~ 4-5 minutes) are needed to allow proper stabilization. In general, it appears that solutions with a significant phase difference were waster to stabilize than those with only a slight difference. Additionally, the data is mostly relationally indicative, which means that the values do not always agree, but will always agree compared to the other samples in that same fluid [20].
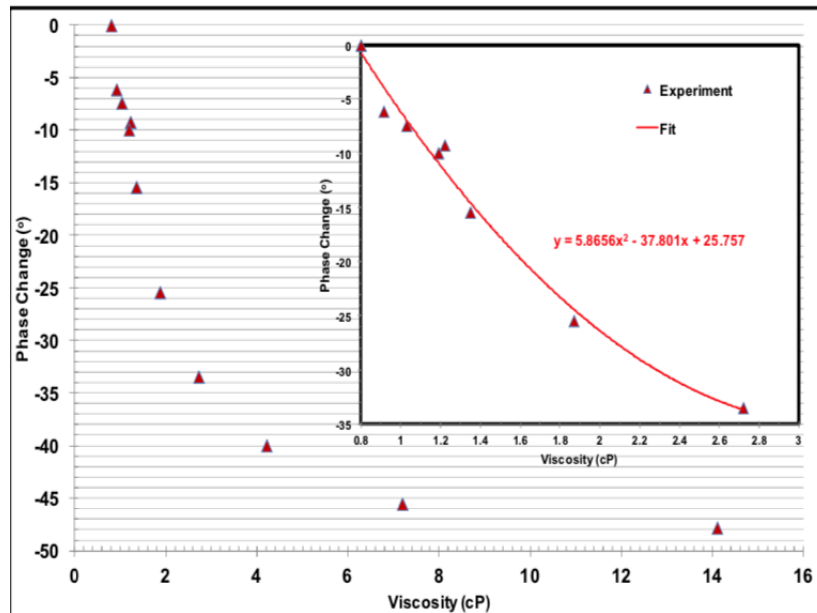
Figure 16: Phase Change vs. Viscosity [20] © 2013 IEEE.

There were issues in measuring unhealthy sample readings, so no proper conclusions were made. While there are advantages to the addition of wireless connections due to the coiling, there is a lot to be desired from this device. In particular, future work should be focused around understanding the changes in viscosity, as well as developing a better model to verify their design against. As seen in other works, numerous biological fluids have significant non-Newtonian aspects, which will impact the values read. The data collected in this was too sparse, which makes meaningful conclusions about the spiking in response meaningless.

Understanding the variation in measurement techniques is important in characterizing real-time systems. M. McAfee and G. McNally focused their work on the issues of process dynamics in single-screw extrusion through the comparison of side-stream rheometers (on-line) and in-line rheometers [21]. Side-stream rheometers measure viscosity by removing a small amount of oil through a side stream and using capillary tube device to measure pressure drop due to the oil, whereas in-line rheometer samples the complete stream. It is important to measure as close to the actual process as possible to provide accurate test readings, which would suggest the use of in-line methods, while at the same time it is important to take measurements without impacting the actual device flow, suggesting the use of side-stream measurement methods [21]. Figure 17 shows a comparison between the two methods, demonstrating how side-stream rheometer measurements were much lower than what the in-line pressure measurements found [21].
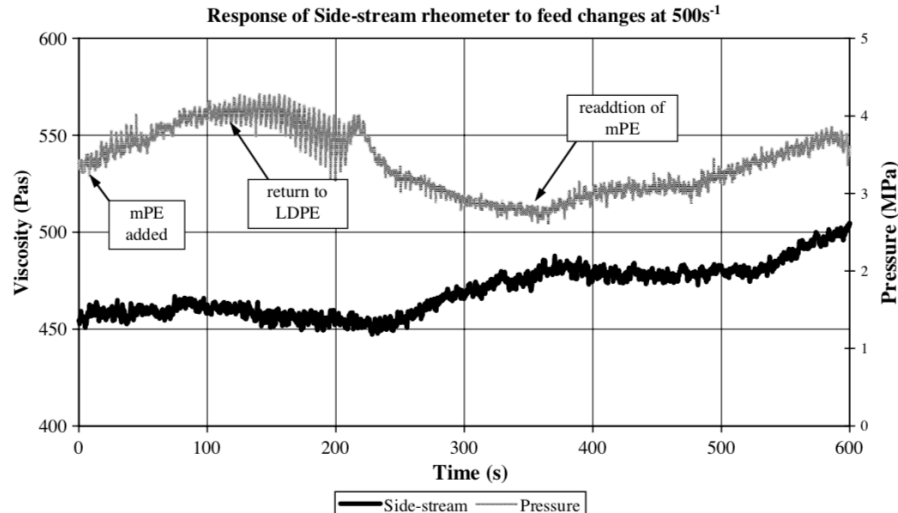
Figure 17: Response of rheometers to feed material changes [21]
© 2006, Document 274943534 Sage.

Additionally, it is easily seen that the side stream method has an extremely slow response time, leading to the loss of fine signal fidelity. In Figure 17, the material change was seen by the in-line measurement but no change was seen at all from the side-stream measurements. A higher

viscosity addition was detected towards the end, but in cases where the change is from higher viscosity to lower viscosity, the less viscous material tends to move through rather than flush all of the preceding material in the measurement lines. One of the issues with in-line rheometry is that a lot of the design needs to be constant to observe consistent readings. Figure 18 shows how cases where the rheometer is further from the entrance capillary, which will lead to lower shear stress measurements and thus incorrect viscosity measurements [21].
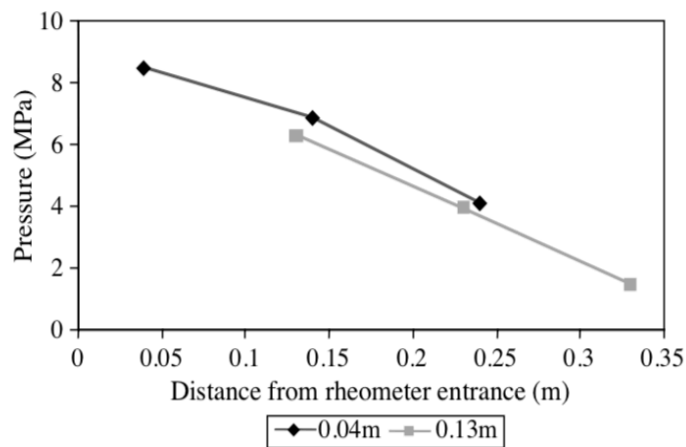
Figure 18: In-line rheometric Pressure Comparison [21] © 2006, Document 274943534 Sage.

The work by N. Ahmed et. al. focused on the use of atomic force microscopes (AFM) to measure the viscosity of liquids through measurement of the resonant frequency. While AFMs originally focused on imaging, they are able to measure intermolecular forces, which allows for the measurement of fluid property changes [22]. N. Ahmed et. al. expanded on this work by investigating the ability for AFMs to measure biochemical reactions through the measurement of viscosity over time. Similar to other works, being able to measure the viscosity change is simply an intermediate towards understanding the chemical reaction as a whole. The operation at a high level is similar to other cantilever-based designs, where in this case the measurements were taking using a single of the "V" cantilevers on the AFM tip. A photodiode was then used to collect a laser beam signal to measure the thermal oscillations.

The sample sizes needed were on the order of 50 µl. Furthermore, the temporal resolution was found to be much larger than ideal and ultimately not great for small time changes. Initially, the resonant frequency of the cantilever was measured in various fluids to demonstrate the static uses, as shown in Figure 19, where (a) is air, (b) is water, and (c) is a 60% glycerol solution by molar mass [22].
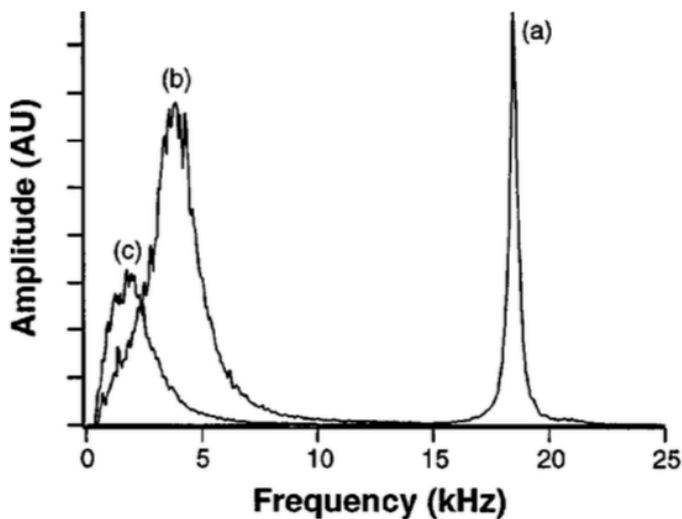
Figure 19: Cantilever frequency response [22] © 2001 AIP Publishing LLC.

It was then determined that the resonant frequency is ultimately dependent on the product of the density and viscosity of the fluid medium, which can be used to measure physical state changes. By measuring the resonant frequency with a known density, the viscosity can then be determined for a changing system, which is this case was verified through the hydrolysis of herring sperm DNA. The solution was allowed to stabilize and then DNase I was mixed into the solution, triggering the hydrolysis process, leading to a frequency shift from 2.9 to 3.5 kHz, as shown by Figure 20 [22].
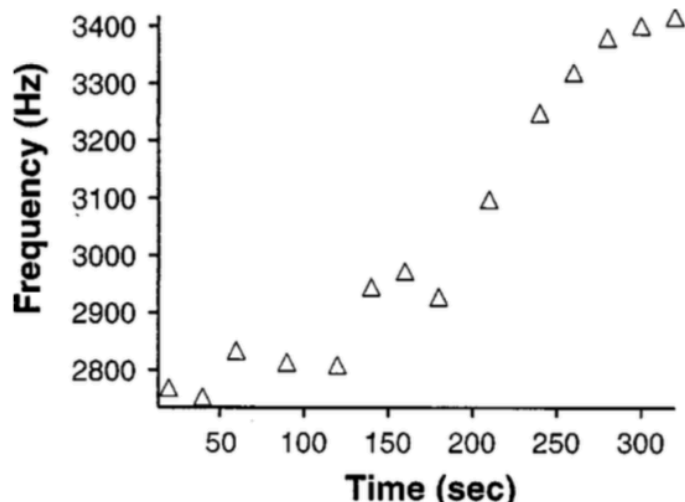
Figure 20: Kinetics of DNA hydrolysis [22] © 2001 AIP Publishing LLC.

"The oscillations of the cantilever are damped as a result of the added drag on the cantilever. The resulting increase in effective mass shifts the resonant frequency to a lower value" [22]. While this work was only demonstrated on simple fluids as well as DNA hydrolysis, there are vast applications of this tool on other bodily fluids such as plasma, whole blood, and potentially other organic molecules. This set an important precedent that time-variant measurements can be taken on existing sensors, and that there might not be a need for specialized tools under most circumstances [22].

All the different works presented above show that real-time viscosity sensing has been approached from a number of different ways, including the conversion of separate tools such as an AFMs as well as numerous specialized MEMS devices. To measure time-varying systems, static measurements are taken to verify basic operation followed by a chemical reaction or material change measurement. Numerous methods for collecting data were identified and the differences between in-line and side-stream measurements were highlighted. By measuring these changes, it becomes possible to track how far a reaction runs as well as any changes in material flow, which has applications primarily in the biomedical industry as well as nearly any product involving liquid

flow. As a whole, these devices have paved the way for more advanced real-time sensing to provide a tighter feedback loop for better system precision. Other than the case for the polymerization, the responses between the various systems behaved in a similar manner. When the medium was changed, there was an initial response time of a few minutes before stability was achieved. Most methods produced an initial response on the order of a few seconds, however significant spiking due to fluid mixing meant that these results were unreliable for immediate responses. It is also noted that the response time varied greatly with the phase difference seen. In most cases a larger phase difference actually led to a faster stabilization than that of the smaller phase difference.

CHAPTER 3

THERMALLY ACTUATED MEMS VISCOSITY SENSOR

The device used in this thesis is fabricated at RIT and is based on thermally induced vibrations of a silicon diaphragm and its damping due to the surrounding fluid. The device is shown in Figure 21 and utilizes thermal actuation through an in situ resistive heater and piezo resistive sensing, both of which are CMOS compatible. An in-situ piezo resistor bridge is used to monitor membrane deflection. Factors involved in measuring viscosity are material composition of the membrane, size of the actuation heater, natural frequency of vibration, effects of temperature, viscosity of oil. Viscosity of the fluid dampens and changes the natural frequency of vibration.
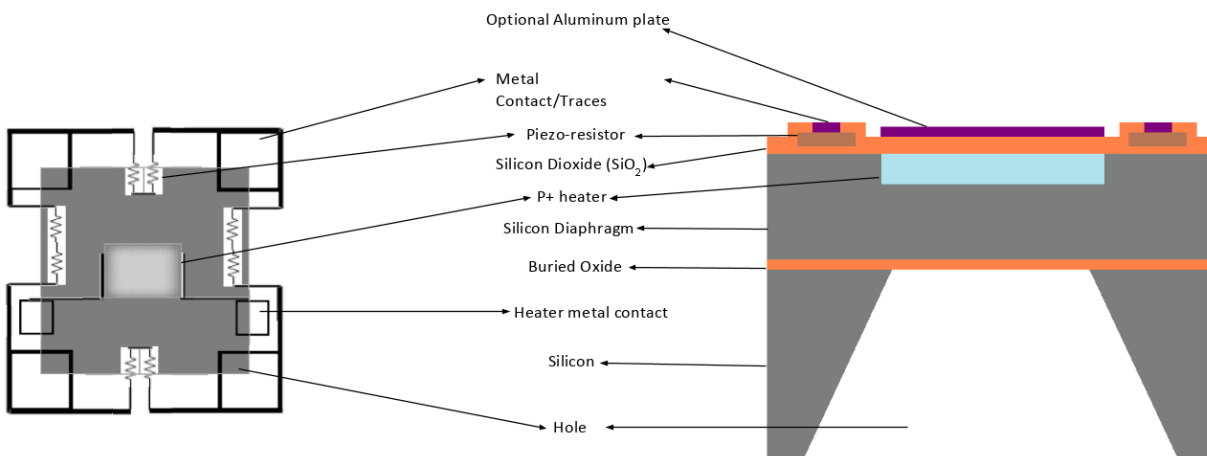
Figure 21: Top - view (left) and cross - sectional view (right) of the viscosity sensor.

The MEMS viscosity sensor works on the heat principle, so it is important to continuously monitor temperature of diaphragm actuation. The sensor is actuated by a thermal pulse which activates the diaphragm making the diaphragm resonate at its natural frequency.

27

3.1   Device Fabrication

The sensor/actuator fabrication researched and done under Ivan Puchades Ph.D. thesis [23] used a bulk MEMS process on SOI wafers with a 15 μm top layer and a 1 μm buried oxide. A blocking oxide layer was grown to mask a P+ spin-on-dopant process to act as the membrane heating element. A stress-relief oxide was then grown to allow a silicon nitride LPCVD deposition on the backside of the wafers. These layers were then patterned and etched using SF_6 and buffered oxide etch. This was then followed by an LPCVD polysilicon layer on both sides of the wafers, where the front-side poly was phosphorus doped to create the Wheatstone sensor bridge.

A 1 μm low temperature oxide was then deposited, patterned and etched to form the poly and P+ contact openings. A 1μm layer of aluminum was then deposited and patterned to form both the electrical connections as well as to act as the bimetallic layer. A secondary passivation layer of 1 μm was deposited on the diaphragm front to further isolate the sensor, and the top was then protected using PROTEK[TM]. The diaphragms were then formed from a back-side KOH etch, using the buried oxide layer as the etch-stop. The final device from this fabrication process is shown in Figure 22.
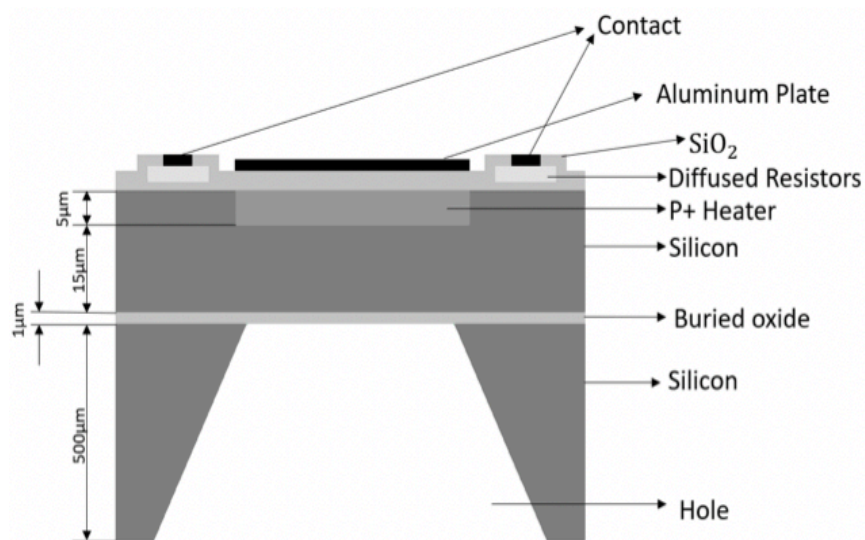
Figure 22: Cross-section view of thermally actuated MEMS viscosity sensor.

3.2 Sensor Packaging and Integration of Conditioning Electronics

Packaging plays a crucial role in testing of the viscosity sensor as the sensor relies on diaphragm movement and no type of external stress should interference in membrane movement causing damping of the vibrations. Specific packaging procedure was followed for minimization of any stress that could be applied onto the sensor. The sensor is wire bonded and glued using epoxy onto a PCB board with an access hole drilled in the back to facilitate these vibrations, any interference in the vibrations can cause changes in frequency readings. The access hole allows the membrane to be in contact with the liquid under test on both the sides as the liquid causes dampening of the natural frequency of vibration. PCB board is designed with 6 solder pins connected with copper line connections reaching towards the drilled hole. PCB board is cleaned with sand paper and wool made of iron to remove aged/oxidized copper and any other impurities present on the top layer. The sensor is glued on to the PCB by applying epoxy on the back of the die as shown in the Figure 23.
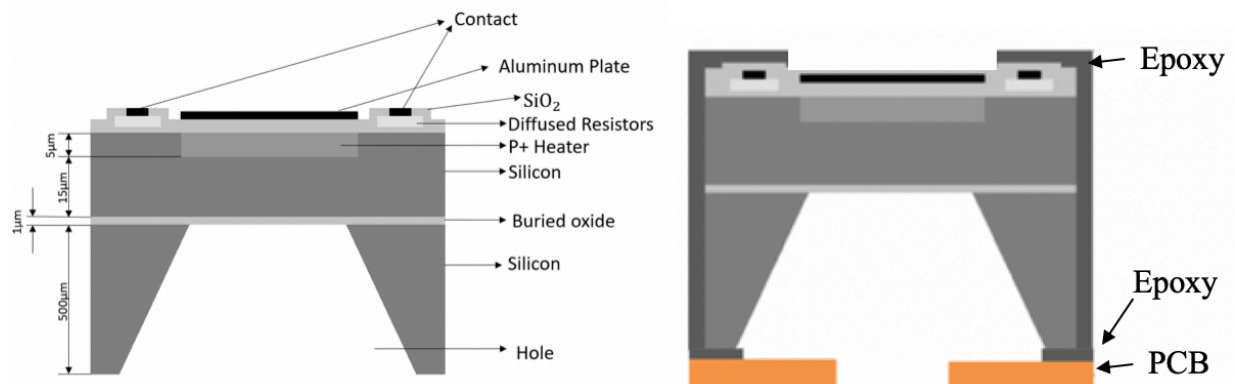
Figure 23: Cross-section view of the sensor before (left) and after (right) packaging.

After the sensor is glued, it is placed in a convection oven for 5-7 minutes at 50°C for the epoxy to change its state from liquid to solid. Now that the sensor is attached to the board, wire

bonding step comes into place, which allows electrical connections to be made between the die and the PCB with an aluminum wire of diameter ~ 25 µm ultrasonically bonded. The connections are made accurately and precautious, epoxy is applied after the bonding on the sensor to prevent wire breakage, loose connections and short circuiting. It is important to note that no epoxy is applied over diaphragm as the sensor highly depends on membrane displacement and fluid interaction. To apply epoxy on the top of the sensor, a paper clip is used for precision where epoxy is applied to the surrounding of the sensor and moved towards the die using clip, covering the borders and the contact pads. Epoxy is hard baked again for 5-10 minutes at 50°C. The sensor is placed flat in the oven to prevent epoxy flow onto the diaphragm. During test external stress could be added if the PCB rested on the bottom or against the sides of the container. It is important that the devices always be position the same way as shown in Figure 24 to not affect the natural vibration behavior.
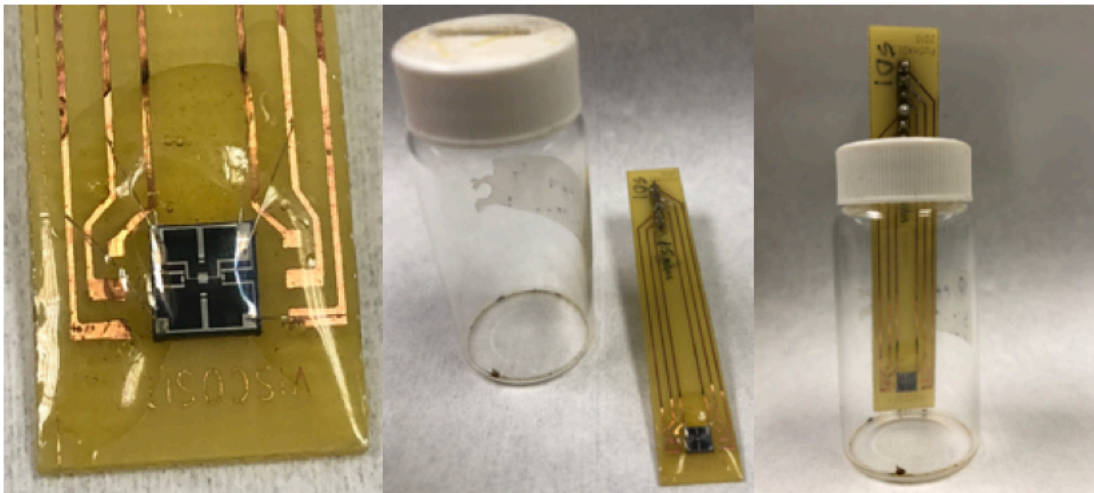
Figure 24: Packaged sensor and test setup to minimize the external stress.

This specific test setup was followed, the sensor was placed in the center of the far filled with oil under test to minimize the external stress which can be caused by the walls of the jar.

The sensor was immersed slowly in oil to avoid the formation of a bubble that could cause error in readings. The packaging should also be free from residual stresses as it could cause output signal shift.

MEMS devices have wide variety of applications due to properties like low power consumption, small size, bulk manufactured and fast response time. If the devices are designed and packaged correctly they can withstand extreme weather conditions and pressure. For instance, application of a sensor in automotive industry would require long term reliability and involve packaging issues like working with constant quivering and extreme temperatures involving snow and humid climate. Packaging of MEMS is a challenge due the involvement of movements such as vibrations, rotations, sliding or a combination of these causing devices to be very fragile hence the need of proper packaging. Biggest concern during packaging is the cost as Tai-Ran mentions in his MEMS packaging book "The packaging cost of microsystems may vary from a moderate 20% for simple plastic encapsulated pressure sensors to a staggering 95% of the total production cost for special pressure sensors that are expected to sustain extremely harsh environments at high pressure with steep rates of temperature rise" [24].

While MEMS devices can be simulated to provide basic characteristics, a large number of secondary factors will impact overall operation such as the final chip packaging. In particular, devices which rely on stress to measure a force such as accelerometers, vibrational sensors and gyroscopes suffer in performance due to the addition of external stress from chip packaging [25]. Numerous papers investigate this by identifying adhesive characteristics such as thickness and other material properties to minimize injected stress. A basic understanding of the packaging process is important to identify the source of the device stress. At a high level, the process can be

broken down into a die attach stage, a sealing stage, a reflow stage, and multiple thermal cycles at the end, where each stage is characterized by a temperature heating cycle. The majority of the injected die stress, shown in the Figure 25 is due to the curing portion of adhesives in the die attach portion of the packaging process, which is then in turn made worse from later thermal cycles [26].
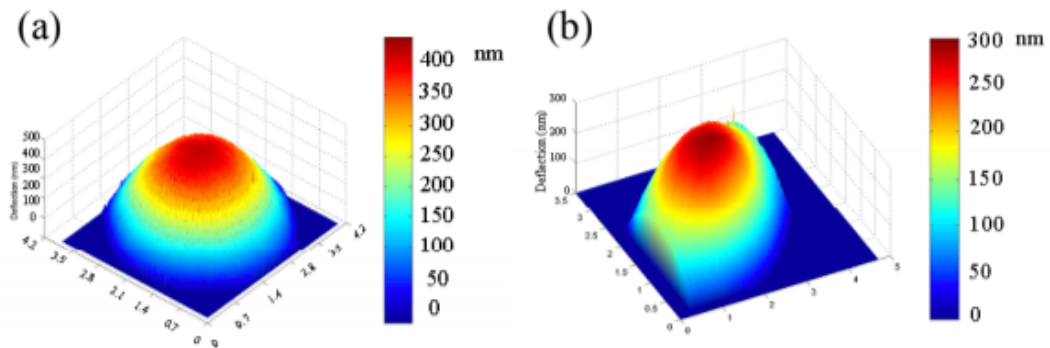
Figure 25: 3-D surface profile of the silicon die showing (a) uniform deflection (b) non-uniform deflection for the side braze package assembled with the silver glass and the polyimide adhesive [26] © 2006 IEEE.

This change in deflection is due to stress evolution, which is partially from the fact that a number of materials are used which have different coefficients of thermal expansion, and thus generate stress at elevated temperatures. Unfortunately, it is often difficult to directly measure the stress, so the out of plane warpage of the die is often measured using an optical profilometer to identify stress without destroying the packaging. In general, it appears likely that the use of packaging materials with similar thermal properties generates less devices stress [26].

One of the primary methods of minimizing die stress is by changing the thickness of the adhesive itself, which can help alleviate the stress between the die and substrate. In general, it is seen that the stress decreases for an increase in adhesive thickness of materials such as silver glass, however it does not appear to make much of a difference in polyimide and silicone adhesives [27].

32

This raises questions about what other properties adhesives may have such as shrinkage. Additionally, it is suggested that after a certain adhesive thickness, the induced stress is no longer due to the substrate, but instead on the bulk properties of the adhesive material itself. In reality, it appears that there is not a way to entirely prevent stress from impacting MEMS performance, so it is necessary to characterize the expected stress and compensate for it through simulation and process modification [27].

3.3 Test Setup

As previously mentioned the device works on thermally induced vibrations of a silicon diaphragm. The membrane is actuated via a short pulse of heat delivered by the heater resistor R_H provided by an external voltage, as shown in the Figure 26. The pulse width is controlled by a waveform generator and a power MOSFET. The MEMS actuator works on the heat principle therefore it is important to continuously monitor temperature of diaphragm actuation, which acts as a vibrating viscometer when actuated by a thermal pulse. The movement of the membrane is measured with the in-situ piezoresistor arranged in a Wheatstone Bridge configuration, which is powered by an external voltage source, and amplified with and instrumentational amplifier before the resulting vibrating signal is analyzed in LabView. Diffused polysilicon heater activates the diaphragm when required voltage is applied resonating the diaphragm at natural frequency, and through Joule Heating $[Q \propto I^2R]$, the applied current across the resistor is dissipated as heat or power where 'R' is the resistance of the heater. Thermal pulse used to actuate is generated by waveform generator (Agilent 33220A) and voltage supply to the heater goes into the MOSFET. An N-channel power MOSFET is used due to its low on-resistance characteristics and functions as a switch completing the circuit between voltage source and heater as constant voltage could burn the resistor heater.
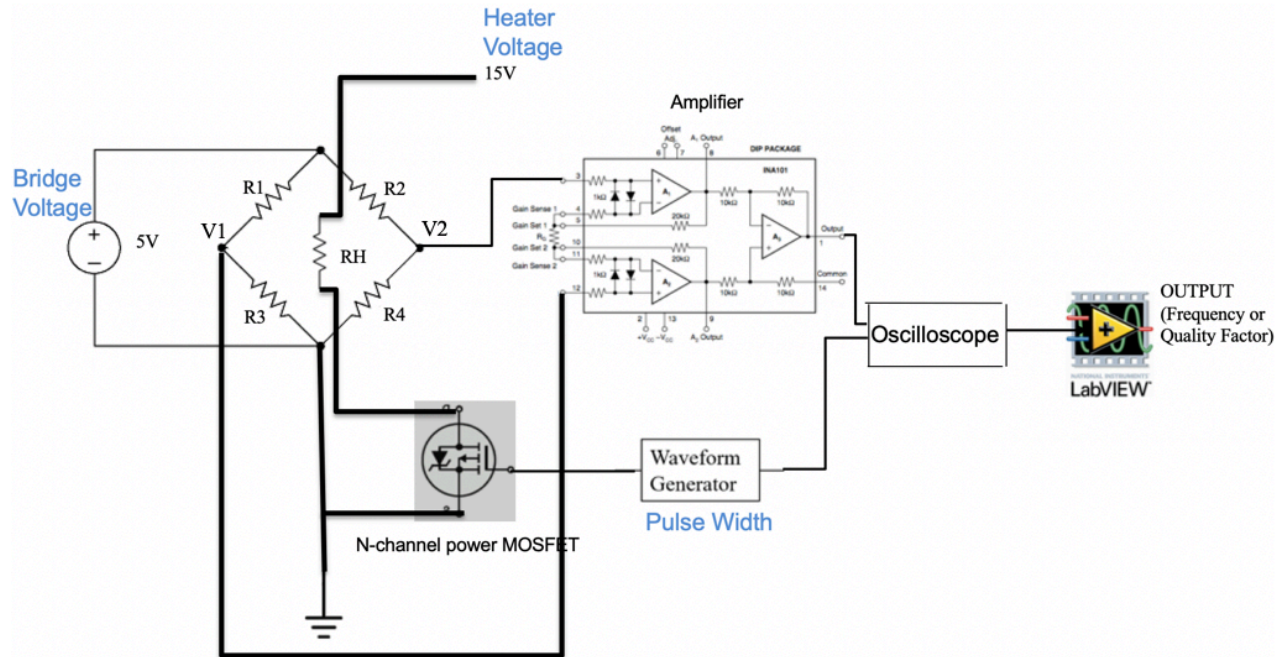
Figure 26: Testing overview for viscosity detection.

The circuit in the sensor is arranged in a Wheatstone Bridge configuration to measure small changes in resistance. Two series-parallel placed resistors connected between voltage source terminal and ground, voltage difference is obtained from the circuit using probes at V_1 and V_2 to find stress on resistors while the diaphragm vibrates. During testing, all the resistors must be functional and the bridge must be balanced with no open circuits. Amplifier INA101HP is used to amplify the signal from the Wheatstone Bridge with a low-level amplification and has three op amps for high accuracy. The amplifier has a resistor R_G which is connected to a potentiometer to increase/decrease gain output and $\pm$ 12 V input is needed to power up the amplifier. The inputs of amplifier are connected to V1 and V2, the nodes between resistors giving the voltage difference which is small hence the need of amplifier. Output of amplifier is sent to LabView to obtain the frequency and quality factor data.

The device measures viscosity through three different characteristics of the vibrating silicon diagram; the resonant frequency, its amplitude and the quality factor. The heat pulse through the waveform generator sets the diaphragm into motion where the diaphragm vibrates at its natural frequency in air. The natural frequency also known as the preferred frequency often measured in cycle per second depends on the shape and the elasticity of the material vibrating. Frequency in air of a square thin plate can be calculated using the equation (3.1) where a is the length of the plate, E is the Young's Modulus of silicon (190 GPa), ρ is the density (2330 kg/m³), h is the thickness of plate and λ is the Poisson's ratio (0.3) [28].

$$Frequency_{air} = \frac{19.74}{2\pi a^2}\left[\frac{Eh^3}{12\rho h(1-\lambda^2)}\right]^{\frac{1}{2}} \tag{3.1}$$
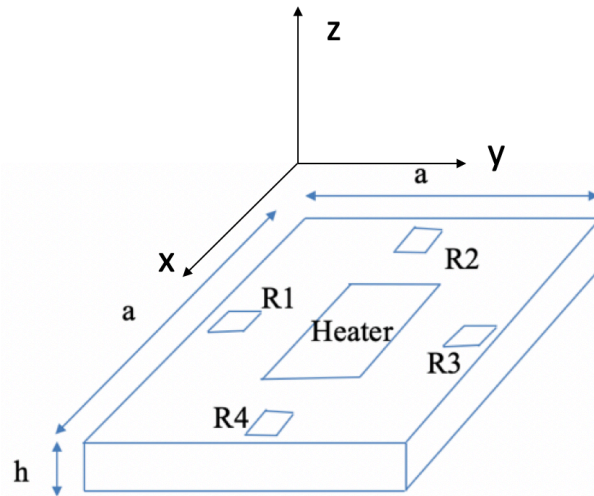
Figure 27: Thermally actuated MEMS viscosity sensor 3D layout.

The frequency of vibration in air calculated for dimensions 2.5 mm x 2.5 mm and height 15 μm was 20,500 Hz. It is important to note that Young's Modulus of silicon is a constant value under ideal conditions however change in temperature could cause change in this value by

deformation of atoms in silicon permanently. Quality factor is the energy loss rate which is the ratio of the energy stored to the energy dissipated per cycle. Easiest way to measure Q factor is the number of vibrations before the amplitude of vibration becomes negligible It is important to understand the need of quality factor (Q) and energy dissipation (ξ) as the sensor is surrounded by fluid that dampens the frequency and reduces the Q factor of oscillation [29,30]. Q factor and ξ can be given by the equations (3.2) and (3.3).

$$Q = \frac{energy_{stored}}{energy_{\,dissipated_{per_{cycle}}}} \approx \frac{0.95}{ξ} \tag{3.2}$$

$$ξ = \sqrt{\frac{v}{wa^2}} \tag{3.3}$$

In equation 3.3, v represents the kinematic viscosity, w is the radial frequency of vibration, and a is the radius of the membrane. Viscous effects can be neglected if v is really small, only become important for large viscosity values. Using the above equations frequency shift due to density of fluid can be calculated by a simple addition of a virtual added mass $β$ shown in equation 3.4 [29,30].

$$Frequency_{fluid} = \frac{Frequency_{air}}{\sqrt{1 + β}} \tag{3.4}$$

$$β = 0.669 \frac{ρ_{fluid}a}{ρ_{plate}h} \tag{3.5}$$

$$β = 0.6538 \frac{ρ_{fluid}a}{ρ_{plate}h} (1 + 1.082\,ξ) \tag{3.6}$$

Equation 3.4 is based on the operation principle of plate vibration in fluid. Frequency in fluid, and the frequency in air both depend upon the density of the fluid (ρ_{fluid}), the density of the material (ρ_{late}), the radius a, and thickness h of the plate. Using theses equations frequency in air and fluid can be calculated, important to note that if kinematic viscosity 'v' is really small in value then the frequency in fluid would be equal to frequency in air.

Figure 28 shows real time viscosity measurements in time domain where the sensor is tested in standard and commercial motor oils (S3) used at room temperature, which has kinematic viscosity value of 4.035 cSt and was obtained from Koehler Instrument Company, Inc. A typical membrane vibration is seen when excited with a pulse of heat as expected by the device working theory [23].
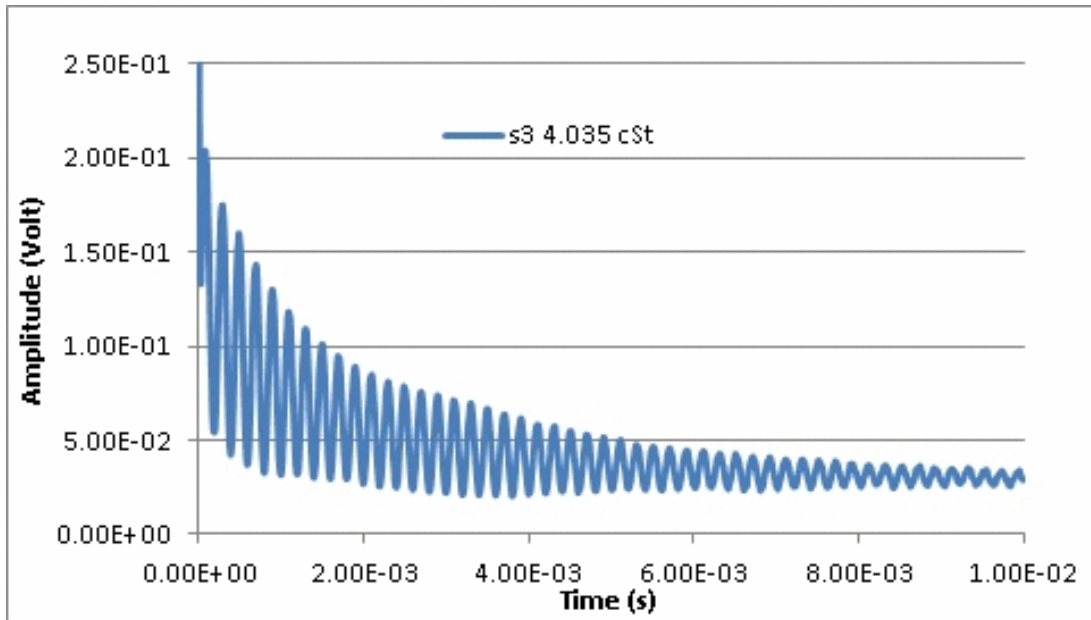
Figure 28 Real time viscosity measurements in time domain of device 4D10 in S3.

Figure 29 shows the real time viscosity measurements in frequency domain by performing a Fast Fourier Transform of the signal. The data collection was automated through LabView to extract the frequency of vibration, quality factor and the amplitude of the oscillation.
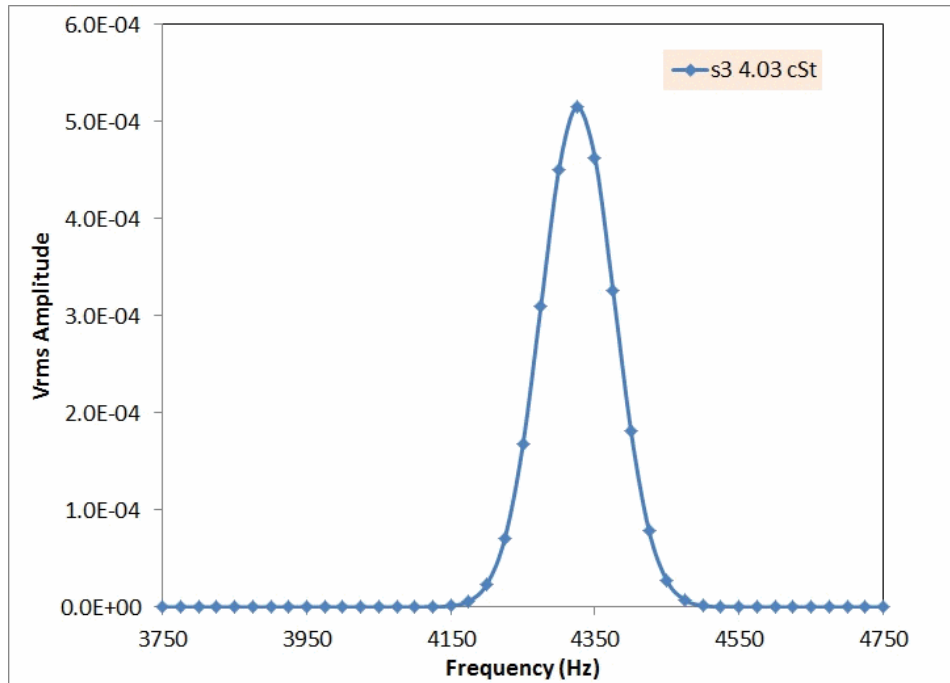
Figure 29: Real time viscosity measurements frequency domain of device 4D10 in S3.

CHAPTER 4

IMPROVEMENTS OF THERMALLY ACTUATED MEMS VISCOSITY SENSOR

Some MEMS viscosity sensors measure flow properties of liquids through vibrations of a beam or diaphragm. The proposed thermally actuated MEMS viscosity sensor monolithically integrates actuation and piezoresistive sensing in a silicon membrane, which results in a simple and reliable device structure. The device measures viscosity through three different characteristics, the frequency, amplitude and the quality factor of the vibrating diaphragm. Improvements were made in the process flow and test setup to incorporate an anisotropic etch process, eliminate bubble formation during test and optimize test bias condition. As such, it is necessary to determine appropriate test bias conditions that do not affect the measurement. As viscosity is dependent on temperature, when the membrane is actuated by heat, the effects of locally changing the fluid temperature will affect the sensitivity of the sensor.

Process flow improvements were needed to adapt Deep Reactive Ion Etching to achieve an anisotropic process with deep, high-aspect ratio trenches. DRIE is highly beneficial to the viscosity sensor fabrication process as alternate route would be to etch wafers using KOH solution for a long period of time which could damage the devices.

Viscosity measurements were performed and compared on different grades of motor oil at room temperature. Error during testing can be caused in viscosity measurement if the diaphragm of the sensor is damaged, sensor not aligned correctly causing the diaphragm to not move freely resulting in external stress, sensor not cleaned after each oil testing giving the wrong measurement

and bubble formation on the backside of the diaphragm when submerged in liquid. To achieve proper functioning of the device and learn on these errors and their effects we focused the testing on the bubble formation in 10W40 grade oil and compared to frequency with all same conditions but without bubble in the same oil.

The main challenge with actuation approach is that the vibration characteristics are also affected by thermal stresses and test bias conditions (bridge voltage, heater voltage and pulse width) due to changes in temperature. The signal produced by these test bias conditions could, at times, be larger than the produced by changes in viscosity. Test bias conditions were optimized to drive further improvements to the viscosity sensor.

4.1   Adaptation of Deep Reactive Ion Etching in Process Flow

A new fabrication flow was adopted post metal etch step to include DRIE process discussed. Additionally, a new front masking method was used to further protect the membranes from damaging as shown in Figure 30. A layer of photoresist was deposited on the front of the carrier wafer and device wafer, placed front to front and aligned to major flat on top of carrier wafer. A hard-bake was then done to effectively bond the two wafers together for the etching step, which provides additional protection. It is very important to note that the carrier wafer must not have any topology and is clean, otherwise it will not attach well. This is particularly important to prevent front-side etching during long BOE etch.
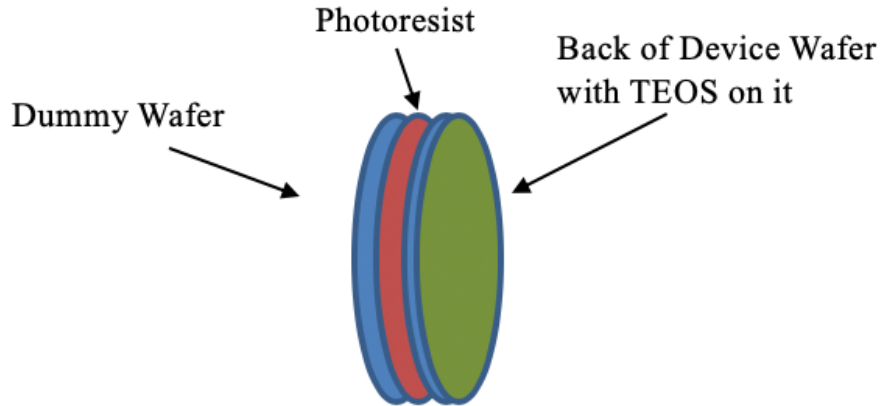
Figure 30: Masking of device wafers using a dummy wafer and photoresist as adhesive.

Following the long BOE etch to remove patterned oxide from the back, 500 μm of silicon is etched using the deep reactive ion etcher. This was followed by wafer saw process to saw whole device wafer and 200 μm into carrier wafer ~ 700 μm such that devices are still attached to carrier wafer. The individual devices are later separated from the carrier wafer in water or solvent that dissolves PR to release the chips. The new flow helped to achieve anisotropic etch on the backside and create more precise designs.

Deep Reactive Ion Etching (DRIE) is an anisotropic process aimed at creating deep, high-aspect ratio and steep-sided holes and trenches in wafers/substrates. This results in an accurate transfer of the mask pattern, free of any damage due to undercutting. In MEMS, DRIE is used to create trenches of depth ranging from a few micrometers to 0.5 mm. Practical etch depths for RIE (as used in IC manufacturing) are usually limited to around 10 μm at a rate of 1 μm/min. What makes DRIE so useful is its ability to etch features greater than, up to 600 μm or more with rates of at least 20 μm/min.
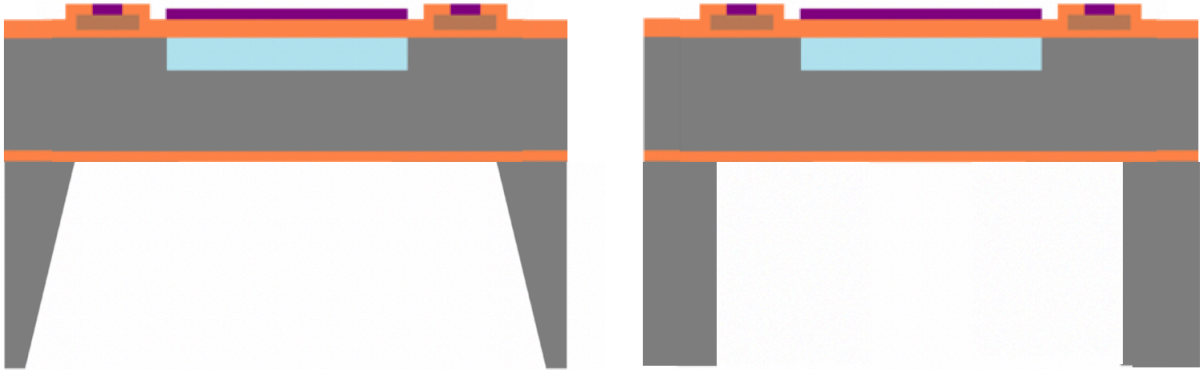
Figure 31: Cross - section view after adaptation of DRIE.

DRIE process was adapted for the fabrication of the viscosity sensor for the above reasons and uses Bosch process to achieve straight sidewalls shown in the Figure 31. Bosch process runs alternative cycles of fluorine-based etchant gas (SF_6, CF_4) to etch the bulk silicon and carbon-based gas (C_4F_8) to create polymer as a passivating layer for sidewalls, this helps to achieve uniform trenches. DRIE is highly beneficial to the viscosity sensor fabrication process as alternate route would be to expose wafers to KOH solution for a long period of time which could damage the devices. Some challenges were faced in achieving center to edge etch rate uniformity which depends on the chuck temperature, gas flow and uniform spread of exposed silicon areas being etched.

700 Cycles   760 Cycles   820 Cycles
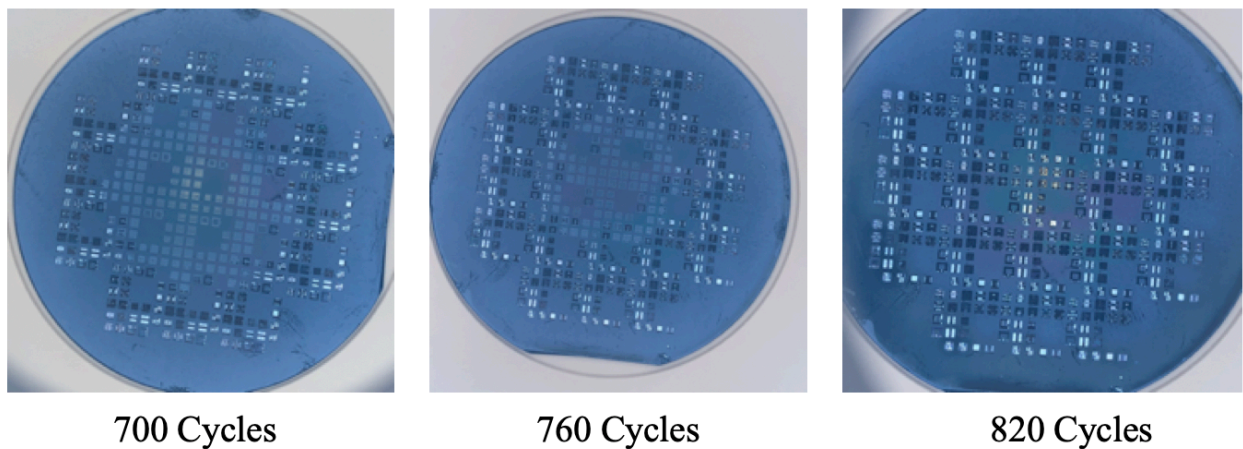
Figure 32: Edge to center (left to right) nonuniformity for backside etch of 500 μm using DRIE process.

Wafer in the Figure 32 was processed using the Bosch process where the recipe ran multiple etch cycles and each etch cycle is 7 seconds passivation 14 seconds etch. It was observed after 700 cycles edges start to clear whereas the center is still completely intact. After 820 cycles center clears which shows there is around 100 μm edge to center etch rate difference (non-uniformity). As the fabricated viscosity sensors are 4 mm x 4 mm and are fabricated on Silicon on Insulator (SOI) wafers with a 1 micron of buried oxide layer which acts as a masking layer, this non-uniformity does not affect the sensors greatly. Improvements were made in fabrication processes flow to provide additional support to membrane and a smoother release mechanism of the devices during the back-side bulk etch.

Before etching the bulk silicon, 3 μm of patterned TEOS is needed to be removed from the back-side through buffered oxide etch (BOE 5.2:1). Long-time exposure in BOE causes front side damage to the protective photoresist and damage to field oxide and aluminum. To prevent this a dummy wafer was attached to the front side of the device wafer while processing is done on the back side. Photoresist is span on device wafer and dummy wafer, later hard-baked on a hot plate for good adhesion. After processing the wafers were sawed and dipped in acetone to release the devices. More work is needed to optimize this recipe to achieve uniform etch rate but was not the focus of this thesis.

4.2 Air Cavity (Bubble) Formation

Discussed previously, the number of vibrations decay as the viscosity increases, and the frequency is expected to decrease with the increase in both density and viscosity. Some non-ideal conditions could arise during testing of the sensor and one such condition is air cavity (bubble) formation. When sensor is placed in oil a bubble could form that causes less mass loading of the

membrane resulting in higher vibration frequency. Mass loading happens when mass of the object alters the natural frequency of vibration of the membrane. Shown in Figure 33, the bubble is usually formed in the access hole below the diaphragm when submerged in oil.
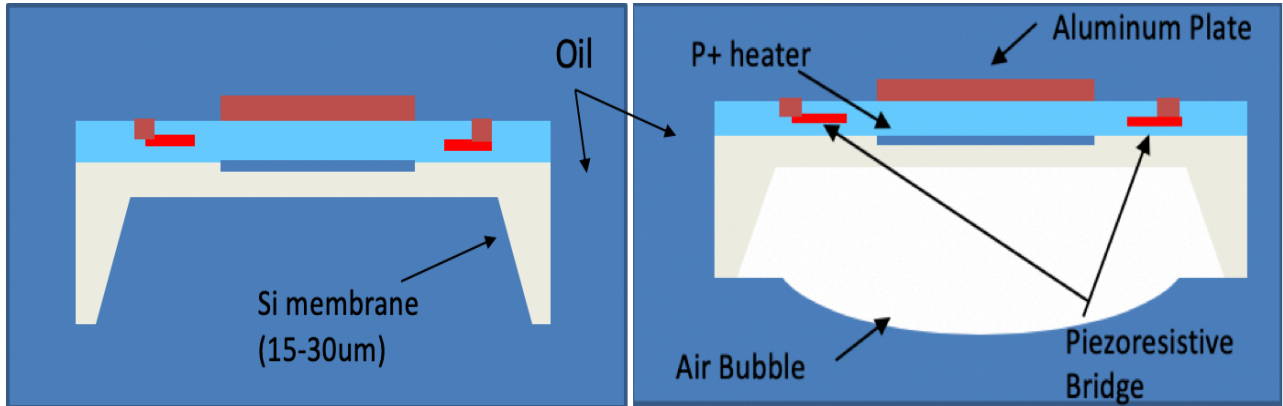
Figure 33: Sensor fully submerged in oil with (right) and without (left) air cavity (bubble) formed.
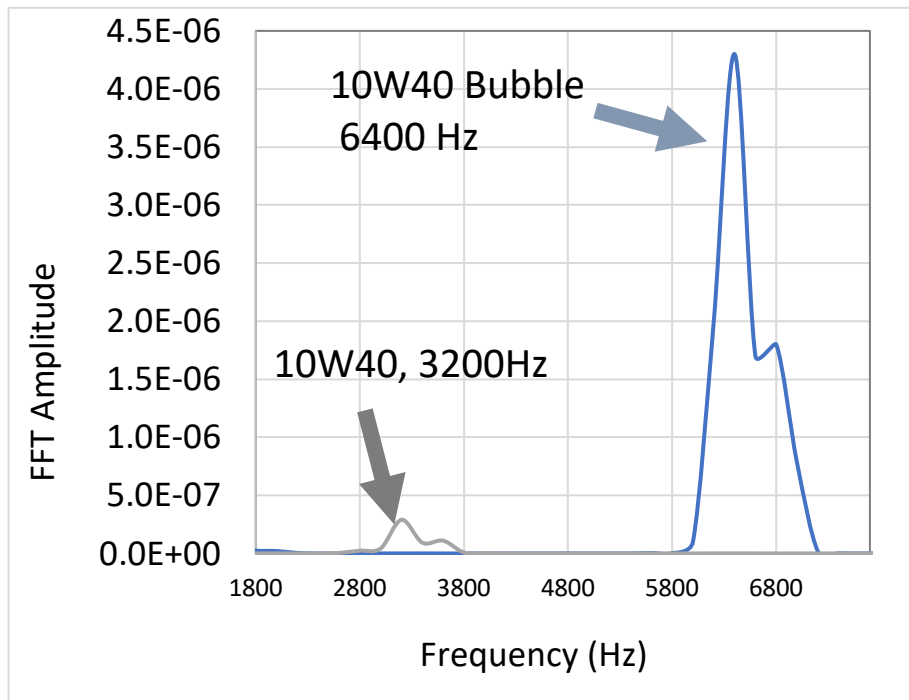
Figure 34: Graph showing the amplitude vs frequency response in 10W40 oil without bubble (left) and with bubble (right).

Figure 34 shows the test results on the bubble formation in 10W40 grade oil and compared to frequency with all same conditions but without bubble in the same oil. There is a 2x jump in frequency and high amplitude when the bubble is present on the diaphragm. The natural frequency of vibration is increased due to the reduction of mass by the addition of bubble on the membrane, because the bubble is very small and light it vibrates with a much higher frequency. Bubble formation could be prevented on the back of the diaphragm by slowly immersing sensor in fluid so that results are accurate. All future tests were monitored and bubble formation was avoided.

4.3 Thermal Actuation Bias

The sensor is actuated via a short pulse of heat delivered by the resistor RH and provided by an external voltage. The pulse width is controlled by a waveform generator and a power MOSFET. The movement of the membrane, including the measurement of the resonant frequency, its amplitude, and Q-factor, is measured with the in-situ piezo resistor Wheatstone bridge, which is powered by an external voltage source. As viscosity is dependent on temperature, when the membrane is heated above the ambient, no effects of changing fluid temperature will be seen in results. As such, it is necessary to determine appropriate test bias conditions that do not affect the measurement. Testing was done with varying input conditions (bridge voltage, pulse width and heater voltage). Figure 35 show viscosity detection setup indicating that heat is generated from Wheatstone bridge voltage, heater voltage and pulse width during actuation/sensing.
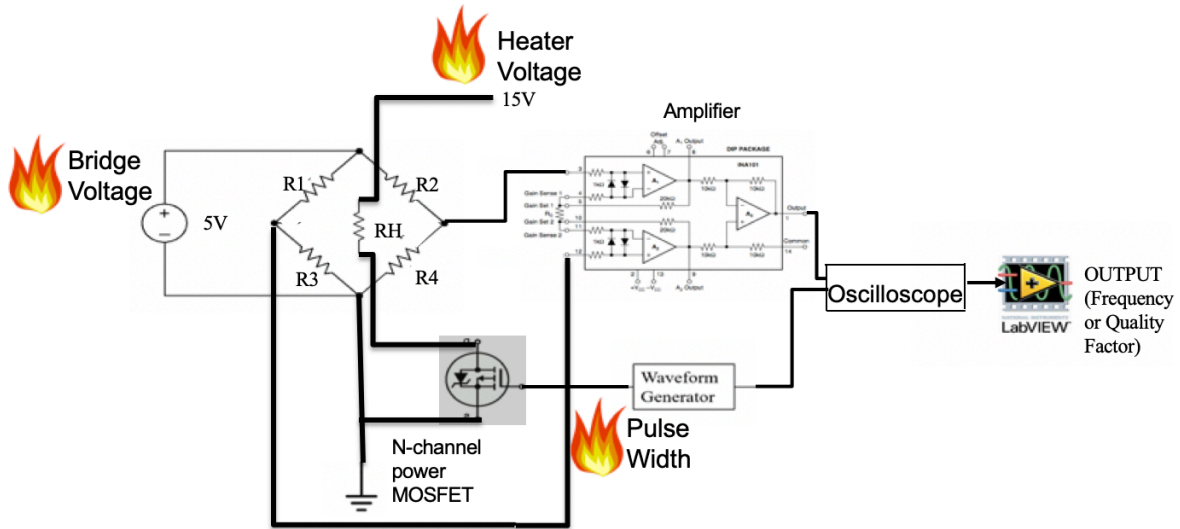
Figure 35: Viscosity detection setup showing places where heat can be generated during testing.

Movement of membrane is measured with the in-situ piezoresistor Wheatstone bridge in Figure 36. Resistors (~0.5 KOhm) are placed at locations that experience maximum stress which is near the edge of the membrane. As the device is epoxied to PCB which is not a perfect heat sink it is important to make sure the device does not heat up above ambient temperature or it could modify the temperature of surrounding fluid.
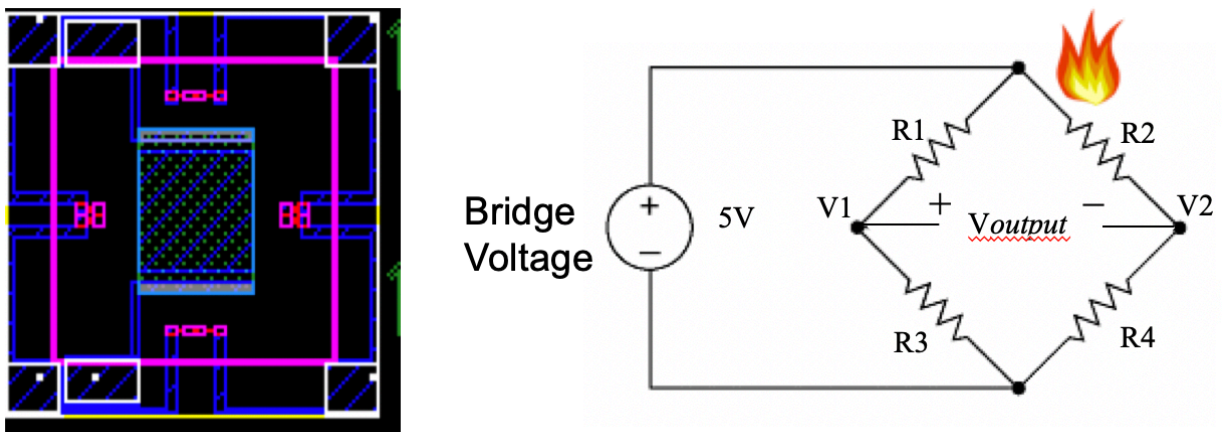
Figure 36: Thermally actuated viscosity sensor MEMS sensor top view (left) and Wheatstone bridge design used for analysis.

Four resistors arranged as two parallel branches with two resistors in series in each branch. A voltage difference can be recorded through the use of two probes on the opposite sides from where the +5V and ground (GND) connections are made. As the diaphragm vibrates, the stress changes the resistance hence changing the voltage difference. It is important to note that output signal is proportional to bridge voltage. Sensitivity increases as Wheatstone bridge voltage output is linearly related to input.

$$V_{output} = \left[\left(\frac{R_4}{R_2 + R_4}\right) - \left(\frac{R_3}{R_1 + R_3}\right)\right] V_S \qquad (4.1)$$

To understand the actuation bias, we need to know that the heat is released when current applied to the heating resistor $R_H = 200$ Ohms. Short thermal pulse sets the membrane in motion and the membrane vibrates at its natural frequency. The pulse width is controlled by a waveform generator and a power MOSFET shown in Figure 37.
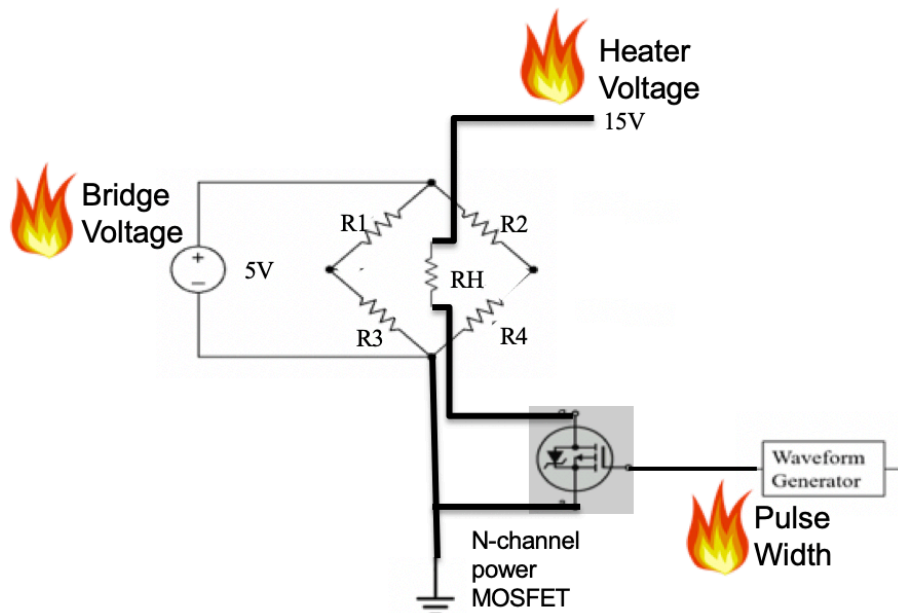
Figure 37: An overview of how the devices were tested with heater and power MOSFET schematics.

Overall the heater works through the process of joule heating, which involves an applied current going through a resistor and releasing heat, or producing power. *Heat (Q), is proportional to the square of the current flowing (I) times the electrical resistance (R), times time [33].*

$$Q = I^2 \text{ x } RT \qquad\qquad (4.2)$$

Each input conditions (Bridge Voltage, Pulse Width, Heater Voltage) were individually optimized to understand the thermal actuation bias effects on sensor response. Under ideal conditions the bias applied to the actuator and sensor do not result in enough heat to modify the local properties of the fluid being tested or affect/modify the sensor performance (frequency of oscillation, amplitude or quality factor).

4.4 Different Test Bias Conditions Results

Test bias condition optimization of the viscosity sensor was needed for proper functioning of the sensor and to make sure the bias conditions would not affect the temperature of the surrounding fluid readings as the sensor measures properties of liquids through thermal vibrations of a silicon diaphragm.

Figure 38 shows results of varying bridge voltage test where sensor was tested in air under the following conditions: bridge voltage $V_B = 5 - 11$ V, pulse width = 30 μs, pulse heat = 30 V. As bridge voltage (V_B) always ON so constant power is being applied to the resistors. Frequency decreases significantly with increase in V_B (- 28%).

48
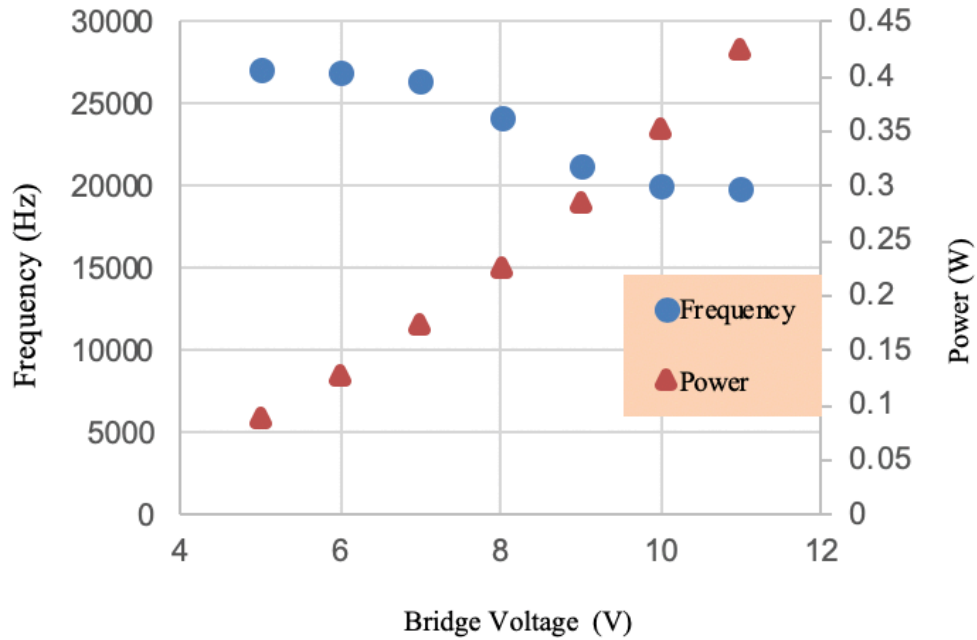
Figure 38: Frequency response of sensor in air with varying bridge voltages.

Quality factor improves as the signal increases but also frequency decreases by -28% which indicates self-heating of the sensor in Figure 39. As previously established in Section 3.3, frequency is dependent on shape, size and material of the device so to further investigate this change in frequency the Youngs modulus of silicon needed to be looked at as the values could change with change in temperature.
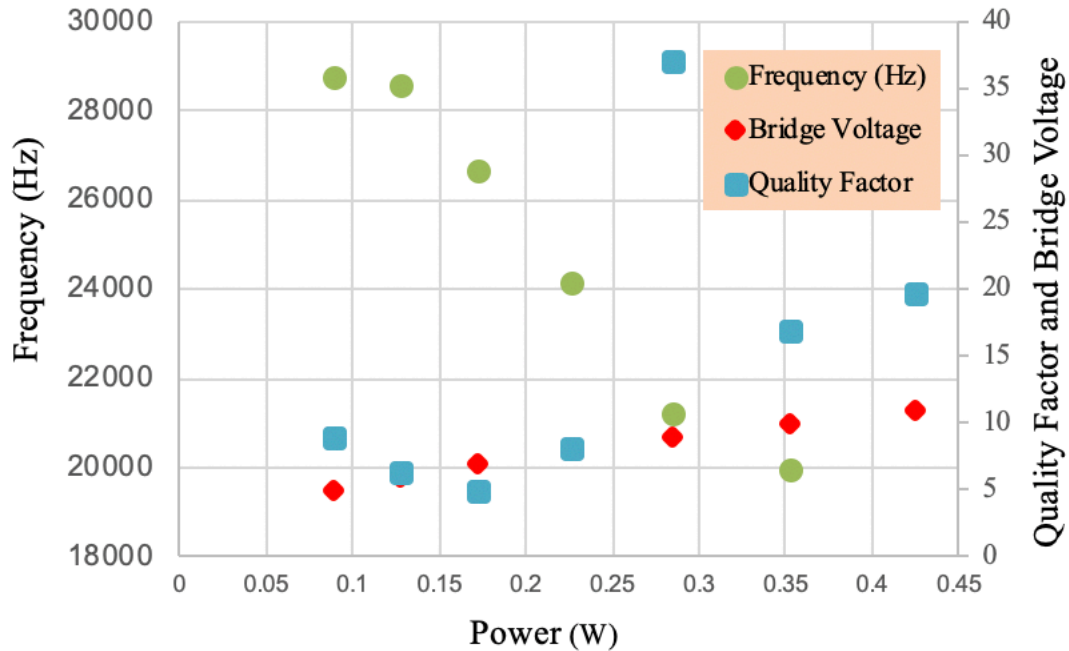
Figure 39: Frequency, bridge voltage and quality factor vs power.

Silicon membrane resonance changes with temperature as Young modulus decreases .1% per °C and coefficient of thermal expansion of silicon is 2.6 ppm/°C [34]. This is a very small change which could not result in decrease of frequency by 28%. Other possible cause could be change in the state of epoxy. Temperature ramp up test was done at increasing bridge voltages to see if epoxy loosening was the cause of decrease in frequency. Figure 40 shows the results of this test where it can be seen that above 5 V, the membrane temperature is affecting the frequency of response. Too high of a bridge voltage results in permanent damage to the sensor as it can be seen for bridge voltage of 12 V when the frequency is different during temperature ramp up and ramp down. The cause of this frequency shift was due to operation of device over the epoxy's service temperature limits as the manufacturer reports the use of epoxy between -23°C to 49°C for long term continuous exposure [35].
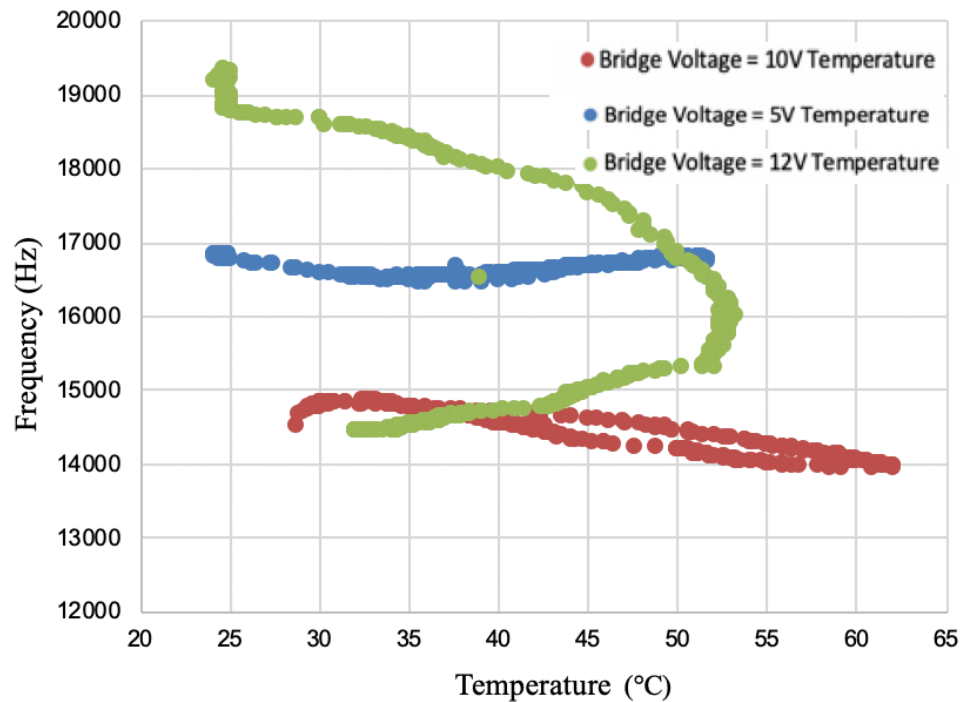
Figure 40: Temperature Ramp Results in Air with varying bridge voltages.

From the above results it was concluded that although increasing the bias of V_B improves signal integrity, the self-heating of the sensor could affect the viscosity. Constant power through V_B and increasing temperature causes epoxy under sensor to loosen up, so maintaining V_B below 7 V to prevent any epoxy damage should not affect the natural frequency of resonance of the sensor.

Figure 41 shows results of varying heater resistor bias when sensor was tested in air. Heater resistor is designed to be $R_H = 200$ Ohms and was tested under the following conditions: bridge voltage = 10 V, pulse width = 30 μs, pulse heat = 6, 8, 10, 12, 14 V. The results show no specific pattern. Frequency is stable and only changes by 4.6%.
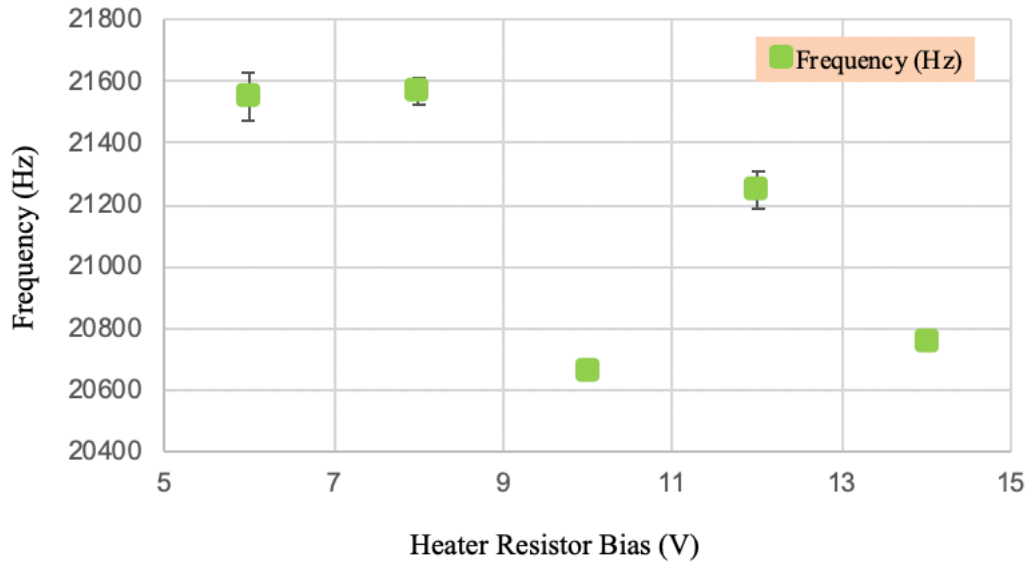
Figure 41: Graph showing change in frequency with change in heater resistor bias voltage.

It can be seen in Figure 42 that heater bias does affect the sensor performance, signal quality is improved with higher heater voltage. Heater bias value can be adjusted for optimum sensor response (within reason).
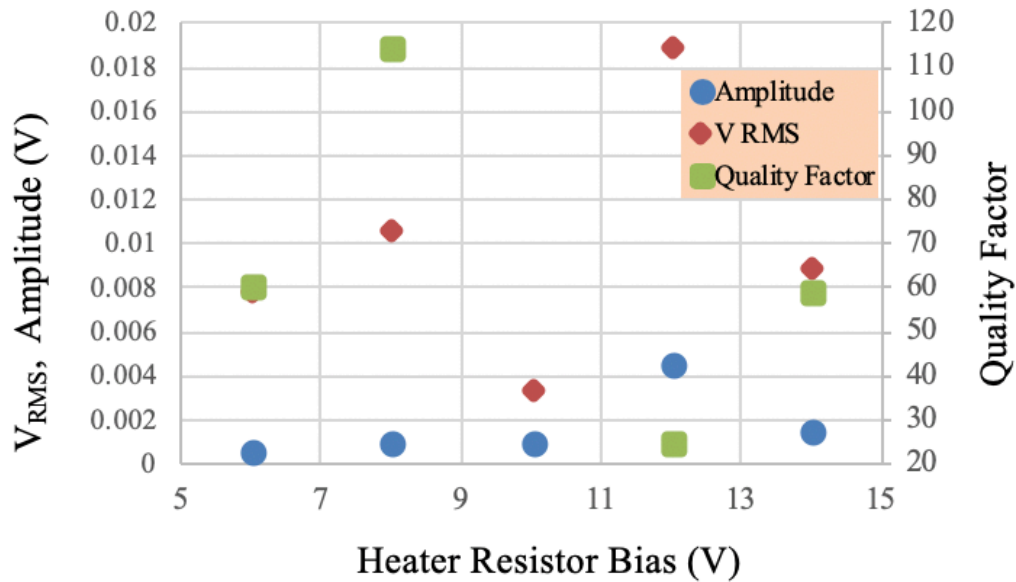
Figure 42: Graph showing change in quality factor, V_{RMS} and amplitude with respect to heater resistor bias.

Figure 43 shows results of varying pulse width when sensor was tested in air under the following conditions: bridge voltage = 10 V, pulse width = 20, 25, 30, 35, 40 µs, pulse heat = 10 V. Results show that the frequency is stable and does not shift more that 10%. Pulse width does not significantly affect the silicon membrane when kept below 30 µsec. Sudden jump at 35 µsec could mean resonant modes could be changing of thin membrane [36].
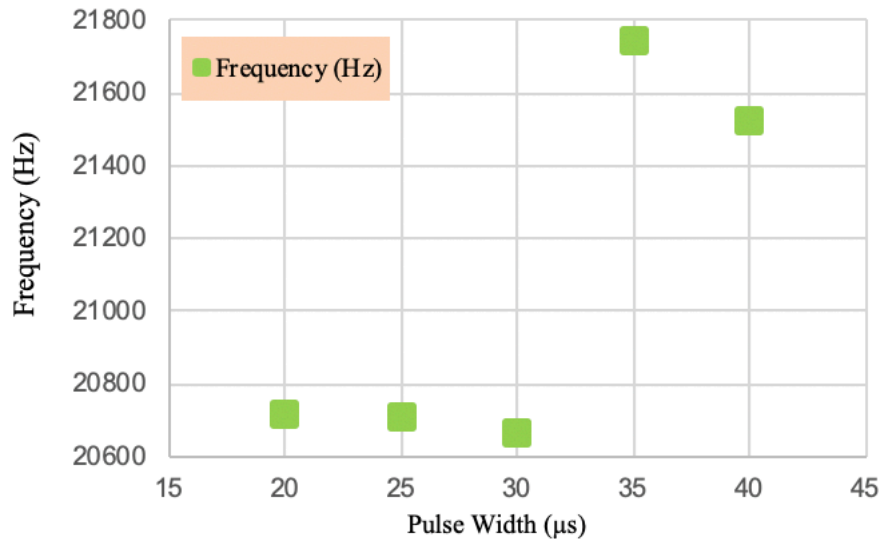
Figure 43: Graph showing change in frequency with varying pulse width.

Seen in Figure 44 pulse width does not affect the sensor performance significantly as this is a very fast pulse. Even though the instantaneous power deliver is between 200 mWatt and 1 W *(Power = V^2/R)*, the energy deliver is less than 30 µJoule *(Energy = Power* x *Time)* with a 30 µsec pulse. At a typical 20 Hz actuation rate, the duty cycle is 0.6 msec per second, or 0.0006 %. It was observed that higher heat pulse improved waveform quality factor.
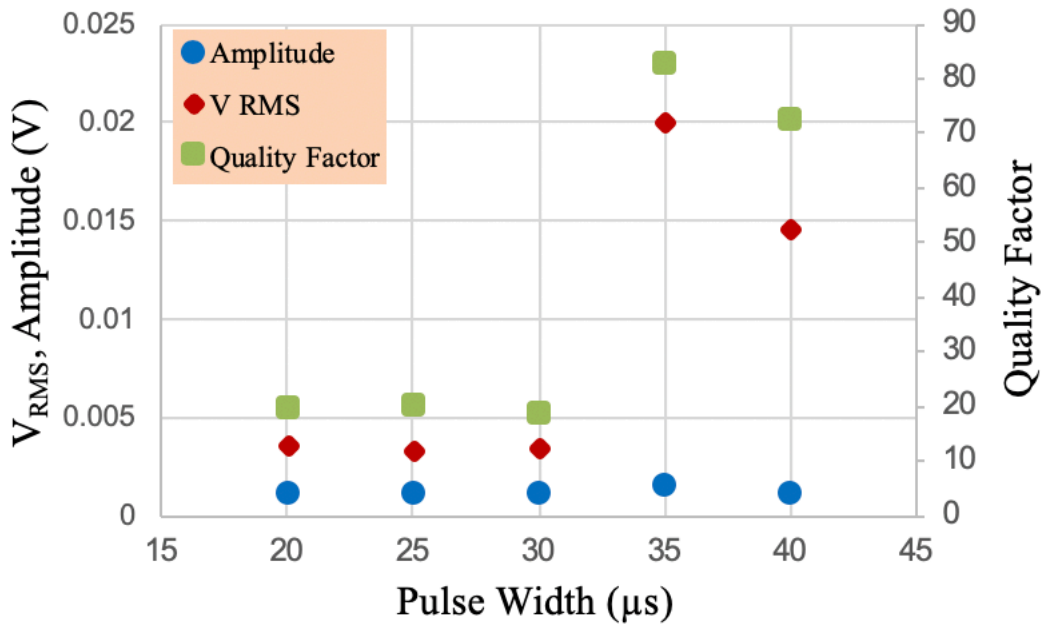
Figure 44: Graph showing quality factor, V$_{RMS}$ and amplitude vs varying pulse width.

Based on all the results we can conclude that frequency is most stable when the pulse width is between 20 and 30 µs and heater voltage between 6-15 V. Pulse width and heater bias do not affect the sensor performance significantly as this is a very fast pulse. Maintain V$_B$ below 7 V to prevent epoxy damage. Too large of a bridge voltage (V$_B$), results in significant heating of the silicon membrane, affecting its resonant frequency and softening of die attach epoxy.

CHAPTER 5

EVALUATING REAL TIME SENSOR RESPONSE IN OIL

To characterize the real-time response and sensitivity of the thermally actuated MEMS viscosity sensor, three different motor oils (5W30,10W40 and 20W50) were bought and the sensor was tested in each individual oil to get baseline readings for frequency, amplitude, and quality factor. Later, the sensor was tested with increasing viscosities and response time was measured. The measured viscosity values were compared to commercial viscosity values which measured using a Brookfield DV2T rotational viscometer to verify operation. The specifications for the different oils used during testing is shown in Table 1. Room temperature viscosity values were obtained using the values from Table 1 and an online calculator from Widman International SRL [39]. To understand the response time, the step response of the frequency, amplitude and quality factor changes (not the step response of the oscillations) were examined.

Table 1: Physical Characteristics of different grades of oil used for experiments [36], [37], [38].

Properties		5W30 Oil	10W40 Oil	20W50 Oil
Density	(kg/m^3)	860	871	880
Kinematic Viscosity @ 40℃	(cSt)	63	104	161
Kinematic Viscosity @ 100℃	(cSt)	10	15	17
Kinematic Viscosity @ 23℃	(cSt)	143	249	455

Viscosity values from the commercial oils were validated using a Brookfield DV2T rotational viscometer. It measures dynamic viscosity by applying low torque to a liquid, resulting in mechanical deformation. The torque required to induce rotation in the horizontal plane is measured and this torque is proportional to the viscosity of the liquid. In DV2T a spindle is attached to a calibrated spring. As the spindle rotates in the liquid sample, the calibrated spring deflects. This deflection of the spring is measured by a rotary transducer [40].

Table 2: Viscosity measurements using Brookfield DV2T rotational viscometer at room temperature.

#	Oil	Commercial Dynamic Viscometer Readings (cP)	Density (g/mm^3)	Kinematic Viscosity (cSt)	Kinematic Viscosity Delta
I	5W30	126	0.860	146.51	0
II	5W30 : 10W40 [2:1]	150	0.863	172.21	25.7 cSt 17.50%
III	5W30 : 10W40 [2:2]	165	0.865	189.43	17.22 cSt 10.00%
IV	5W30 : 10W40 : 20W50 [2:2:1]	199	0.868	228.41	38.98 cSt 20.60%
V	5W30 : 10W40 : 20W50 [2:2:2]	222	0.870	254.24	25.83 cSt 11.30%

Sensor D49 was tested for real time response. The sensor is comprised of a 2.5mm membrane with a P+ heater covering 2% of the membrane, no passivation, no metal on top. To calculate the viscosity vs vibrations relationship for our sensor, we tested the sensor in 5W30, 10W0 and 20W50 oil to get baseline data. Figure 45 shows the raw data in time and frequency domain for the baseline tests in 5W30, 10W0 and 20W50 oil. Frequency, quality factor and average amplitude of oscillation values were extracted by lab view from the raw data.
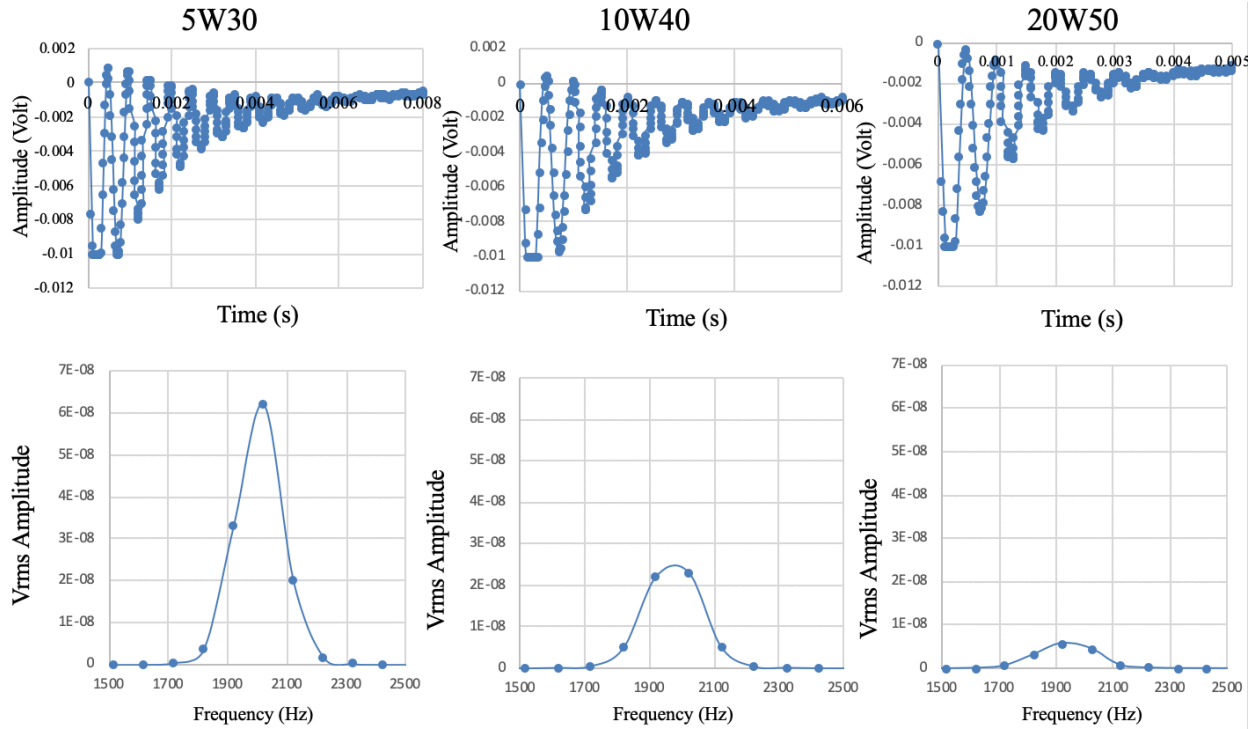
Figure 45: Raw data in time domain and frequency domain for 5W30, 10W40 and 20W50 oil.

Based on the viscosity values measured using the commercial viscometer and average frequency values obtained from baseline tests, a curve for best fit / trendline was added to achieve R^2 (coefficient of determination) closer to 1 as shown in Figure 46. A power trendline was used with data sets as it compares measurements that increase/decrease at a specific rate and the R-squared value achieved is 0.9946, which is a nearly perfect fit of the line to the data. The power trendline equation was:

$$y = 2344.5 \, x^{-0.032} \tag{5.1}$$

In the equation 'y' is the frequency and 'x' is the viscosity value.

Using the measured viscosity values from commercial viscometer, and the power trendline equation shown above, the expected frequency values were calculated for different mixtures of oil.
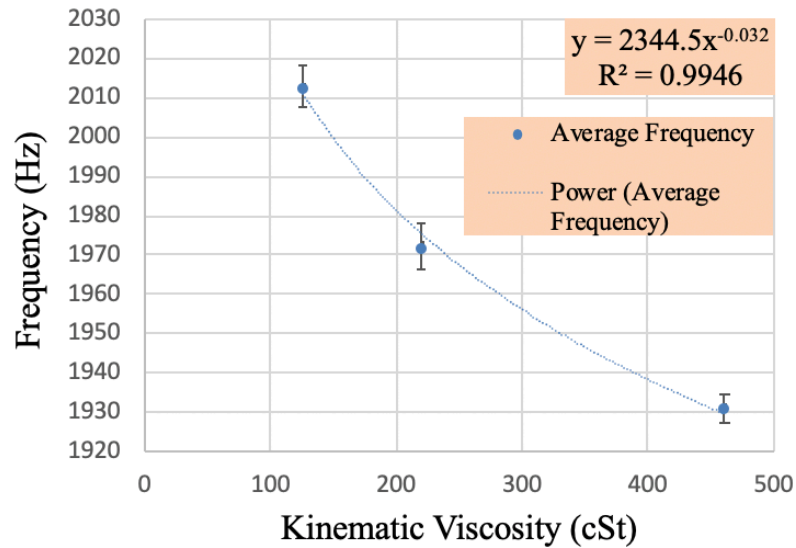
Figure 46: Plot for frequency vs kinematic viscosity with a trendline fit to predict frequency for different viscosity.

Amplitude and viscosity relationships were drawn based on the viscosity values measured using the commercial viscometer and average amplitude values obtained from baseline tests for oil 5W30, 10W0 and 20W50. An exponential trendline curve was found to be the best fit as the data values fell at increasingly higher rates, shown in Figure 47. The exponential trendline equation was:

$$y = 0.0011\,e^{-0.03x} \tag{5.2}$$

In the equation 'y' is the amplitude and 'x' is the viscosity value.

Using the measured viscosity values from commercial viscometer and the exponential trendline fit in Equation 5.2, the expected amplitude values were calculated for different mixtures of oil.
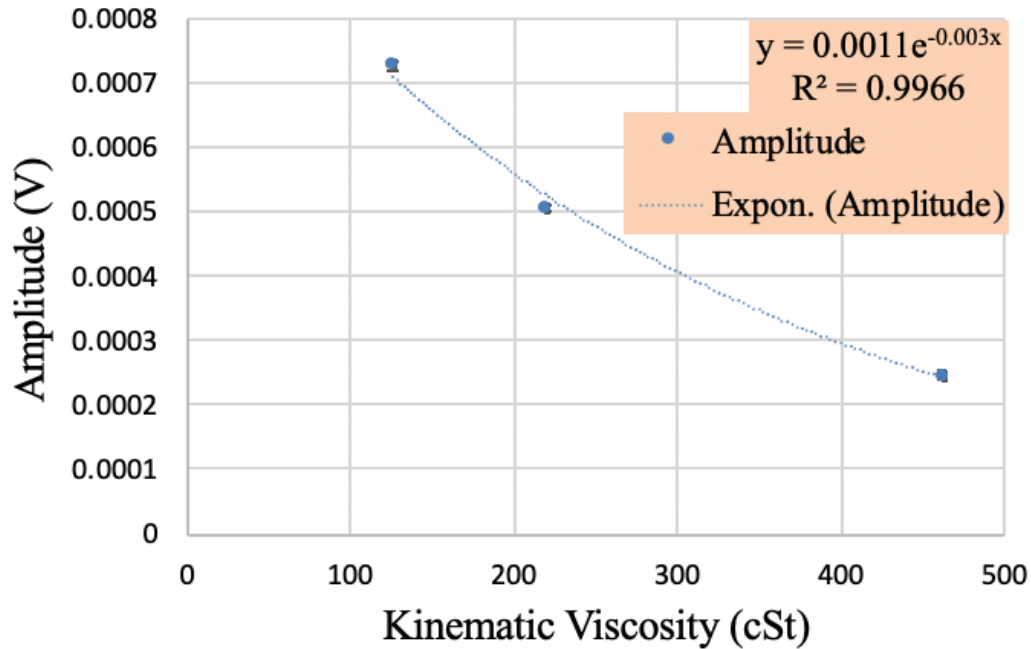
Figure 47: Plotted exponential fit for baseline amplitude values vs. kinematic viscosity.

Three different test scenarios were investigated (1) no agitation, (2) continuous agitation and (3) short-term agitation to evaluate the response. Between tests the sensor was cleaned by using wipes to soak oil particles on both sides of the diaphragm. Cleaning is also a very important factor, because leaving any residues from previous test could cause shift in frequency, amplitude and quality factor. The same test bias conditions were used through the testing. The settings were a Wheatstone Bridge bias of 7 V, a heating resistor bias at a frequency of 20 Hz with a voltage of 15 V for 25 microseconds.

(1) <u>No agitation</u>

The device was tested in the commercial motor oils with increasing viscosity and data being recorded every 5 seconds. The test setup used for no agitation can be seen in Figure 48.
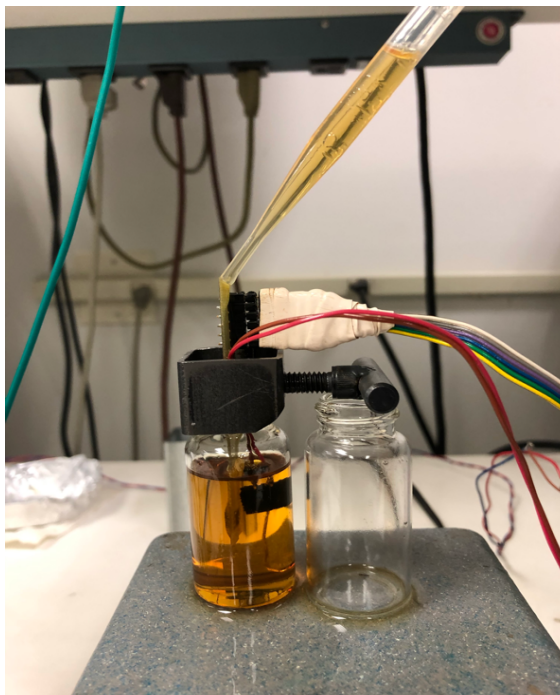
Figure 48: Test setup for no agitation.

The no agitation test was performed in the following order: I: 5W30 (7 mL), II: 10W40 (3.5 mL), III: 10W40 (3.5 mL), IV: 20W50 (3.5 mL) and V: 20W50 (3.5 mL). Table 2 above indicated the expected results. Figure 49 shows that as viscosity increases, or the fluid becomes more viscous the frequency tends to decrease except for the second addition of 10W40 oil. This is because when 10W40 is added the second time, kinematic viscosity change is the lowest (17.22 cSt or 10 %) as compared to all the other mixtures. The kinematic viscosity delta change values are shown in Table 2 above for all the different mixtures. As seen in Figure 49, after adding oil the frequency spikes by 6.7% within the first 5 seconds, remains high for a minute, and then slowly starts to decrease to the expected frequency value shown in Table 3. To determine if the frequency has stabilized for our system, frequency values must not shift larger than ±10 Hz for time greater that 5 minutes. Keeping the same test bias conditions and cleaning the sensor very thoroughly seems to help with repeatability of the results.

60

Initial conclusions behind the spike in frequency and amplitude in Figures 49, 51 was due to a temperature change but the results show that temperature is stable with an average of 25.26 ± 0.24 °C. In this case, potential other reasons for the spike could be due to perturbations / vibrations being added by the way the oil is dropped in the vial or due to the change in volume of the liquid. More tests would need to be performed to investigate the cause of the spike such as addition of same oil twice and see if changing volume causes the spike in frequency or by adding small quantities of oil to eliminate any type of perturbations getting added on. Initial spike in response, then overdamped. Higher viscosity oil seems to settle down faster than low viscosity oil
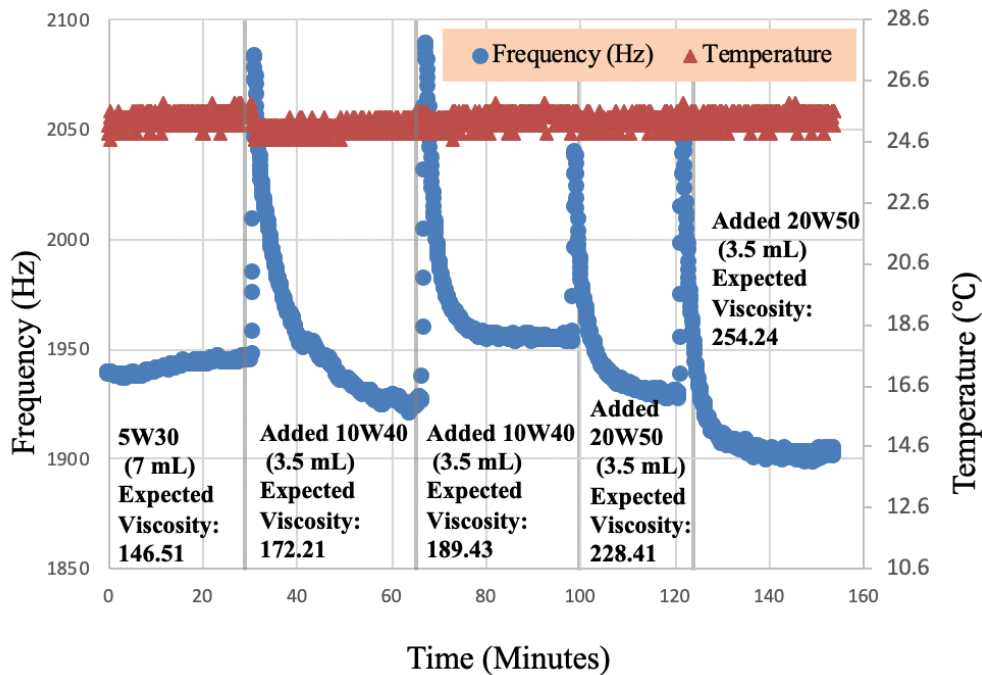
Figure 49: Graph showing frequency response to different oils with no agitation.

Figure 50 shows normalized response of frequency. Initial upward spike in response then overdamped. It was seen that higher viscosity oil settle down faster (10 minutes) than low viscosity oil (12-15 minutes).
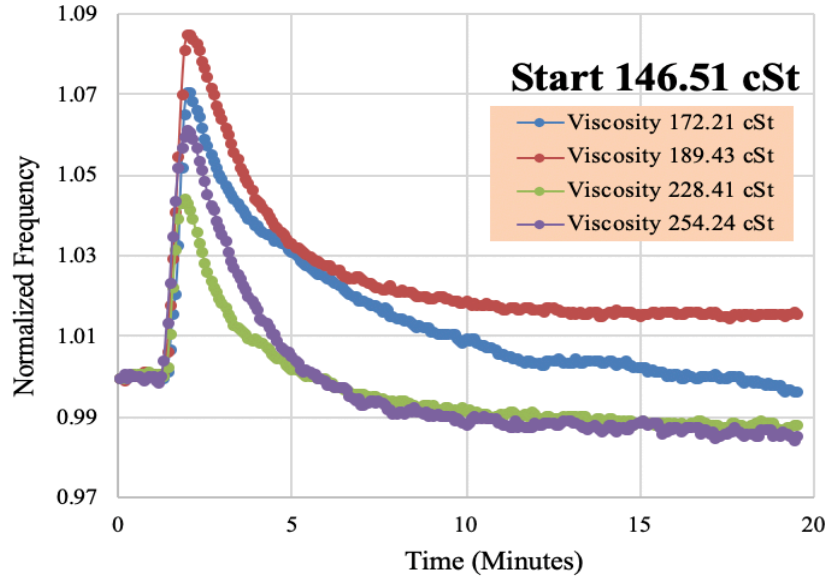
Figure 50: Graph showing normalized frequency response to different oils with no agitation.

The results for amplitude of oscillations (average of all the oscillations of the waveform) from the sensor with varying viscosities shows a similar response to frequency. Figure 51 shows that when oil is added, the amplitude spikes to a lower value within 5 seconds and then quickly settles down to a value lower than previous. The change between II and III is much lower than others, as expected. This is consistent between regions II and IV, however region V shows a much lower value that is more consistent with the results in previous works. Underdamped response is seen with similar settling time for all oils.
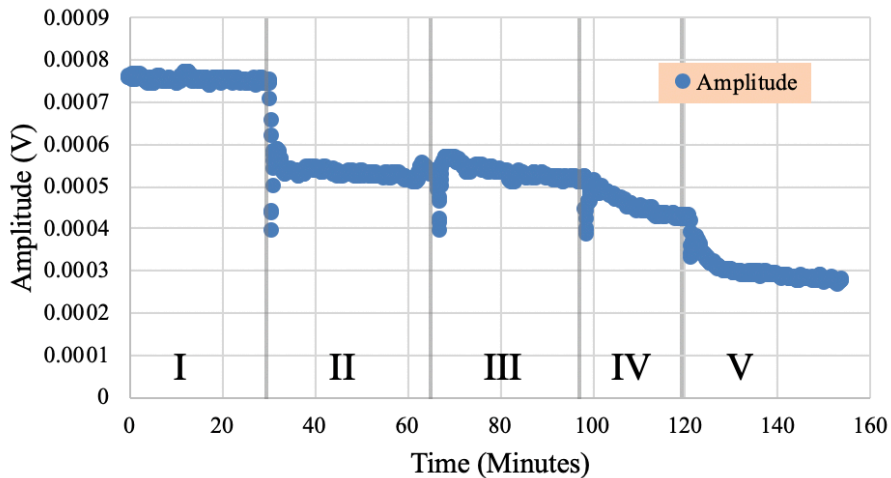
Figure 51: Graph showing amplitude response to different oils with no agitation.

Figure 52 shows normalized response of amplitude. Initial downward spike in response then underdamped. Similar settling times around 7 minutes were seen for all oils.
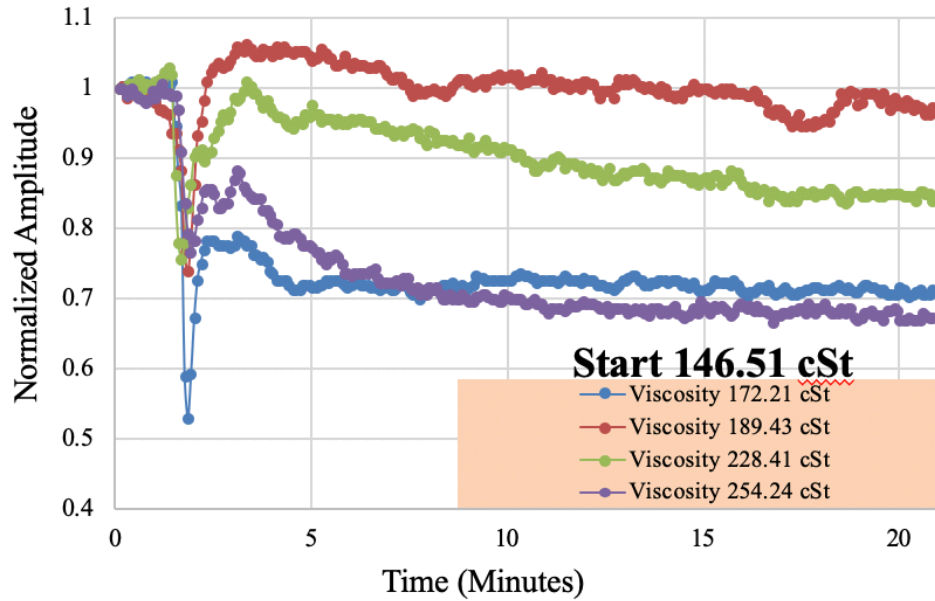
Figure 52: Graph showing normalized amplitude response to different oils with no agitation.

Figure 53 shows an increase in quality factor (number of oscillations) which is consistent with increase in frequency (spikes in frequency), but opposite to what is expected. As the viscosity oil increases the number of oscillations should reduce. The likely reason behind the higher number of oscillations was due the way the oil was added. The oil was added using a pipette, during the dropping of oil perturbations could be introduced leading to an initial sampling of pure oil, which then spikes back up due to the fluid mixing. Additionally, these perturbations could cause the sensor to shake or move from its original position and increase the quality factor values.
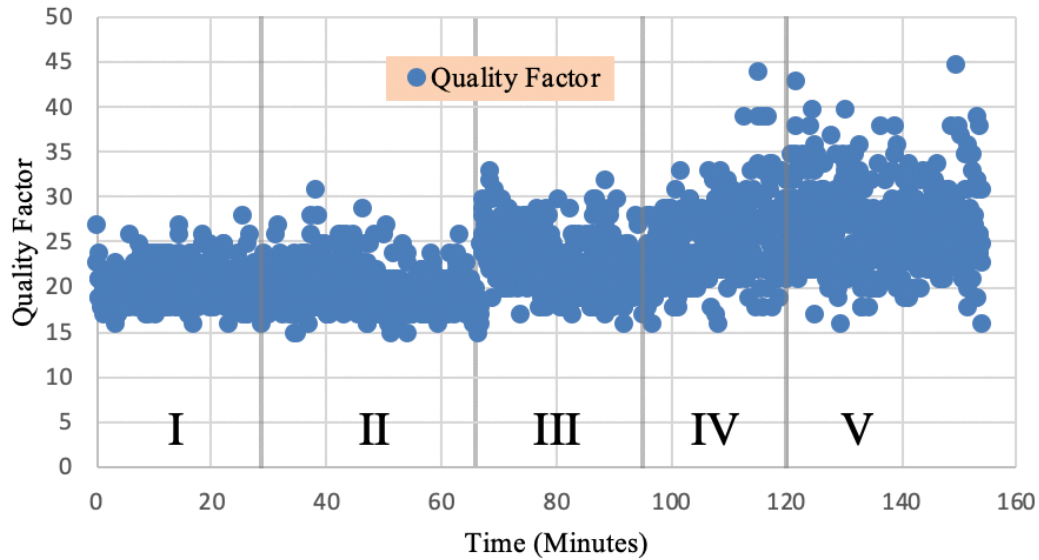
Figure 53: Graph showing quality factor response to different oils with no agitation.

(2) **Continuous agitation**

The test setup used for continuous agitation can be seen in Figure 54. This new setup focuses on the sensor relying on thermal vibrations, where these vibrations must not get affected by any external forces such as the rotation of magnetic stirrer bar. The vibrations from the stirrer bar can give false results if placed too close to the sensor. A bigger jar was used to place the stirrer bar and sensor far apart and the sensor was clamped using a piece holder to avoid any movements due to agitation. As the sensor must be submerged in the oil under test, for this setup to work, larger quantities of oil were needed.
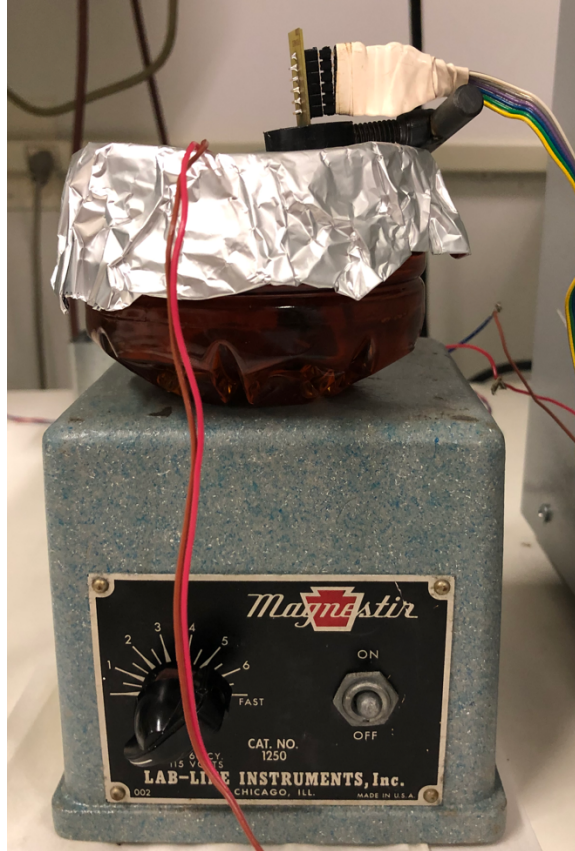
Figure 54: Test setup for continuous agitation.

Figures 55, 56, and 57 show frequency, amplitude, and quality factor responses to continuous agitation test, respectively. Note the scale of the time axis is in hours instead of minute. The device was tested in the commercial motor oils with increasing viscosity and data being recorded every 10 seconds. Continuous agitation test was performed in the following order: I: 5W30 (100 mL), II: 10W40 (50 mL), III: 10W40 (50 mL), IV: 20W50 (50 mL) and V: 20W50 (50 mL). This test was performed for a longer duration as it takes time for the magnetic stirrer to reach a stable temperature. The magnetic stirrer system heats up slowly heating the fluid under test to 33-34 °C but when new oil is added it is at room temperature, so monitoring temperature is very important for this test setup. Figure 55 shows that when new oil is added it reduces the vial temperature from around 33°C to 27 °C causing changes in frequency. Continuous agitation test

results show a similar trend to no agitation where the frequency decreases when 10W40 is added first but increases when more 10W40 is added. Later the frequency drops for 20W50 as expected and as more 20W50 is added the frequency starts to decrease further, but then due to changing temperature, the frequency does not see any decrease and instead increases. Stabilization time and response time is higher for continuous agitation because large quantity of oil is used. To start, 100 mL of 5W30 oil was used for baseline measurements and 50 mL of oil was added for each different case as opposed to 5 mL for "no agitation" test.
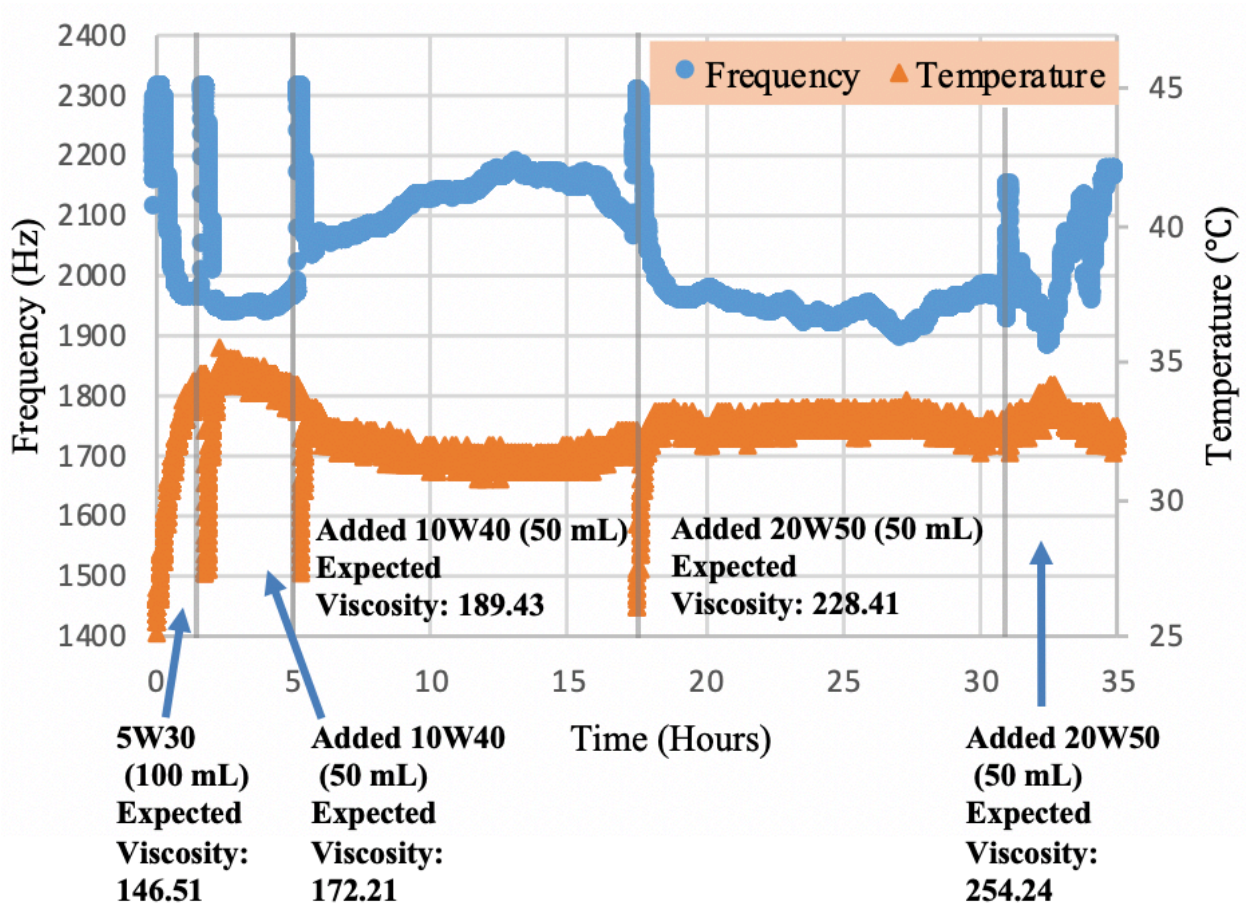
Figure 55: Graph showing frequency and temperature response to different oils for continuous agitation test setup.

The upward spike in frequency in Figures 55 and downward spike in amplitude in Figure 56 is due to the change in temperature as the fluid getting added is room temperature (24°C) whereas the

liquid in the vial is around 33°C. There is a high amount of dampening in the system because the signals seem to stabilize in temperature quickly and only slightly adjust from that point onwards. The magnetic stirrer system setup used for continuous agitation is very unstable as the temperature keeps changing. When 10W40 is added the second time the viscosity does not change much but the density is changing more significantly. The frequency is more responsive to both viscosity and density whereas the amplitude only to viscosity. Improvements are needed to investigate this method further. Future work should rely on heated fluids for testing, that way the temperature in the system could remain nearly constant to eliminate this source of error. This will likely improve the initial spiking; however, it might not change some of the later system responses. There appears to be some amount of dampening in this system, where a slight amount of oscillation is seen in the signals.
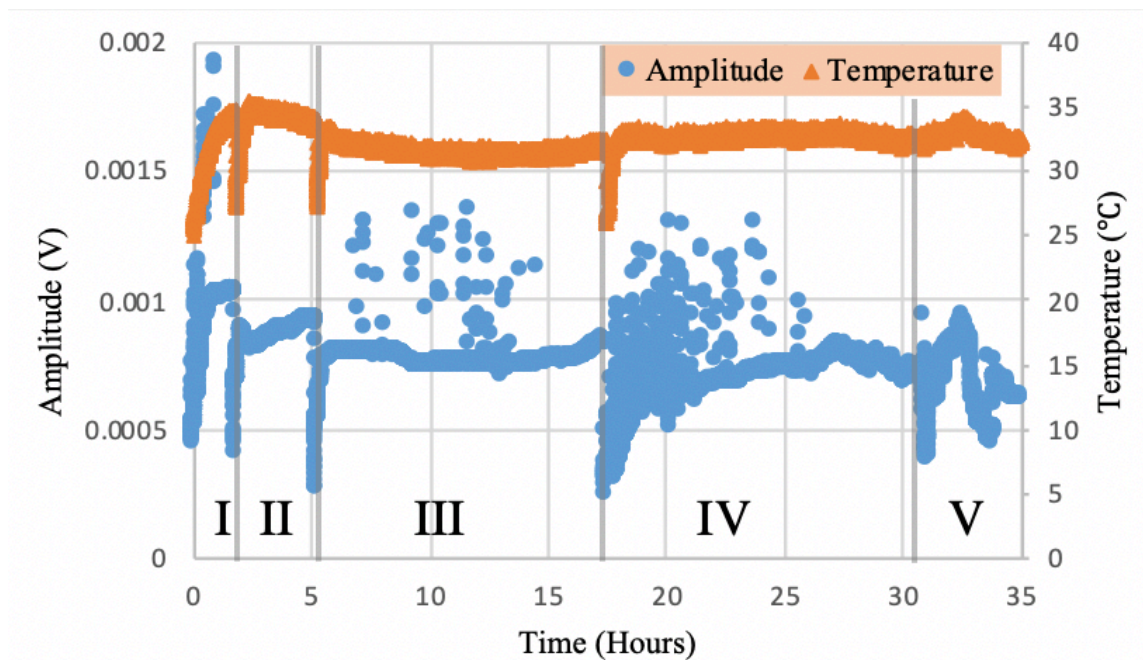
Figure 56: Graph showing amplitude and temperature response to different oils for continuous agitation test setup.

Figure 57 shows that with increasing viscosity, the value of quality factor does not seem to response and the values are all relatively similar. Similarly, the temperature and quality factor are closely related, and the change in temperature is distinctly related to some of the sources of error seen. The quality factor doesn't seem as affected as the amplitude, but comes at the cost of an extremely wide range of results to begin with. Future work should focus on reducing this quality factor variability because it is difficult to make meaningful conclusions in this case.
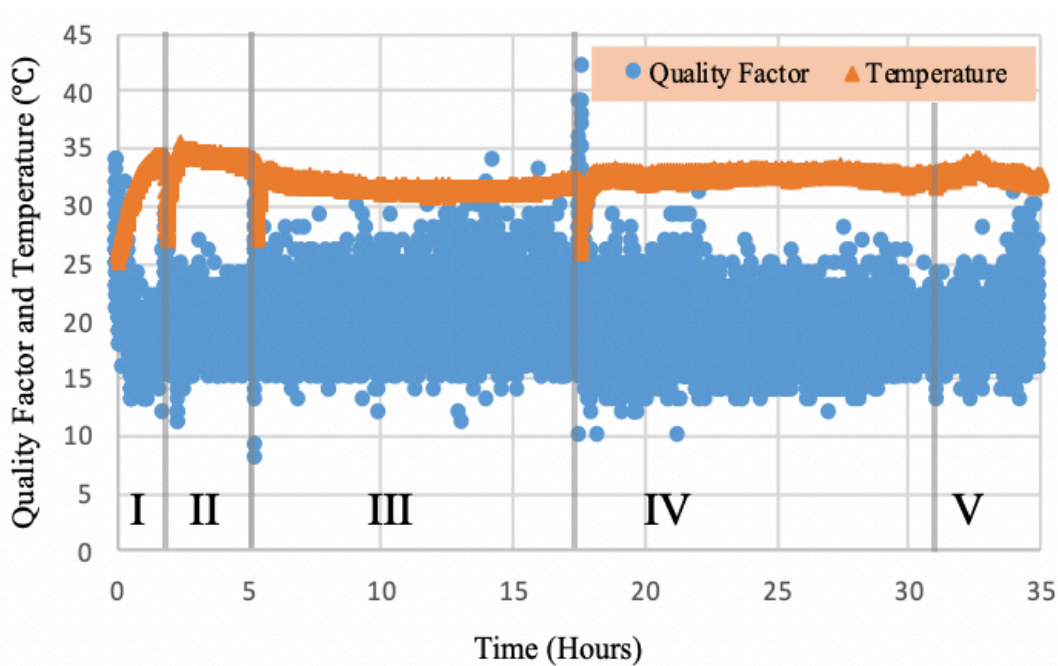
Figure 57: Graph showing quality factor and temperature response to different oils for continuous agitation test setup.

(3) **Short-term agitation**

Figure 58 shows a newer setup to incorporate agitation to the test procedure. The sensor was clamped using a piece holder to place the device in the middle of the vial, avoid touching any of the sides of the vial and avoid any movements that could be caused due to magnetic stir bar

placed inside the vial. In this setup, the stirrer was only turned on for 5 minutes when higher viscosity oil was added, the rest of the time the stirrer was off.
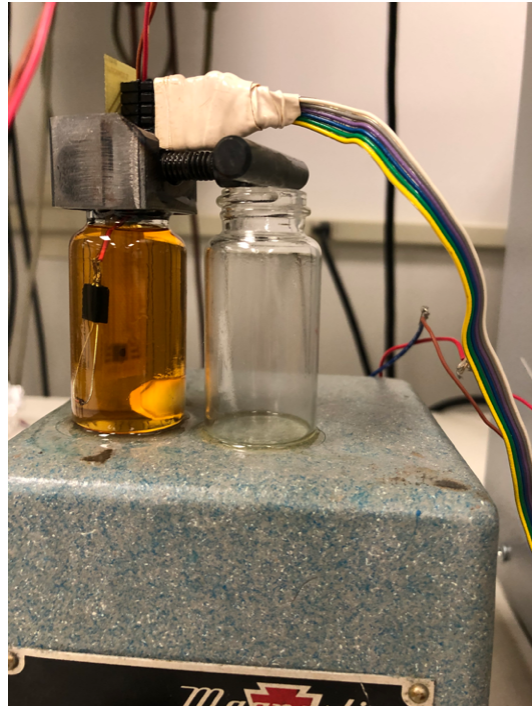
Figure 58: Vial placed on top of magnetic stirrer with a PN diode for temperature sensing, a stir bar and sensor D49 placed using the piece holder inside.

The short-term agitation procedure was a 5-minute agitation, when new oil is added. This setup does not seem to work as expected, as it can be seen in Figure 59 the frequency increase with the addition of higher viscosity 10W40 oil. Results are not stable and show high deviation as the agitation is not continuous or it could also be due the short-term agitation causing system error or the stirrer bar touching the sensor as we see in Figure 60 amplitude is not stable after the addition of 20W50 oil.
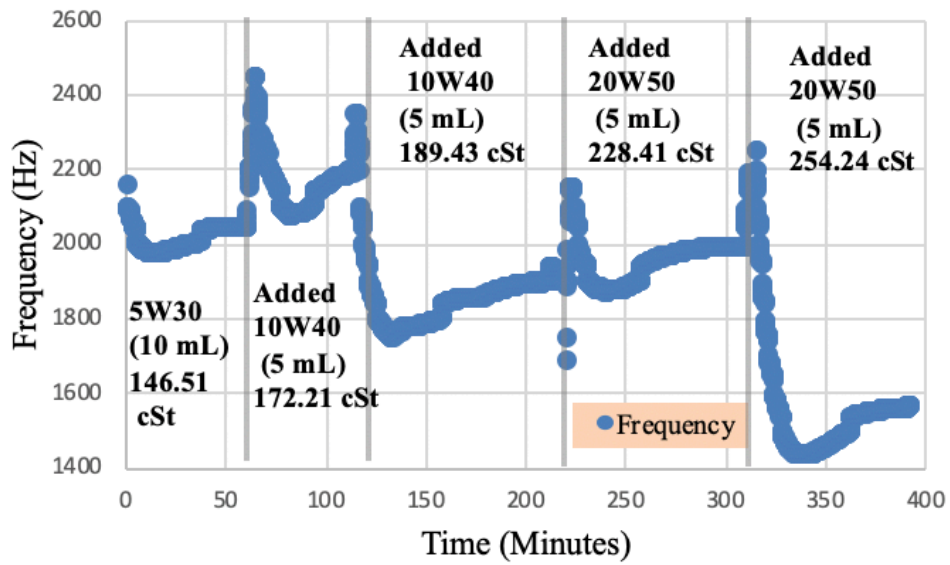
Figure 59: Graph showing frequency response to different oils with agitation only during addition of oil.

Figure 60 shows the amplitude and temperature response for short term agitation setup. The setup is not stable, does not respond to increasing viscosity as well as an opposite response to temperature.
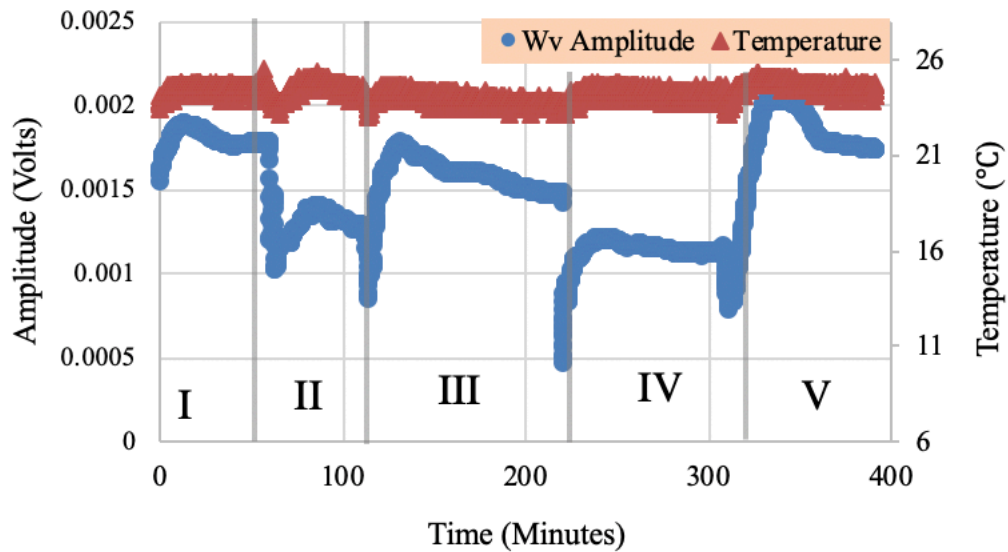
Figure 60: Graph showing amplitude response to different oils with agitation only during addition of oil.

70
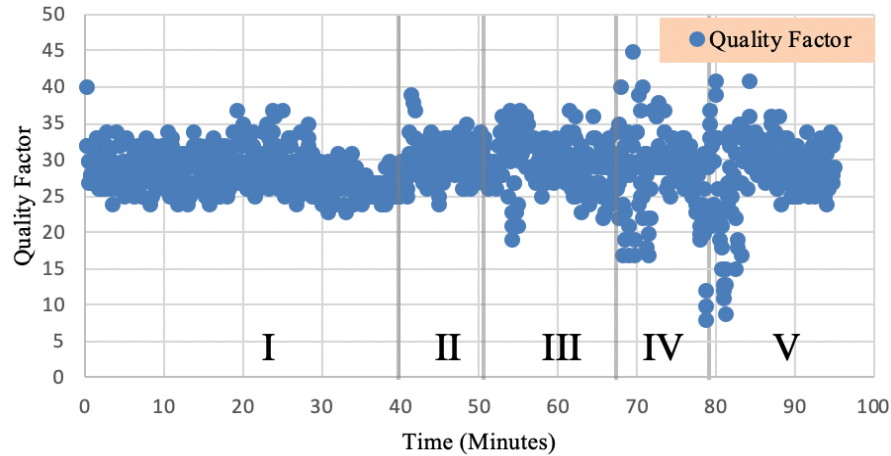
Figure 61: Graph showing quality factor response to different oils with agitation only during addition of oil.

Using the measured viscosity values from commercial viscometer and the power trendline equation shown above the expected frequency values were calculated for different mixtures of oil. These results are shown in Table 3. The expected frequency values were used as a comparison and conclusions were drawn for the cases of no agitation, continuous agitation, and short-term agitation procedures.

Table 3: Expected and measured frequencies for various test conditions.

Test Case	Measured Kinematic Viscosity (cSt)	Expected Frequency (Hz)	No Agitation Measured Frequency (Hz)	Continuous Agitation Measured Frequency (Hz)	Short-Term Agitation Measured Frequency (Hz)
5W30	146.51	1998.68	1942.13	1963.92	2005.40
5W30 : 10W40 [2:1]	172.22	1988.36	1938.02	1939.32	2103.86
5W30 : 10W40 [2:2]	189.44	1982.31	1956.21	2064.20	1892.98
5W30 : 10W40 : 20W50 [2:2:1]	228.42	1970.48	1933.59	1929.51	1883.39
5W30 : 10W40 : 20W50 [2:2:2]	254.25	1963.73	1903.64	1992.81	1553.53

71

Figure 62 is a graphical representation of Table 3 which shows the frequency results of different tests procedures and can be compared to the expected frequency result. The frequencies for different test procedures were obtained by averaging the values after the response has stabilized and the spike seen in all the test scenarios was disregarded.
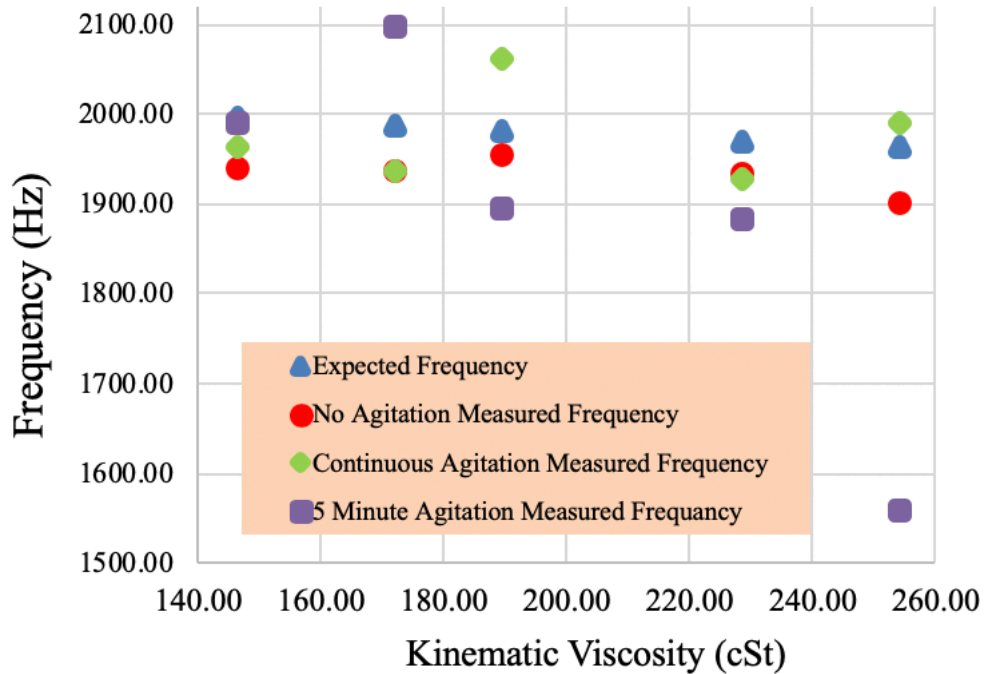
Figure 62: Plot of frequency vs. viscosity for all different methods.

The short-term agitation procedure was disregarded because the result does not follow any trend and too much randomness, which could be due the vibrations of agitation. Future work should investigate a better method of doing short-term agitation through shorter time for stir-bars rotations, as well as potentially changing how the fluids are added.

Using the measured viscosity values from commercial viscometer and the exponential trendline fit in Equation 5.2, the expected amplitude values were calculated for different mixtures of oil. These results are shown in Table 4. The expected amplitude values were used for comparison and to draw conclusions for the no agitation, continuous agitation, and short-term agitation procedures.

Table 4: Expected and measured amplitudes for various test conditions.

Test Case	Measured Kinematic Viscosity	Expected Amplitude (mV)	No Agitation Measured Amplitude (mV)	Continuous Agitation Measured Amplitude (mV)	Short Term Agitation Measured Frequency (mV)
5W30	146.51	0.71	0.76	1.02	0.65
5W30 : 10W40 [2:1]	172.22	0.66	0.53	0.88	0.47
5W30 : 10W40 [2:2]	189.44	0.62	0.53	0.75	0.34
5W30 : 10W40 : 20W50 [2:2:1]	228.42	0.55	0.45	0.73	0.30
5W30 : 10W40 : 20W50 [2:2:2]	254.25	0.51	0.29	0.66	0.39

Figure 63 shows that the amplitude response for all the different methods follow the downward trend similar to expected amplitude. The amplitude values for no agitation procedure are the closest to the expected amplitude result.
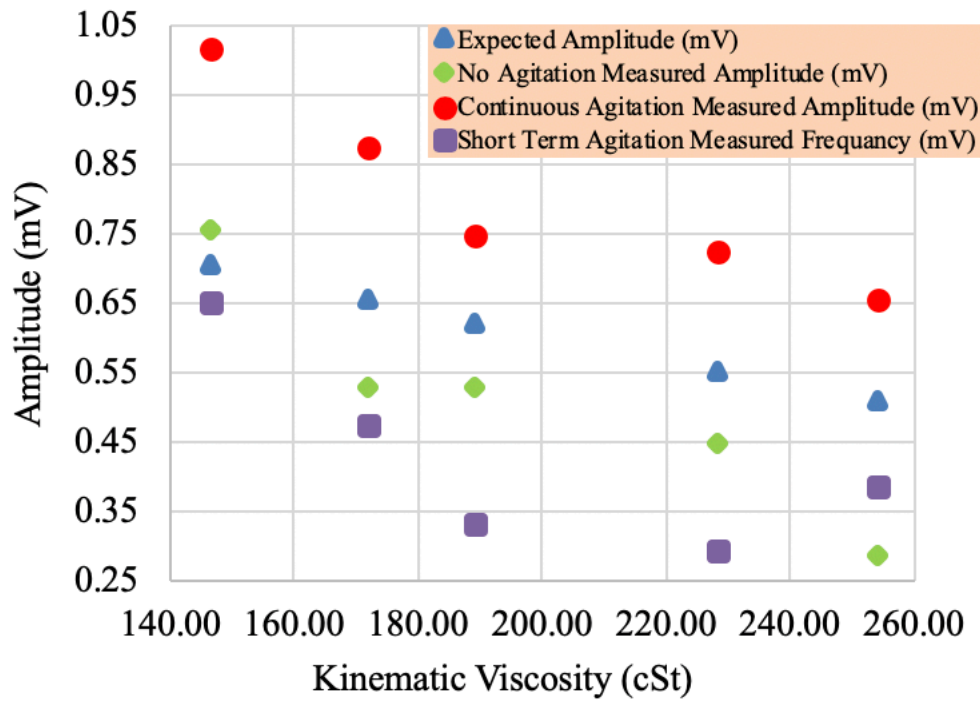
Figure 63: Plot of amplitude vs. viscosity for all different methods.

Out of the three results obtained from the sensor, amplitude has the best characteristic representation for the different fluids, followed by frequency and lastly the quality factor. With changes occurring to the frequency, similar changes can be seen occurring to the sensors amplitude but the quality factor does not seem to respond to change in frequency. Further investigation needs to be done to understand the spiking or after addition of oil, thus the first 10 minutes of data must be disregarded as the sensor takes time settle down. Temperature monitoring in the system is extremely important and it is clear that external variables such as this need to be tightly locked down for better response characterization.

Explaining response signal / spike:

To understand the response signal and possible theories for the spikes and data instability, three separate tests were done. A first one to see if change in volume causes the spike, which is done by adding the same oil and seeing if there is any spike, the second by not changing the oil temperature by adding small quantities of oil, and the third to see if epoxy is softening by testing with a lower bridge bias.

In Figure 64, 5W30 oil was tested as a baseline and more 5W30 was added after 60 minutes. The results show that when adding the same oil, the spikes are still present. This means that changes in the viscosity of oil and volume are not causing the spike. It can also be seen that viscosity change is not a big factor– other things affect it such as epoxy or temperature.
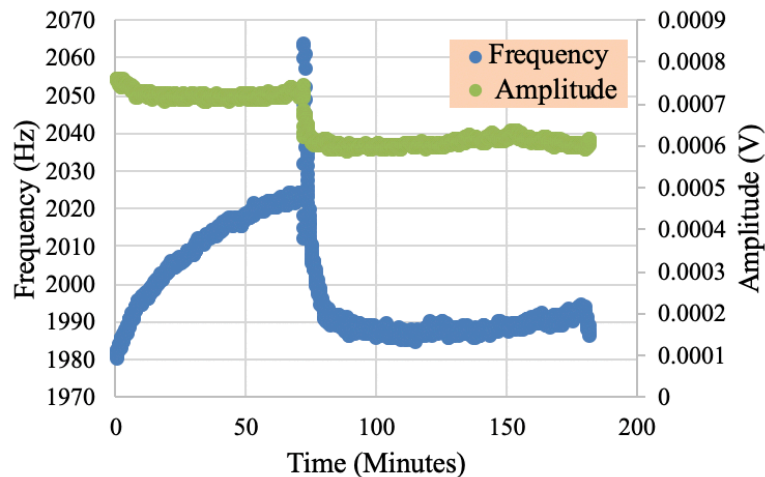
Figure 64: Graph showing frequency and amplitude response with same oil added after some time.

The second test focused on controlling the change in temperature of the oil and to do so oil was added 1 drop (50 µL) every second. This reduced the sudden temperature variation and also any external vibrations due to oil addition. Figure 65 shows that amplitude does not see any spike and is an underdamped response whereas frequency did see a spike, but because the temperature

increased due to higher bridge voltage (7V), the frequency did not come back down. A slower oil addition technique could help fix the spike but temperature is the major cause. In future tests oil would be added 1 drop (50 µL) every 5 seconds or potentially in a continuous monitored flow.
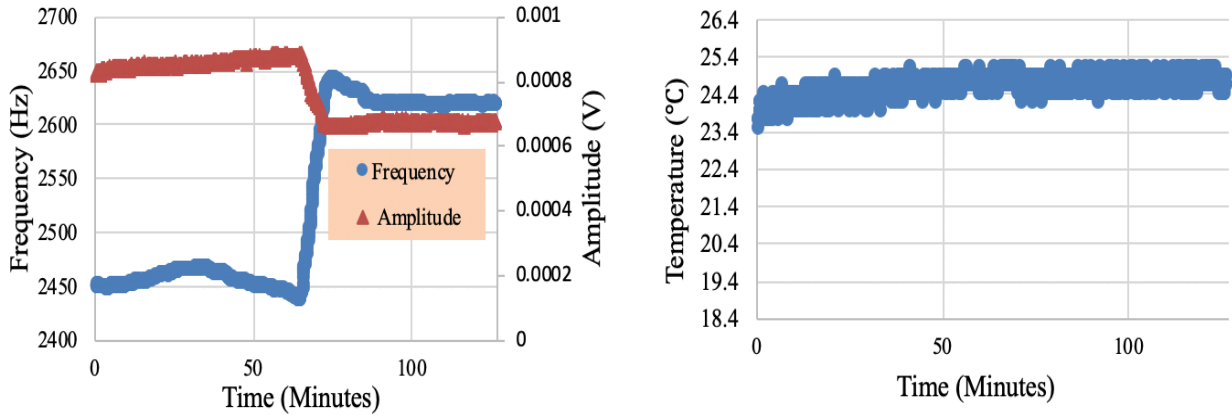
Figure 65: Graph showing frequency and amplitude response with new oil addition method.

Third test was to see if epoxy softening was causing the spike. Bias conditions were changed to run test with a lower bridge bias. Sensor test conditions were bridge voltage = 3 V, pulse width = 25 µs, pulse heat = 15 V. Figure 66 shows frequency and amplitude response with lower bridge bias.
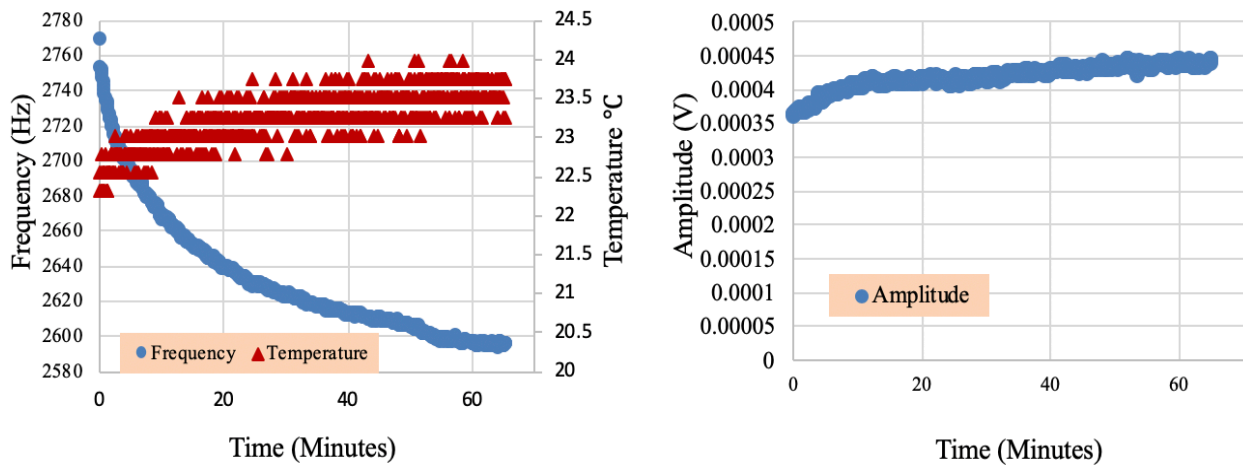
Figure 66: Graph showing frequency and amplitude response with lower bridge bias.

76

In the test above, same oil was added after 50 minutes and results show no spike in frequency or amplitude. This is due to the fact that because bridge voltage is continuously ON, which causes significant heating up of the sensor and loosening of epoxy. Mentioned in Section 4.4, as bridge voltage (V_B) is always ON, constant power is being applied to the resistors which caused frequency to decrease significantly with increase in V_B (- 28%). The possible cause for this frequency shift stated earlier could be change in the state of epoxy. It is important to note that natural frequency of vibration could change if there is changes in stress of epoxy when submerged in oil changing due to the change in Poisons ratio of epoxy. Based on the epoxy technical data sheet the maximum heat resistance of epoxy should be no more than 40 °C, and this temperature value is highly dependent on the resin-to-hardener proportion as it corelates the glass transition temperature values [41]. The ratio of resin-to-hardener used for our packaging purpose was 1:1 as suggested by the manufacturer. The manufacturer also states that cure time and shear strength is dependent on temperature, humidity and thickness of epoxy applied [41]. "The tensile strength of all resins depends linearly on the test temperature with respect to the particular glass transition temperature (T/TG)" [43]. The results from the testing of our sensor show that the temperature is increasing due to higher bridge voltage which could be impacting the viscoelastic properties of epoxy and changing the tensile shear strength of the epoxy, causing loosening and stress onto the sensor directly.

The final solution to eliminate spike was to lower bias voltage to reduce any significant heating and addition of oil in very small quantities ~ μL range. To completely remove any packaging influence on the viscosity sensor, using an epoxy which is more resistant to elevated temperatures and marine is recommended as it would provide high bonding strength when sensor is exposed to any liquid. One example of such epoxy would be 'The Loctite 0.85 fl. oz. Marine

Epoxy'. The manufacturer claims that this epoxy will cure underwater, resistant to water, moisture, solvents and impact and also has a higher adhesion level [42].

The no agitation test was repeated with the lower bridge bias condition and the newer method of adding oil to see if any improvement is seen response time. The frequency and amplitude responses with lower bridge bias are shown in Figure 67.
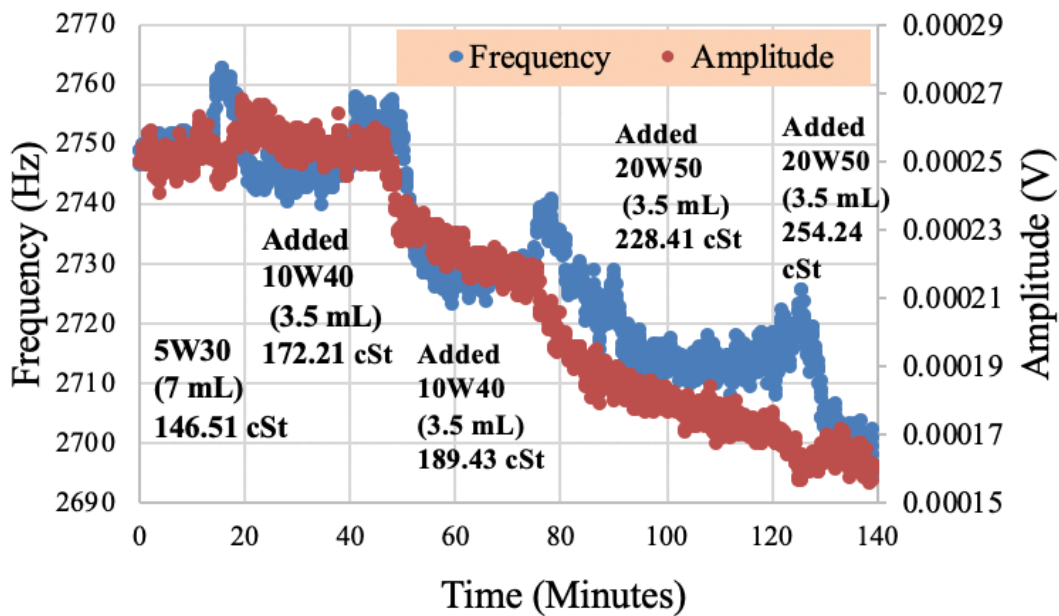
Figure 67: Graph showing frequency response to different oils for no agitation test setup with lower bridge bias.

Lowering bridge voltage and new oil addition method reduces variability as seen in Figure 67. Result also show improved response (3 minutes) and lower stabilization time for each test case. Frequency only spikes 10-20 Hz as compared to previous testing 120-150 Hz. The amplitude shows an overdamped response whereas frequency is underdamped.

Figure 68 shows normalized response of frequency. Initial upward spike in response then underdamped. No agitation response with $V_B = 3$ V settle down faster for all the different viscosity.
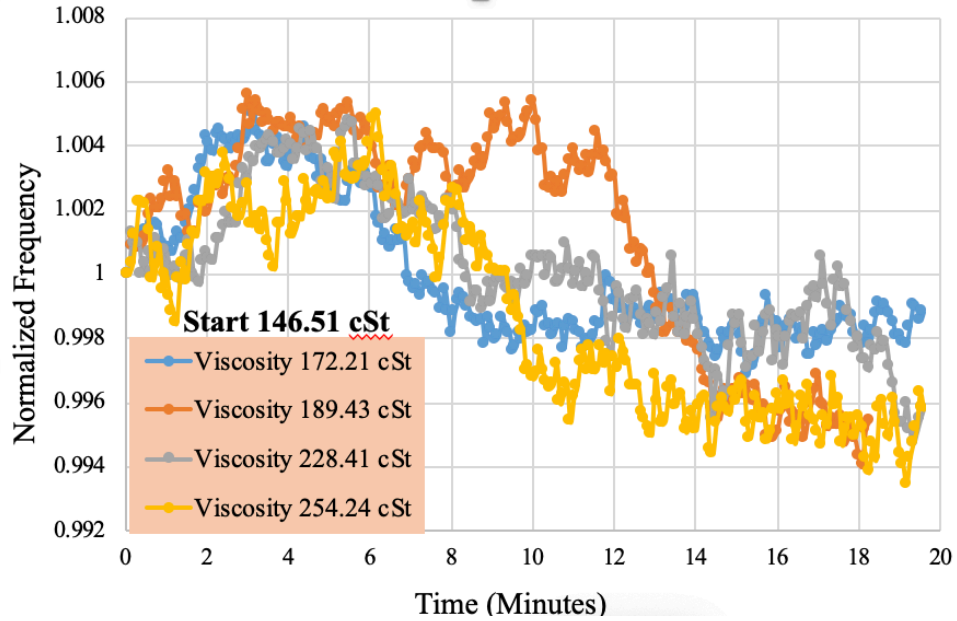
Figure 68: Plot of normalized frequency response to different oils for no agitation with $V_B = 3$ V.

Figure 69 shows normalized response of amplitude with $V_B = 3$ V. Overdamped response is seen with stabilization time around 10-12 minutes. No agitation response with $V_B = 3$ V shows same response times for all the different viscosity.
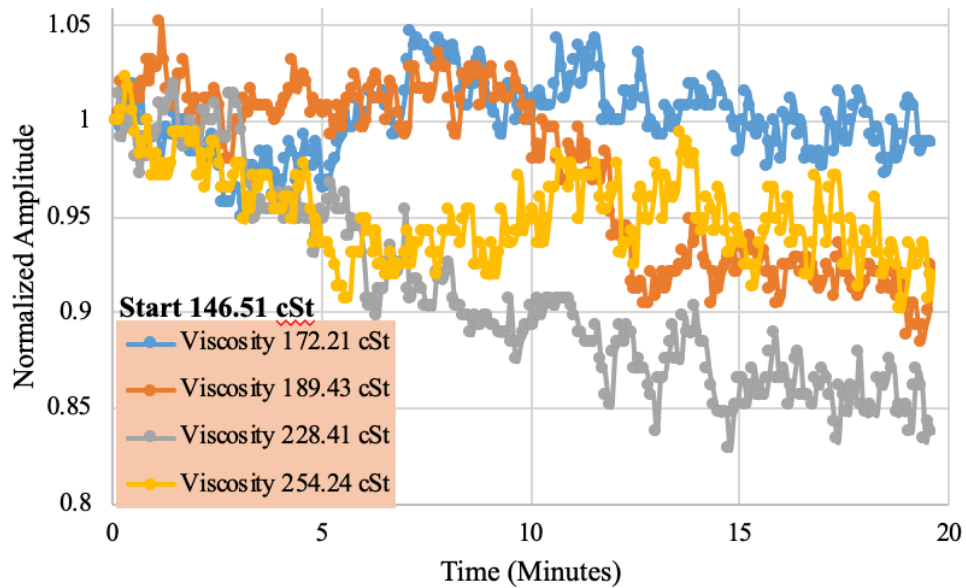
Figure 69: Plot of normalized amplitude response to different oils for no agitation with $V_B = 3$ V.

79

Figure 70 shows the raw data in time and frequency domain for the baseline tests in 5W30, 10W0 and 20W50 oil with $V_B = 3$ V. Frequency, quality factor and average amplitude of oscillation values were extracted by lab view from the raw data.
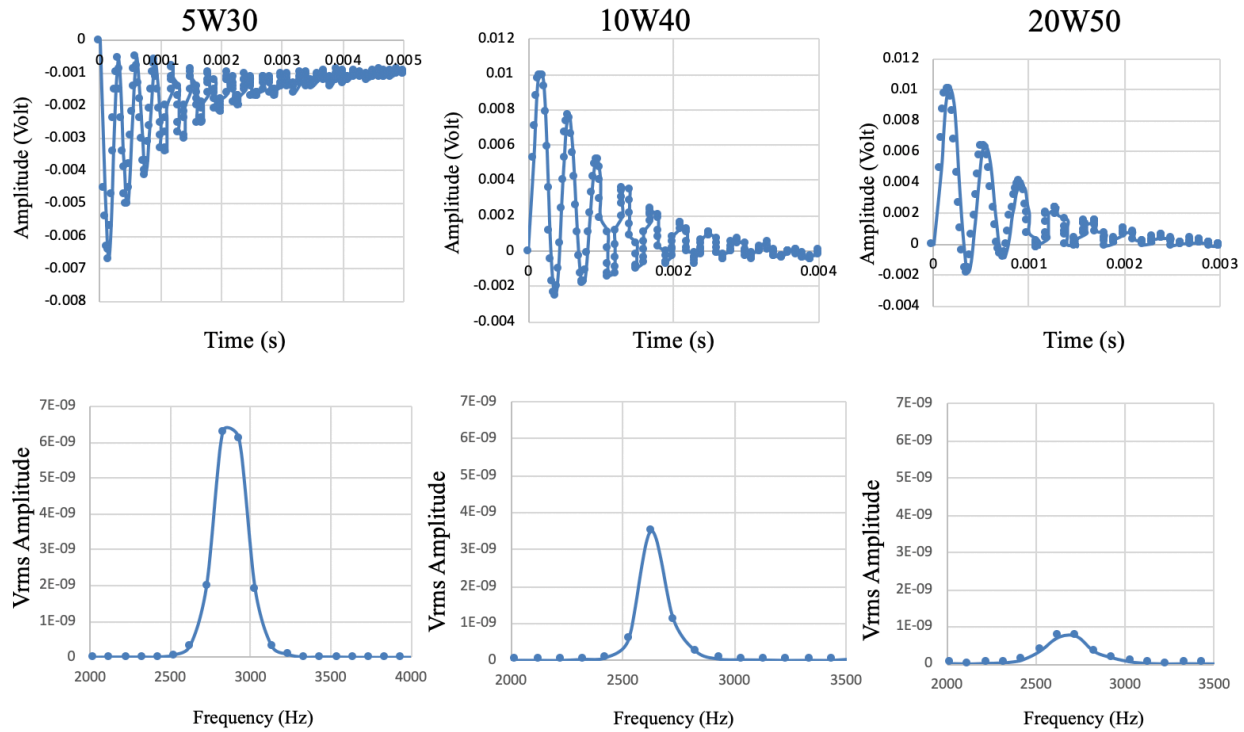
Figure 70: Raw data in time domain and frequency domain with $V_B = 3$ V for 5W30, 10W40 and 20W50 oil.

To calculate the expected amplitude and frequency at $V_B = 3$ V, sensor was tested again with new bias condition in 5W30, 10W40 and 20W50 oil to get baseline values. A curve of fit was used to predict the viscosity and amplitude relationship. Figure 71 shows a power trendline was used with data sets and the R-squared value achieved is 0.9991. The power trendline equation was:

$$y = 0.1459\, x^{-1.269} \tag{5.3}$$

In the equation 'y' is the amplitude and 'x' is the viscosity value.
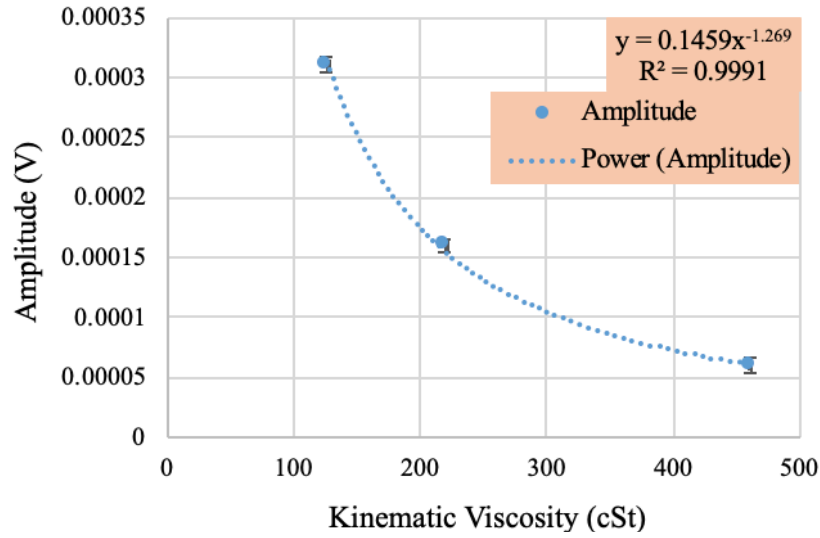
Figure 71: Plot for amplitude vs kinematic viscosity with a trendline fit to predict amplitude for different viscosity with bridge bias 3 V.

A similar trendline curve was plotted to predict the expected frequency at $V_B = 3$ V. Shown in Figure 72, a power trendline was the best fit and the R-squared value achieved is 0.9989, which is a nearly perfect fit of the line to the data. The power trendline equation was:

$$y = 3297.8.5 \, x^{-0.036} \tag{5.4}$$

In the equation 'y' is the frequency and 'x' is the viscosity value.
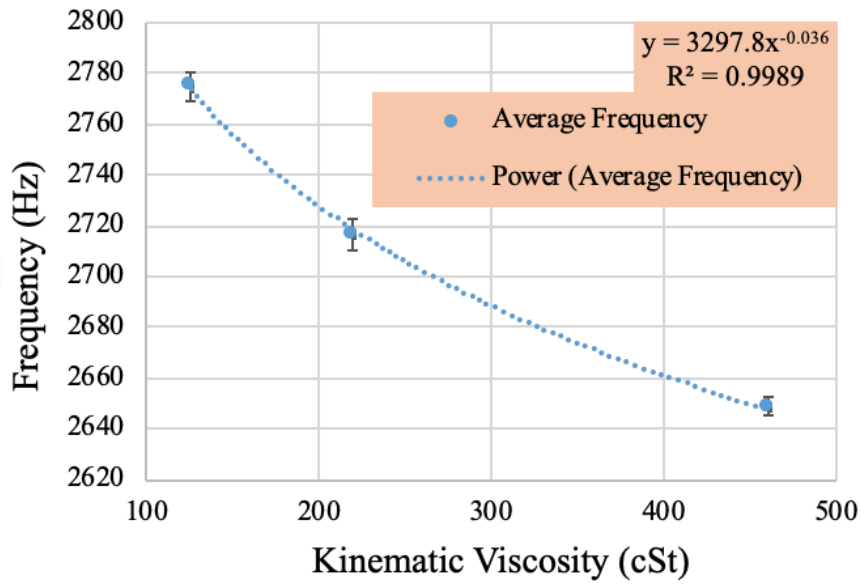
Figure 72: Plot for frequency vs kinematic viscosity with a trendline fit to predict frequency for different viscosity with bridge bias 3 V.

Table 5: Expected and measured frequency and amplitudes for lower bridge bias conditions.

Test Case	Measured Kinematic Viscosity (cSt)	Expected Frequency (Hz) for V_B = 3 V	No Agitation Measured Frequency (Hz) for V_B = 3 V	Expected Amplitude (mV) for V_B = 3V	No Agitation Measured Amplitude (mV) for V_B = 3 V
5W30	146.51	2755.83	2747.96	0.26	0.24
5W30 : 10W40 [2:1]	172.22	2739.48	2742.02	0.21	0.25
5W30 : 10W40 [2:2]	189.44	2730.46	2727.76	0.19	0.21
5W30 : 10W40 : 20W50 [2:2:1]	228.42	2713.17	2712.84	0.15	0.17
5W30 : 10W40 : 20W50 [2:2:2]	254.25	2701.61	2696.38	0.13	0.15

Table 5 shows the expected amplitude and frequency values that were calculated using the power trendlines in Equation 5.3 and 5.4 and can be compared to the no agitation test repeated with the lower bridge bias condition. These baseline tests were needed to be repeated because the expected frequency and amplitude values obtained earlier were from tests at a higher bridge voltage (V_B = 7 V).

Figure 73 shows the frequency and amplitude response for the lower bridge bias condition follow the downward trend similar to expected amplitude. The expected and measured frequency values are < 1 % different for all the test cases. The expected and measured amplitude values are a close match with a difference of ± 0.03 mV.
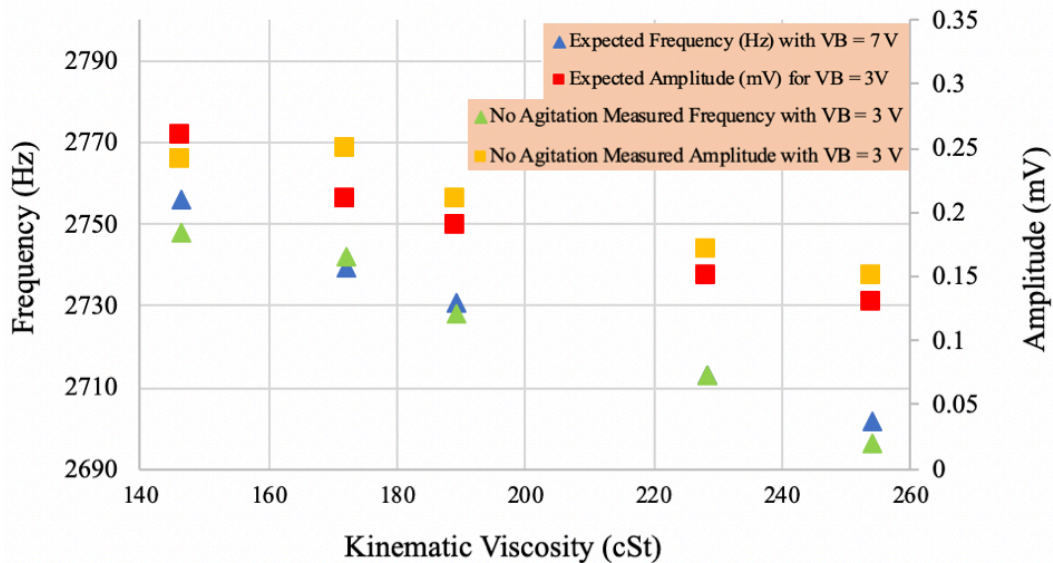
Figure 73: Plot of expected and measured frequency and amplitudes for lower bridge bias conditions.

In general, the results agreed with what was seen in literature [18], with a few **notable exceptions.** Beginning of testing in 5W30 oil response time is longer as it takes time to the setup to stabilize due to the temperature differences. When the viscosity is increased by adding different oils to the mixture, there is an initial downward/upward spike before the signals stabilize. After

this initial spike there was settling seen which was consistent with what was expected if compared to response seen of a micro cantilever sensor by M K Ghatkesar et al [18].

Results compared to [18] where we see that a kinematic viscosity shift of 0.129 cSt (15 % increase) results in a 0.68 % decrease in frequency shift, as shown in Figure 12. Whereas for our sensor when 10W40 oil is added to the initial 5W30 [1:2] by volume, viscosity shift of 25.7 cSt (17.5 % increase) results in 0.21 % decrease in frequency. The frequency shift of the cantilever beam sensor seems to be more sensitive than that of the diaphragm sensor due to its comparatively larger surface area interaction with the fluid under test. In [18] when viscosity is increased by 19 %, as the fluid is changed from 5 % glycerol to 12 % ethylene glycol, the amplitude decreases by 9 %. In comparison to this for our sensor when viscosity is increased by 20.60 % during 5W30:10W40 [2:2] to 5W30:10W40:20W50 [2:2:1], amplitude shift observed was from 0.21 mV to 0.17 mV seen in Table 5. This is a 20 % decrease, which is larger than the 9 % decrease seen in [18]. The amplitude change of the diaphragm sensor seems to be more sensitivity than that of the cantilever beam sensor. Further investigation is needed in order to understand this behavior. The response times seen were similar 3-5 minutes and overdamped matching for the most part. Quality factor measurements were not reliable for our test setup.

CHAPTER 6

CONCLUSION

It was shown that the MEMS sensor fabricated in this work performed similarly to the works previously examined, with some notable process improvements. Issues such as the temperature difference in samples and different agitation methods were examined and necessary future work was identified.

As viscosity is dependent on temperature, when the membrane is heated above the ambient, no effects of changing fluid temperature must be seen in results. As such, it was necessary to determine appropriate test bias conditions that do not affect the measurement. Test bias condition optimization results showed that frequency is most stable when the pulse width is between 20 and 30 μs and heater voltage between 6-15 V. Pulse width and heater bias do not affect the sensor performance significantly as this is a very fast pulse. Even though the instantaneous power deliver is between 200 mW and 1 W, the energy deliver is less than 30 μJoule with a 30 μsec pulse. At a typical 20 Hz actuation rate, the duty cycle is 0.6 ms per second, or 0.0006 %. Pulse width and heater bias value can be adjusted for optimum sensor response (within reason). It was important to note that too large of a bridge voltage (V_B), resulted in significant heating of the silicon membrane, affecting its resonant frequency and softening of die attach epoxy. The local temperature of the sensor is changing due to the bias, affecting the response – possibly affects the epoxy very significantly.

Testing with the optimized bias conditions, the real-time response of the thermally actuated MEMS viscosity sensor was evaluated. Using the measured viscosity values from commercial

viscometer and the trendline equations the expected frequency and amplitude values were calculated for different mixtures of oil. Three different test scenarios were investigated (1) no agitation, (2) continuous agitation and (3) short-term agitation and compared to the expected frequency and amplitude. No agitation results were the closest match to the expected values, within $\pm$ 5 % range for frequency and $\pm$ 15 % for amplitude.

Out of the three different ways that viscosity could be compared to for our sensor, amplitude has the best characteristic representation for the different fluids, followed by frequency and lastly the quality factor. It was observed that frequency is very dependent on intrinsic stress, natural frequency responding to viscosity but only as a small factor, other packaging elements affect frequency shift the most. This is due to the fact that frequency is dependent on the shape size and material of the sensor. Also, the Youngs Modulus of silicon changes with the change in temperature and decreases frequency but only by a factor of 0.1 % per °C. Amplitude of oscillations are independent to material properties changing and shows a faster response, within 2-3 minutes.

Results showed spikes in frequency and amplitude, which upon further investigation, seemed to be due to local variations in the temperature affecting the epoxy used for die-attach and wire bond protection. Changes in the state of epoxy causes stress onto the membrane of the sensor and greatly affect the natural frequency of vibrations. On the other hand, the amplitude of the oscillation showed a more stable result as it is not as sensitive to the effect of the stress forces. Spikes and data instability were eliminated by lowering the bias voltage to 3 V, which reduced any significant heating, and proved that when the sensor is heated near the glass transition temperature of the epoxy its response is very sensitive to any temperature variations. In addition, oil was added

in very small quantities (~ µL) to minimize drastic temperature changes.   The no agitation test, repeated with lower bridge voltage, showed a faster response (3 minutes), low stabilization time, and frequency only spikes of 10-20 Hz as compared to previous testing 120-150 Hz. Amplitude does not see any spike with the new conditions and is an underdamped response.

Future work would involve repeating agitation experiments with new test bias conditions (3 V) and new oil addition method. Better results, could be seen if sensor packaged in a way where there is no temperature dependence, by either using an epoxy with a higher glass transition temperature or heating up the oil to a temperature higher than system temperature (> 35 °C).

7.0   REFERENCES

1.   D. Nieto, "What are the differences between dynamic and kinematic viscosities?", Web, Rheosense, September 26, 2015

2.   D. Troyer "Kinematic Viscosity Explained", Machine Lubrication [online] URL: https://www.machinerylubrication.com/Read/294/ absolute-kinematic-viscosity

3.   R. Arun "Importance of Viscosity in Real Life Properties of Fluid Mechanics", Fluid Mechanics, 2017 URL: https://www.careerdune.com/ 2017/10/importance-of-viscosity-in-real-life.html

4.   Lowe, G. & Lee, Aj & Rumley, A & Price, J & Fowkes, F. (1997). Blood viscosity and risk of cardiovascular events: The Edinburgh Artery Study. British journal of haematology. 96. 168-73. 10.1046/j.1365-2141.1997.8532481. x.

5.   Acree Technologies Incorporated "Thin Films Coating Technologies for the 21st Century", Coatings for Medical / Biomedical Devices and Surgical Instruments. URL: http://www.acreetech.com/index.php/products/medical-biomedical-surgical

6.   Lowe, G. & Lee, Aj & Rumley, A & Price, J & Fowkes, F. (1997). Blood viscosity and risk of cardiovascular events: The Edinburgh Artery Study. British journal of hematology. 96. 168-73. 10.1046/j.1365-2141.1997.8532481. x.

7.   D. Troyer "Kinematic Viscosity Explained", Machine Lubrication [online]URL: https://www.machinerylubrication.com/Read/294/ absolute-kinematic-viscosity

8.   C. Akbay and O. Koçak, "Vibrational Viscometer Design for Biomedical Purposes," *2018 Medical Technologies National Congress (TIPTEKNO)*, Magusa, 2018, pp. 1-4

9.   Engineering ToolBox, (2003). *Absolute, Dynamic and Kinematic Viscosity*. [online] Available at: https://www.engineeringtoolbox.com/dynamic-absolute-kinematic-viscosity-d_412.html [Accessed 12, October 2019].

10.   Ghader Rezazadeh and Mina Ghanbari, On the mathematical modeling of a mems-based sensor for simultaneous measurement of fluids viscosity and density, Sensing and Imaging 19 (2018), no. 1, 27.

11.   L. Zhao *et al*, "A MEMS Resonant Sensor to Measure Fluid Density and Viscosity under Flexural and Torsional Vibrating Modes," *Sensors,* vol. 16, *(6),* pp. 830, 2016.

12.   Yu Hongbin, Lou Liang, and Alex Gu Yuandong, Capacitive micromachined ultrasonic transducer (cmut) based micro viscosity sensor, Sensors and Actuators B: Chemical 227 (2016), 346 – 351.

13. Po-Cheng Chen and A. Lal, "Ultrasonic viscometer with integrated depth measurement," *2015 IEEE International Ultrasonics Symposium (IUS)*, Taipei, 2015, pp. 1-4. doi: 10.1109/ULTSYM.2015.0247

14. A. Ebisui, Y. Taguchi, and Y. Nagasaka, Novel optical viscosity sensor using laser-induced capillary wave, MOEMS and Miniaturized Systems VII (David L. Dickensheets and Harald Schenk, eds.), vol. 6887, International Society for Optics and Photonics, SPIE, 2008, pp. 155 – 164.

15. A. D. Gomes, J. Kobelke, J. Bierlich, K. Schuster, H. Bartelt and O. Frazão, "Optical Fiber Probe Viscometer Based on Hollow Capillary Tube," in *Journal of Lightwave Technology*, vol. 37, no. 18, pp. 4456-4461, 15 Sept.15, 2019. doi: 10.1109/JLT.2019.2890953

16. T. Manzaneque *et al*., "Density-viscosity sensor based on piezoelectric MEMS resonator and oscillator circuit," *SENSORS, 2014 IEEE*, Valencia, 2014, pp. 241-244. doi: 10.1109/ICSENS.2014.6984978

17. R. Thalhammer *et al*., "Viscosity sensor utilizing a piezoelectric thickness shear sandwich resonator," in *IEEE Transactions on Ultrasonics, Ferroelectrics, and Frequency Control*, vol. 45, no. 5, pp. 1331-1340, Sept. 1998. doi: 10.1109/58.726459

18. M K Ghatkesar, E Rakhmatullina, H Lang, C Gerber, M Hegner, T Braun, "Multi-parameter microcantilever sensor for comprehensive characterization of Newtonian fluids", Sensors and Actuators B: Chemical, Volume 135, Issue 1, 2008, Pages 133-138, ISSN 0925-4005

19. B A Bircher, L Duempelmann, K Renggli, H P Lang, C Gerber, N Bruns, T Braun, "Real-Time Viscosity and Mass Density Sensors Requiring Microliter Sample Volume Based on Nanomechanical Resonators" Analytical Chemistry 2013 85 (18), 8676-8683 DOI: 10.1021/ac4014918

20. O. Cakmak, E. Ermek, H. Urey, G. G. Yaralioglu and N. Kilinc, "MEMS based blood plasma viscosity sensor without electrical connections," *SENSORS, 2013 IEEE*, Baltimore, MD, 2013, pp. 1-4. doi: 10.1109/ICSENS.2013.6688342

21. M. McAfee, G. McNally, "Real-time measurement of melt viscosity in single-screw extrusion", Transactions of the Institute of Measurement and Control 28, 5 (2006)

22. N. Ahmed, D. F. Nino, V. T. Moy, "Measurement of solution viscosity by atomic force microscopy", Review of Scientific Instruments 72, 2731 (2001)

23. Ivan Puchades and Lynn F. Fuller, "A Thermally Actuated Microelectromechanical (MEMS) Device for Measuring Viscosity," *Journal of Microelectromechanical Systems*, vol. 20, no. 3, pp. 601-608, 2011.

24.	T.R. Hsu "MEMS and Microsystems-Design and Manufacture", McGraw-Hill, Boston, 2002

25.	S. S. Walwadkar, J. Cho, "Evaluation of Die Stress in MEMS Packaging: Experimental and Theoretical Approaches", IEEE Transactions on Components and Packaging Technologies, Volume 29, No. 4, December 2006

26.	S. Walwadkar, P. W. Farrell, L. E. Felton, J. Cho, "Effect of die-attach adhesives on the stress evolution in MEMS packaging", Proc. 36th International Symposium for Microelectronics (IMAPS), Boston, MA, November, 2003, Pages 847-852

27.	R. H. Krondorfer, Y. K. Kim, "Packaging Effect on MEMS Pressure Sensor Performance", IEEE Transactions on Components and Packaging Technologies, Volume 30, No. 2, June 2007

28.	R. Blevins, "Formulas for Natural Frequency and Mode Shape," in *Van Nostrand Reinhold*, New York, 1979

29.	Philip M Morse and K. Uno Ingard, *Theoretical Acoustics*. Princeton: McGraw-Hill Inc, 1968.

30.	Y Kozlovsky, "Vibration of Plates in Contact with Viscous Fluid: Extension of Lamb's Model," *Journal of Sound and Vibration*, vol. 326, no. 1-2, pp. 332-339, 2009.

31.	K. Nojiri and SpringerLink (Online service), Dry Etching Technology for Semiconductors. 2015;2014;.

32.	Wikipedia.org.	(2011,	December)	Joule	Heating.	[Online].	URL: http://en.wikipedia.org/wiki/Joule_heating

33.	Ahmed, Abdelaziz & Dennis, John & Khir, M. & Mohamad Saad, Mohamad Naufal. (2012). Simulation and modeling the effect of temperature on resonant frequency of a cmos-mems resonator. AIP conference proceedings. 1482. 32-36. 10.1063/1.4757433.

34.	Loctite®	Epoxy	Quick	Set™,	features	and	benefits	Url: https://www.loctiteproducts.com/en/_products/build/epoxies/loctite_epoxy_quickset.html

35.	Wikipedia.org.	(2009,	October)	Step	response.	[Online].	URL: https://en.wikipedia.org/wiki/Step_response

36.	Pennzoil Conventional Motor oil [Online]. URL: https://www.pennzoil.com/ en_us/products/blends-conventionaloils/conventional/_jcr_content/par/productDetails .stream/1460058457626/87085ca215d8b53603881d61ab788decce877c67/Pennzoil-SAE-5W-30-Motor-Oil.pdf

37. Pennzoil Conventional Motor oil [Online]. URL: https://www.pennzoil.com/en_us/products/blends-conventional-oils/conventional/_jcr_content/par/productDetails.stream/1460058456388/3fe6772b7145eecac142d08e6d639534fa238b70/Pennzoil-SAE-10W-40-Motor-Oil.pdf

38. Pennzoil Conventional Motor oil [Online]. URL: https://www.pennzoil.com/en_us/products/blends-conventional-oils/conventional/_jcr_content/par/productDetails.stream/1460058458136/eac3a5c91a14ac315eef72ff85b7bce1b8f008d8/Pennzoil-SAE-20W-50-Motor-Oil.pdf

39. Widman International SRL Mantenimiento Proactivo, Calculate the Actual Oil Viscosity at the Operating Temperature of your Equipment calculator, URL: https://www.widman.biz/English/Calculators/Operational.html

40. Brookfield Engineering, laboratory-viscometersDV2T Touch Screen Viscometer [Online]. URL:https://www.brookfieldengineering.com/products/viscometers/laboratoryviscometers/dv2t-touch-screen-viscometer

41. Loctite® Instant Mix™ 5 Minute Epoxy, Henkel Corporation - Professional & Consumer Adhesives [Online].URL: https://www.loctiteproducts.com/en/products/build/epoxies/loctite_epoxy_instantmix5minute.html

42. Loctite® Marine Epoxy, Henkel Corporation - Professional & Consumer Adhesives [Online]. URL : https://www.loctiteproducts.com/en/products/build/epoxies/loctite_epoxy_marine.html

43. B. Fiedler, T. Hobbiebrunken, M. Hojo, K. Schulte, "Influence of Stress State and Temperature on The Strength of Epoxy Resins" Polymer Composites Section, Technical University Hamburg-Harburg, Germany August 26-30, pp. 533-539, 2009

8.0 APPENDIX A

MCEE770 – 2181
MEMS PROCESS FLOW
P+, STS DRIE (option)

Step	Instructions	Review/Sign
1.	Obtain qty 2, 6" n-type wafers SOI, N-type region 20um, BOX 1um, 1-10 ohm-cm Obtain qty 2, 6" n-type wafers (non SOI for Nitride option)	ALL WAFERS
2.	Take res map measurements Average: _____ ohm-cm	ALL WAFERS
3.	RCA clean	ALL WAFERS
4.	Grow 5000A oxide recipe 350	ALL WAFERS
5.	81pt Spectro map measurement Average oxide thickness_____ stdv_____	ALL WAFERS
6.	Photo level 0: alignment marks Coat wafer Resist OIR 620-10 (recipe 6 on SVG to hand dispense): Recipe:_____ Develop in wafer track. CD-26 Recipe 1 Expose using ASML Stepper Stepper job: _____ Stepper Mask: Level 0 Combi reticle	ALL WAFERS

7.	Etch Alignment Marks BOE 10:1 about ~550A/min For 11 minutes Inspect resolution	ALL WAFERS
8.	Solvent Strip	ALL WAFERS
9.	RCA clean	ALL WAFERS
10.	Grow P+ masking oxide 5000 Å, Recipe 350 tube 1 -critical to set up ASML alignment marks- Enter Nanospec thickness: 1_____, 2_____, 3_____, 4_____, 5_____ Should be around ~7500A	ALL WAFERS
11.	Photo 1: P+ diffusion Coat in wafer track using OiR620 resist. Soft bake 90C Recipe:_____ Expose using ASML Stepper Stepper job: MCEE770 *(modified?)* Stepper mask: Level 1, Diffusion Develop in wafer track. CD-26 Recipe:_____ Enter minimum resolution line: _____ um	ALL WAFERS
12.	Etch Alignment Marks BOE 10:1 about ~550A/min ~18 minutes Inspect resolution	ALL WAFERS
13.	Strip Resist 10 min solvent clean + 5 min DI water rinse + SRD	ALL WAFERS

	Enter minimum resolution line: _____ um	
14.	RCA Clean Standard	ALL WAFERS
15.	Grow 200A of screen oxide recipe 215 Ramp in O2 for 20 min Soak for 36min	ALL WAFERS
16.	Ion implant Boron: Ion: B11 Dose = 1E15cm-2 Energy = 100KeV Time ~10min at 100uA	ALL WAFERS
17.	BOE 10:1 screen oxide for 2 minutes	ALL WAFERS
18.	Dopant Diffusion/4000Å Oxide - Recipe:_____ Soak: ramp up 30min O2 + 5minO2 1100C + 25wetO2 at 1100C + 20min **anneal N2** + ramp down N2 60min	ALL WAFERS
19.	Photo 2: contact cuts Coat in wafer track using OiR620 resist. Recipe: Soft bake 90C Expose using ASML Stepper Stepper job: _____ Stepper mask: Level 2 CC Post exposure bake 110C Develop in wafer track. CD-26 Recipe: DEVELOP.rcp Enter minimum resolution line: _____ um	ALL WAFERS

20.	BOE 10:1 Etch CC oxide Need to Etch through field oxide ~0.75um on SOI wafers)	ALL WAFERS
21.	Deposit 3µm of TEOS on to the BACK of the wafer Enter Nanospec thickness: 1_____, 2_____, 3_____, 4_____, 5_____ Measure back of wafer	ALL WAFERS
22.	RCA clean and Pre metal HF dip: 50:1 H2O:HF for 30 seconds DI water 5 minutes Followed by SRD	ALL WAFERS
23.	CVC 601 sputter metal deposition of Al Pressure 5mT Power: 2000W Time: 30minutes Thickness: 1um hot/cold sputter Ar 20sccm Power: 2000W Pressure: 5mT Pre sputter: 300 seconds Standard Al sputter for 250 seconds Turn on heater per 601 manual instructions Set timer to 17 minutes temp 200C After 15 minutes set to hot sputter for 1200 seconds	ALL WAFERS
24.	Photo 3: Metal Coat in wafer track using OiR620 resist. Recipe: Expose using ASML Stepper Stepper job: _____ Stepper mask: Level 3 metal Develop in wafer track. CD-26 Recipe:	ALL WAFERS

	Enter minimum resolution line: _____ um	
25.	Aluminum etch wet - allow bath to sit for an hour before etch to achieve a uniform 40C throughout bath Constant agitation – etched for 5.5 minutes in 2018.	ALL WAFERS
26.	Solvent strip resist	ALL WAFERS
27.	Sinter aluminum Use short course recipe. 425C for 30minutes.	ALL WAFERS
28.	Photo 4: Bottom Hole Hand coat back of wafer. ASML stepper without alignment. Photoresist: OIR 620 Soft-bake: 90C Post exposure bake: 110C CD 26 develop Hard bake: 140C on spacer ring.	ALL WAFERS
29.	Coat the front with resist to mask BOE: **Attach wafer _to a clean and new_ Si wafer carrier to protect backside:** **(very important that the carrier wafer does not have any topology and is clean, otherwise it will not attach well)** Coat front of carrier wafer 2500 rpm, 30 seconds Do not bake Coat front of wafer 2500 rpm, 30 seconds Place front to front and align to major flat on top of carrier wafer. Back of the wafer should be up. Hard bake at 130C for 3 minutes.	ALL WAFERS

30.	BOE Wet Etch into the 3um of TEOS back hole to expose the Silicon Oxide left after etch should be <100A	ALL WAFERS
31.	Separate from carrier: Place device and carrier on hot plate at 140C Use razor or sharp edge of tweezers to separate wafers. Remove resist in solvent strip or acetone bath. Spin rinse dry. Inspect front aluminum:	ALL WAFERS
32.	Front hole lithography Photo 5: Front Hole Coat by hand using OiR620 resist Recipe: Expose using ASML Stepper Stepper job: _____ Stepper mask: Level 5 top Hole Develop in wafer track. CD-26 Recipe: Enter minimum resolution line: _____ um	ALL WAFERS
33.	Wet etch oxide in 10:1 BOE	ALL WAFERS
34.	STS (1um per cycle) SOI to buried oxide layer SOI is 20 microns thick Etch and passivate pressure: 5mTorr 600W Etch(sccm) Passivate (sccm) C4F8 0 85 SF6 130 0 O2 12 0 Ar 20 20 Number of cycles:_____ P2 measurement:_____ Etch rate_____	ALL WAFERS

35.	Recoat and redo Top Hole litho if necessary to finish BOX etch. Attach wafer to carrier to protect backside (see previous for instructions). 5.2:1BOE Wet etch the 1um of buried oxide	ALL WAFERS
36.	Separate from carrier: Place device and carrier on hot plate at 140C Use razor or sharp edge of tweezers to separate wafers. Remove resist in solvent strip or acetone bath. Spin rinse dry.	ALL WAFERS
37.	Attach carrier wafer and device wafer with OIR 620 resist: 1. Coat front of carrier wafer and set it down (no softbake) 2. Coat from of device wafer and place on top of carrier wafer lining up the flats (no softbake) 3. Hard bake a 140C for 7 minutes	ALL WAFERS
38.	STS etch to carrier wafer from the back ~500um (will need to have careful way to handle wafers post STS even though they are on carrier wafer) P2 measurements:	ALL WAFERS
39.	Saw whole wafer and 200um into carrier wafer ~700um such that cantilever are still attached to carrier wafer	ALL WAFERS
40.	Separate the carrier wafer from the devices in water or solvent that dissolves PR to release the chips Heating chips on hot plate may also work well.	ALL WAFERS
41.	TEST ☺	ALL WAFERS